MATRIX-ASSISTED ULTRAVIOLET LASER DESORPTION / IONISATION MASS SPECTROMETRY OF MACROMOLECULES

by

Tak-Wah Dominic Chan

This thesis is submitted for the degree of Doctor of Philosophy

University of Warwick

November 1992

TABLE OF CONTENTS

2. INSTRUMENTATION AND EXPERIMENTAL METHODS

3. FIELD DESORPTION

4. MATRIX-ASSISTED LASER DESORPTION / IONISATION

5. KINETIC ENERGIES OF IONS

6. CHARGING PROCESSES

7. CONCLUDING REMARKS

LIST OF TABLES

LIST OF FIGURES

ABBREVIATIONS

API	Atmospheric pressure ionisation or electrospray
ASE	Amplified spontaneous emission
B_0	Magnetic field strength
Buc	Buccalin
CCD	Charge-coupled device
CID	Collision-induced decomposition
Da	Daltons
EHC	Field desorption emitter heating current
EHD-MS	Electrohydrodynamic mass spectrometry
EI	Electron impact ionisation
ε_m	Molar absorption coefficient or extinction coefficient
Ep	Epidermal growth factor receptor
FAB	Fast atom bombardment
FD	Field desorption
FI	Field ionisation
FT-ICR-MS	Fourier transform ion cyclotron resonance mass spectrometry
FWHM	Full-width half-maximum
GPIB	General purpose interface bus
Glu	Glucagon
Ins	Insulin chain-B
LA	A synthetic peptide
LD	Laser desorption
LEP	Limiting-extraction-potential
LHRH	Luteinising hormone releasing hormone
MALDI	Matrix-assisted laser desorption / ionisation
M/A	Matrix-to-analyte molar ratio
MIFS	Microline focus spectrometry

MIKES	Mass-analysed kinetic energy spectroscopy
m_i	Mass of incident ion
m_f	Mass of fragment ion
M_m	Mass-average molecular mass
M_n	Number-average molecular mass
MS/MS	Tandem mass spectrometry
m/z	Mass-to-charge ratio
3-NBA	3-nitrobenzyl alcohol
Nd-YAG laser	Neodymium yttrium-aluminium garnet laser
ns	Nanosecond
PAD	Post-acceleration detector
PEEK	Poly(ethene) ether ketone
PD	Plasma desorption
PK	Protein kinase-C fragment (530-558)
RMM	Relative molecular mass
SCSI	Small computer system interface
SIMS	Secondary ion mass spectrometry
SDS-PAGE	Sodium dodecyl sulphate-poly(acrylamide) gel electrophoresis
q	Unit electronic charge
TI	Thermospray ionisation
TOF-MS	Time-of-flight mass spectrometry
VIP	Vasoactive intestinal peptide
ν_c	Ion cyclotron orbital frequency
V_{ex}	Extraction potential
V_{ESA}	Electric sector analyser voltage
V_m	Molar volume
V_{sam}	Sample-stage potential
V_{ret}	Retardation potential

ACKNOWLEDGEMENTS

I would like to thank the following people:

My supervisor Professor Peter J. Derrick, for his constant willingness to listen and discuss my ideas. His guidance, encouragement and conceptual assistance throughout the course of this work is deeply appreciated.

Dr. Les Chewter and Dr. Paul McCombes, my industrial supervisors for their stimulating discussions and euthusiastic supports for the present work.

Mr. Alex W. Colburn, for his technical assistance in the design of the laser-based time-of-flight analyser and for solving the numerous electronic problems.

Dr. Caroline Bradley, for her assistance with the field desorption experiments.

The members of the mechanical workshop, for their workmanship in the construction of the ion source, the off-axis post-acceleration detector and the various bits and pieces.

Dr. Dave Reynolds, for his assistance in electronic interface and program development.

Professor Derek J. Gardiner and Mr. Michael Bowden, for performing the Raman microscopy experiments.

Mr. Gerald Smith, for taking the scanning electron micrographs.

Dr. Stephen Davis, for his assistance in the use of the ion optical calculation programs.

Dr. Mark Dowsett, for his stimulating discussion on ion optical calculations.

Dr. Tracey Madden, for proof reading the manuscript.

Dr. Jonathan Curtis, Dr. Su Chen, Dr. John Trainor, Dr. Caroline Bradley, Desmond Yau, Anastassios Gianakopulos, Emmanuel Raptakis, Jonathan Haywood, my work colleagues, for their companionship.

I wish to thank my secondary school, Rosaryhill School, for providing the essential scholarship for my undergraduate study in England. I am especially in debt to the former secondary school principal, Fr. Lionel Xavier O.P., for his gudiance and encouragement throughout my education.

I am pleased to acknowledge the financial support by Shell Thorton Research Centre, Chester, England, for the work presented in this thesis.

My family and friends have been a constant source of support throughout the course of my overseas study and research work. I particularly wish to thank my parents for their continuous encouragement and my girl friend, Teresa Tong, for her support.

DEDICATION

to

My parents

DECLARATION

I hereby declare that this thesis is my own work and that, to the best of my knowledge and belief, it contains no material previously published or written by another person, nor material which to a substantial extent has been accepted for the award of any other degree or diploma of a university or other institute of higher education, except where due acknowledgement is made in the text.

Tak-Wah Dominic Chan

Abstract

The process of ion formation by matrix-assisted ultraviolet laser desorption / ionisation has been studied, using a time-of-flight mass analyser designed and constructed during the course of the present study. Solid matrices and a liquid matrix have been examined. For solid matrices, the signal reproducibility from one sampling position to another has been found to be generally poor. Raman microscopy and scanning electron microscopy studies of the solid samples have shown that matrix-analyte mixing depends critically on the drying conditions. In the case of nicotinic acid as the matrix, nitrogen-purging during the drying process has been found to improve the matrix-analyte mixing. Protein molecule-ion signals have been registered over a wide range of matrix and analyte molar ratios. A near-elimination of matrix-ion formation has been observed at a relatively low matrix-to-analyte ratio for nicotinic acid matrix, but not for sinapinic acid matrix. For the liquid matrix (3-nitrobenzyl alcohol), the signal reproducibility has been found to be excellent. A typical sample could tolerate hundreds of laser shots. A high degree of molecular clustering has been observed for protein-ions at relatively high protein loadings (~ 100 pmol). It has been found that there is a strong dependence of molecule-ion signals on the extraction field. Strong fields have tended to suppress the formation of protein molecule-ions.

Initial velocities for both positive and negative protein molecule-ions have been determined to be ~ 800 ms^{-1} within the experimental uncertainties. The kinetic energies of the protein molecule-ions after full-acceleration have been determined using a grid-electrode to which a retardation potential was applied. Pronounced energy deficits have been observed. Sample-stage potential and the molecular mass of the analyte have been found to affect the magnitudes of energy deficits. Several factors affecting charging processes in MALDI have been studied. Solution-phase acid/base properties and gas-phase proton affinities has been found not to correlate with ionisation efficiencies in MALDI.

A number of synthetic polymers have been studied using MALDI. Only polymers with polar functional groups have been analysed successfully. Based on the present understanding of the desorption / ionisation processes, it is proposed that ionisation rather than the desorption process is the limiting factor in the formation of gaseous molecule-ions from non-polar polymers. The use of an aprotic matrix, it is proposed, should enhance the ionisation of non-polar molecules through electron transfer.

1

INTRODUCTION

Macromolecular behaviour was recognised in 1861 when Thomas Graham noticed[1] that a number of substances differed markedly in their diffusion properties from ordinary materials such as inorganic salts and sugars. The diffusion properties are nowadays attributed to the high molecular masses of these substances. Such macromolecular behaviour may be a consequence of the aggregation of small molecules through secondary bonds to form association colloids. "Macromolecules", in the context of this thesis, refers to molecules, which contain a very large number of atoms joined together by primary chemical bonds and which cannot be reduced to "small" molecules without irreversible destruction. Synthetic polymers and biopolymers represent major categories of macromolecular substances. Both types of polymer are made up of units with similar structures to each other and are characterised by the number, sequence, configuration and conformation of the units.

Synthetic polymers such as poly(ethylene) and poly(succimide) constitute the foundation of many industries including various manufacturing and petro-chemical industries. The physical properties of these polymeric materials are influenced by a number of fundamental characteristics, which include chemical composition, average molecular size, molecular size distribution, degree of branching, stereoregularity and crystallinity. Understanding of the relationship between molecular structure and physical properties contributes greatly to the development and enhancement of these polymeric materials through the design of chemical species with optimum performance characteristics.

Synthetic polymers are normally composed of oligomeric mixtures, which are characterised by their molecular mass distributions. Various statistical averages are used to describe the molecular mass information, for example, number-average molecular mass (M_n) which is defined as

$$M_n = \frac{\sum N_i M_i}{\sum N_i} \qquad (1)$$

and mass-average molecular mass (M_m) which is defined as

$$M_m = \frac{\sum N_i M_i^2}{\sum N_i M_i} \qquad (2)$$

N_i is abundance of the molecule of mass M_i. At present, gel permeation chromatography[2] is the most commonly adopted analytical technique to provide information about oligomeric distributions. This method requires the use of suitable standards of which the molecular mass distributions are known. In the analysis of new or unknown chemical compounds, such standards are difficult to obtain. For this reason, molecular mass information obtained via this method is often only a gross estimate of the real molecular mass distribution. Structural information becomes extremely difficult to obtain when the molecular mass of a polymer exceeds a few thousand daltons.

Biopolymers, such as proteins, oligonucleotides, lipids and polysaccharides, are typically not composed of identical molecules. There is typically no distribution of oligomers to be considered in terms of the molecular mass information (apart from the isotopic distribution). The most reliable method at present, other than mass spectrometry, for obtaining the relative molecular masses of biopolymers has been the use of sodium dodecyl sulphate in conjunction with poly(acrylamide) gel electrophoresis (SDS-PAGE)[3,4]. The accuracy of this technique depends on the nature of the analytes and is normally about a 5%. In the case of certain substances,

such as glycoproteins, very large errors can occur due to the carbohydrate portions interacting in a very different manner from protein-type structures.

1.1. Mass spectrometry of high-mass polymers

Mass spectrometry is an analytical method used to separate and measure the masses of gaseous ions according to their behaviour under electric and magnetic fields. Relative molecular mass can be obtained directly through the mass-measurement of the molecule-ion peak. Structural information concerning the molecule may be deduced from the masses of the fragment ions resulting from decomposition of the molecule-ion.

The essential requirements in mass spectrometry are to be able to produce characteristic ions and mass-analyse them. The formation of gas-phase ions from gaseous or volatile samples can be achieved by electron bombardment, chemical ionisation[5,6], field ionisation[7,8] and multiphoton ionisation[9,10]. Most molecules with masses above a few hundred daltons, by their very nature, are likely to be involatile and thermally sensitive. They would not have a vapour pressure high enough (10^{-4} Pa) to produce detectable ions using the aforementioned ionisation techniques. Pyrolysis or thermal degradation[11] of these compounds to produce low-mass neutral volatile fragments has been used to prepare such materials for mass spectrometric studies. The use of chemical methods, to increase volatility, to protect a compound during vigorous ionisation or to simplify information generated, have also been employed. The molecular-mass information and structural information obtainable with these approaches is generally not satisfactory. In the case of chemical derivatisation, the sample sizes required of the order of milligrams can be unrealistically high. In the last two decades, a number of desorption / ionisation techniques have been developed to transform these thermally labile and involatile substances from their liquid or solid phase into the gas phase. Commonly adopted techniques include field desorption (FD)[8,12,13], thermospray ionisation (TI)[14],

secondary ion mass spectrometry (SIMS)[15,16], fast atom bombardment (FAB)[17-20], plasma desorption (PD)[21,22] and laser desorption (LD)[23,24].

Analytical applications of these desorption / ionisation techniques depend strongly on the physico-chemical nature of the sample molecules. Bio-polymers, which are highly polar by nature, seem to "work well" with most of the desorption / ionisation techniques. For instance, FD, FAB and liquid-SIMS have been used extensively to analyse biological samples with masses of up to 10 000 Da. Using a 30 keV Cs^+ ion beam in liquid-SIMS, molecules in the mass range of 10 000 - 24 000 Da have been analysed[25]. For the desorption / ionization of bio-polymers in the mass range above 10 000 Da, plasma desorption has been used routinely. Recently, the rapid development of matrix-assisted laser desorption / ionisation (or MALDI in short)[26,27] and the electrospray or atmospheric pressure ionisation (API)[28-29] have extended the capability of mass spectrometric measurements to the region of several hundreds of thousands daltons. Hillenkamp et al, using MALDI, have demonstrated the desorption / ionisation of whole catalase molecules with molecular mass of ~235 000 Da[30]. Our group at Warwick has reported[31] a cluster ion of bovine serum albumin with a mass of ~530 000 Da (as discussed below).

Polar synthetic polymers such as polyglycols have been investigated extensively using different desorption / ionisation techniques. Lattimer et al[32,33] have used FD and FAB ionisation to study poly(ethylene imine) and polyglycols. The number-average molecular masses were found to be higher in the case of FD, compared to those obtained from FAB. The FAB result has been attributed to fragmentation caused by the fast-atom beam. SIMS and PDMS have also been applied to the study of synthetic polymers in the mass range up to 4 000 Da. SIMS has given correct oligomer distributions only for a thin layer of sample coated onto the target[34]. For insoluble polymers, which cannot be prepared as thin layers, PDMS has been preferred[35]. Laser desorption technique has been used to study insoluble polymers. Poly(ethlyene glycols) oligomers of masses up to 97 000 Da[36] have been

observed. Cook et al[37] have studied poly(ethlyene glycols) using electrohydrodynamic (EHD) mass spectrometry. Fenn et al[38] have recently reported the successful analysis of poly(ethlyene glycols) up to 5 millions daltons using the API technique. In their experiments, the formation of multiply-charged adduct ions (possibly Na^+ ion adduction) with charge-states up to 4 100 charges have been claimed.

In spite of their relatively low binding energies, non-polar molecules do not seem to be as easy to analyse as polar molecules using most of the techniques described above. The applications of mass spectrometry to the analysis of less polar synthetic polymers and oligomers has been limited to relatively low molecular-mass samples. Most of the desorption / ionisation techniques have limited success with non-polar polymers, such as poly(styrene) and poly(isoprene). In this aspect field desorption, the original technique in the area, remains the preferred ionisation method. Craig et al[39] have observed ions of masses up to 13 600 Da in the field desorption mass spectrum of poly(styrene). Analysis of very high-mass non-polar synthetic polymers has not been achieved using present mass spectrometric techniques. The newly discovered matrix-assisted ultra-violet laser desorption / ionisation and atmospheric pressure ionisation techniques have considerable potentials in this analytical area, based on the high flexibilities of their experimental conditions.

1.2. MATRIX-ASSISTED LASER DESORPTION / IONISATION (MALDI)

1.2.1. Laser desorption

Attempts to make use of lasers to ablate non-volatile inorganic materials [40,41] in mass spectrometry can be traced back to the mid-1960s. In 1968, Vastola et al[41] demonstrated the first successful desorption of intact molecule-ions from organic compounds using laser desorption. Since then, systematic investigations of generating ions from organic compounds using laser beam have been undertaken,

and extensively reviewed[42,43]. In a typical laser desorption experiment, energy is absorbed by the sample either through direct optical absorption or by heat conduction from the substrate. The sudden input of energy causes a bulk-solid excitation which leads to the phase transition. Several processes may contribute to the expansion of a laser-induced plume into the vacuum system, including thermal vaporization or sublimation[44], vibrational / thermal expansion[45] and coulomb repulsion[46]. During the sample disintegration, a region of high molecular density and high molecular mobility can be formed, which is called the "selvedge region". Within the course of material ablation, different chemical reactions may take place, for example photoionisation, cationisation, proton transfer, fragmentation and rearrangement.

A wide degree of freedom with respect to the experimental parameters such as laser wavelength, laser pulse width, laser focus and photon flux has allowed the creation of "tailor-made" experimental conditions for the analysis of specific materials[24,47]. In spite of the flexibility of the experimental conditions, there seems to be an upper limit to the size of molecules that can be desorbed as intact ions by laser desorption, in the absence of a matrix. This limit for laser desorption in the absence of a matrix is something like 1 000 Da for bio-polymers and 10 000 Da for synthetic polymers.

1.2.2. Evolution and principle of matrix-techniques in mass spectrometry

A matrix technique is one where the sample is added onto or into a suitable medium, known as matrix, during the sample preparation. The matrix-sample composite is then introduced into the mass spectrometer for the subsequent analysis. With the use of an appropriate matrix, labile sample molecules which would otherwise be decomposed, can be desorbed and ionised intact. In the development of nearly all desorption / ionisation techniques, there seems to have been a pattern in which "neat" samples were used initially. The inclusion of either solid or liquid matrices, in a latter stage, has given greater success. With plasma

desorption nitrocellulose has been an efficacious matrix[48]; glycerol has been enormously effective for keV-particle bombardment (fast atom bombardment and SIMS)[17]. The important new technique of atmospheric pressure ionisation requires a dispersive medium (solvent) with appropriate physical properties[28,29,49].

The use of matrix materials to enhance the analyte ion yield in laser desorption has been studied extensively. Early experiments of this kind concentrated on the use of ionisation reagents such as alkali salts[50,51] or metallic substrates[52]. In a systematic study, Hillenkamp et al[53,54] observed a dramatic difference in the yield of the analyte ions depending on the analyte optical absorption coefficient at the wavelength of the laser. In general, absorbing analytes required lower photon fluxes and gave much stronger ion signals corresponding to the intact molecule-ions. The presence of a thin layer of absorbing analyte molecules was sufficient to prevent thermal desorption of the substrate materials. The observation of this exclusive resonant desorption / ionisation gave a clue as to the possibility of channelling the photon energy. Early studies had shown that co-desorption of absorbing and non-absorbing amino acids enhanced desorption of the non-absorbing amino acids[53]. These various observations led to a quite different approach in the search of matrix materials for laser desorption.

The logic of using absorbing materials to enhance the desorption of analyte molecules has subsequently proved extremely useful for the analysis of very large bio-polymers. Hillenkamp et al[26,55] showed that by mixing large molar excesses of nicotinic acid (matrix) with the analytes, intact protein molecule-ions of over one hundred thousand daltons could be desorbed. The first report on matrix-assisted laser desorption / ionisation of large intact proteins was, however, by Tanaka et al[27], employing a rather different experimental approach. Laser desorption was performed on a slurry of ultra-fine metal powder in glycerol, in which proteins and polymer materials were dissolved. The laser energy was said to be absorbed by the ultra-fine metal powder (300Å cobalt powder), which then caused the desorption / ionisation

phenomenon. Nelson et al[56-58] have demonstrated that, using frozen aqueous solutions of analytes, fragments of DNA up to 410 000 Da could be ablated. Matrices such as graphite and crown ethers have also been used[59,60].

1.2.3. General features

The underlying principles of operation for different matrix systems may differ from one another. To date, most of the matrix-assisted laser desorption / ionisation studies have been concerned with the method proposed by Hillenkamp et al in 1988, in which small organic molecules are used as matrices[55,61]. Most of the work presented in this thesis has centred on this particular method. Superficially, at least, the sample preparation method is simple. Typically a few picomoles of the analyte is mixed with 1 000 to 10 000 molar excess of matrix in solution. A few microlitres of the solution mixture is dried onto a metal target before being introduced into the mass spectrometer. The resultant sample deposit can be highly inhomogeneous (see section 4.1). Studies have shown that matrix-to-analyte ratios ranging from a few hundreds to hundreds of thousands can be used[62]. Depending on the matrix material, different amounts of contamination or admixture can be tolerated. Salts, detergent or buffer concentrations in the millimolar range do not significantly reduce the quality of the spectra[63,64].

Matrix-assisted laser desorption / ionisation (MALDI) mass spectra, in general, consist of strong signals, derived presumably from the matrix, in the region $< m/z$ 500 and singly and doubly charged analyte molecule-ion signals. The matrix-ion signals comprise molecule-ions, fragment ions and also higher mass ions presumably formed from photochemical reactions. The relative intensities of the low-mass ions and the analyte molecule-ion signals depend on the experimental conditions and the matrix used. With the correct sample preparation method and at the laser energy set to the threshold for ion production, a near-elimination of the low-mass ion peaks can be achieved using certain matrices such as nicotinic acid[65,66] and

2,5-dihydroxybenzoic acid[67,68]. This will be discussed in detail at section 4.2. The relative intensities of molecule-ion signals of different charge-states depend on the nature of the matrix and analyte molecules. Generally, the intensities of the multiply-charged molecule-ions increase with the mass of the analyte molecule. Oligomeric ions usually appear at relatively high loadings (> 10 pmol) of the analyte molecules.

In the proximity of the molecule-ion peak, satellite-ion peaks of low intensities formed by adduction of the intact or fragments of the matrix molecules have been observed[62]. The degree of chemical adduction has been found to increase with the size of the analyte molecule. A positive correlation[69,70] has been found between the analyte molecule-ion peak-width and the size of the analyte molecule, in cases where the adduct ions are not resolved from the molecule-ions. No cleavage of the covalent bond in the backbone of analyte molecules has been observed to result from the desorption process, although losses of small functional groups such as -COOH and $-NH_2$ have been observed[71]. For large proteins, dissociation of non-covalent interactions between subunits has been reported when using matrices with hydroxy functional group(s)[72]. The collapse of the tertiary structure of the analyte molecules has been attributed to sample denaturation during the sample-preparation stage, rather than to the actual desorption process.

The signal-to-noise ratios of mass spectra generated from the matrix-assisted laser desorption / ionisation technique have been found to be excellent, as compared to other desorption / ionisation techniques such as FAB and PDMS. The sensitivity of the MALDI technique is extremely high. Sample loadings of lysozyme (RMM 14 314) as low as 50 femtomoles has given rise to clear and unambiguous molecule-ion signals[73] It has been estimated that only 10^{-17} mole of sample is actually used up by a single laser shot[67].

1.2.4. Matrices and experimental parameters

Although the idea of using absorbing molecules to enhance the generation of intact molecule-ions for the non-absorbing molecules had been put forward in 1985[53], it took almost two years before the discovery of nicotinic acid as a matrix which gave excellent enhancement of the efficiency of desorption / ionisation for proteins. The essential physical and chemical properties of an ideal matrix remain obscure. Among hundreds of organic molecules, which have the required strong molar extinction coefficients, only about twenty have been found to be effective as matrices for laser desorption. Very little is known about the limiting factors, apart from the prerequisite criterion of a high molar absorption coefficient[74] (ε_m = 30 000 to 160 000 mol cm^{-1}) at the laser wavelength. Nearly all of the working matrices were discovered through screening of various organic molecules. It has been found that even closely related compounds can have very different properties as matrices. For instance, 2-pyridinecarboxylic acid is a very poor matrix, whereas 3-pyridinecarboxylic acid is an excellent matrix[74]. Presence of specific functional groups, such as an aromatic ring or a carboxylic acid, is not essential[62].

It is not certain whether the photochemistry of the matrix materials constitutes a critical factor. Nearly all matrix molecules decompose to a certain extent at the threshold laser energy of ion production through the loss of either hydroxyl functional groups[75] or carboxylic acid functional groups[76]. The excellent desorption characteristics of cinnamic acid derivatives[69] also implies that low sublimation temperature or vaporisation temperature is not essential, because these compounds are fairly involatile under high vacuum.

It has been suggested[61] that the matrix molecules must isolate individual analyte molecule from each other and hence limit analyte aggregation. This proposal has been the subject of discussion[67,77]. The controversy is mainly associated with the fact that experimental methods are not available to measure the matrix-analyte

interactions, especially in the solid state. This subject will be discussed in the connection with results from Raman microscopy and scanning electron microscopy of the solid samples (section 4.1).

In spite of the fact that the matrix must absorb strongly at the laser wavelength, there seems to be no restriction on the selection of the laser wavelength. Various wavelengths in the ultra-violet region including the third- (355 nm)[78] and fourth (266 nm)[26] harmonics of the Nd-YAG laser, the nitrogen laser (337 nm)[63,78] and XeCl excimer laser (308 nm)[80] have been used. Overberg et al have reported[81,82] that specific infra-red photons, such as 2.94 / 2.97 μm and 10.6 μm (strongly absorbed by stretching and bending modes respectively of the -NH and -OH functional groups), together with a proper selection of matrix material, can also lead to the desorption / ionization of massive molecules. The spectral characteristics of IR-MALDI seem to be very similar to those of UV-MALDI[82].

The ability to control the laser beam intensity[62,65] is as important as the selection of the matrix. The analyte molecule-ion intensity depends on the laser energy in a highly non-linear function. There is typically a sharp onset of the analyte molecule-ion signal, followed by a gradual decline of signal intensity as the laser energy is raised above the threshold of ion production. A complete quenching of analyte molecule-ion signals can result from a less than 10-fold increase in the laser energy from the threshold value.

The absolute magnitudes of threshold laser energies for triggering analyte-ion generation have strong implications for the understanding of the desorption / ionisation process. There have been several studies[80,83] concerning the measurement of threshold laser energies. Laser irradiance[55] (or power density) in W cm^{-2} has been used extensively to describe the energy deposited onto the sample. Precise measurement of the experimental factors such as laser-beam temporal and spatial profiles, pulse duration and total energy are essential to

determine accurately the laser irradiance. Most of these parameters are, however, difficult to measure. Even with the most careful design of the experiment, the large variations associated with the experimental conditions, such as laser wavelength, laser pulse-width, ion transmission of the mass spectrometer and detector sensitivity, hinder attempts to verify results through inter-laboratory comparisons. Sundqvist et al[83] have compared the performance of femtosecond lasers with the commonly used nanosecond lasers. It was demonstrated that for a pulse duration in the region of nanoseconds or less, there is no direct influence of the laser pulse-duration on the threshold laser energy for the ion generation process. This implies that "laser irradiance" may not be a good measure of the energy implantation for the triggering of desorption / ionisation. Laser fluence (J cm^{-2}) should, it has been proposed, be used instead of laser irradiance in discussing MALDI[84].

1.2.5. Ion formation

The desorption and ionisation of intact involatile and thermally labile molecules require a method of rapid energy implantation into the material, which presumably needs to be fast enough to avoid thermal degradation. The laser-induced disintegration of the molecular lattice has been described as a non-equilibrium and collective disruption[61,80] process, which transforms the molecules from their solid / liquid forms into a microvolume of gaseous ions. Similar to other desorption / ionisation methods, the sudden input of energy into the condensed-phase induces the formation of both gas-phase ionic and neutral species. Addition of low concentrations of essentially non-absorbing macromolecules should not alter the gross phenomenological event. The challenge in MALDI lies in the discovery of the process(es) responsible for the preferential transfer of translational energy (rather than internal energy) to the macromolecules, and in understanding the factors governing the ionisation of macromolecules.

1.2.5.1. Desorption

In a typical MALDI experiment, the spatial distribution of the excitation process is roughly 10^{-1} to 10^{-2} mm^2 and the time scale for energy deposition is of the order of nanoseconds. With the laser intensity in the threshold region, a linear photon absorption can be assumed. Therefore, the energy deposited per unit volume follows Beer's Law and depends on the molar absorption coefficient (ε_m) of the material at the frequency of the photon. Consider the reduction of photon intensity that occurs when the beam intensity I passes through the matrix lattice. The loss of photon intensity is proportional to the thickness (dx), the molar volume (V_m) and the intensity of the incident laser beam (I).

$$dI = -I\left(\frac{\varepsilon_m}{V_m}\right)dx \qquad (3)$$

The molar absorption coefficient or extinction coefficient (ε_m) depends on the molecule under study and the wavelength of the laser. Rearranging equation 3, gives

$$d\ln I = -\left(\frac{\varepsilon_m}{V_m}\right)dx \qquad (4)$$

Assuming the molecular density is uniformly distributed throughout the sample, V_m is independent of the depth x.

Integrating equation (4) gives

$$\int_{I_i}^{I_f} d\ln I = -\int_0^{l}\left(\frac{\varepsilon_m}{V_m}\right)dx \qquad (5)$$

$$\log\left(\frac{I_f}{I_i}\right) = -l\left(\frac{\varepsilon_m}{V_m}\right) \qquad (6)$$

where l is the penetration depth of the laser.

Taking a beam modulation factor of 0.01%, ε_m = 40 000 mol^{-1} dm^3 cm^{-1} and V_m = 83.5 mol^{-1} cm^3.[44] The penetration depth of the laser is estimated to be ~85 nm. Therefore, the excitation profile is essentially two-dimensional with energy decreasing exponentially with depth. The net momentum caused by lattice disintegration would essentially be an outward expansion and an inward compression.

The laser-induced sputtering of large molecules from a matrix has been studied theoretically. Vertes and Levine[44,85,86] have suggested a thermal-spike model in which the matrix molecules sublime from the sample surface as a result of local heating. In the proposed model, there is ejection at all values of laser fluence, but an effective threshold occurs when the fluence is increased to a certain value at which the ejection yield rises rapidly with the fluence. The survival of very large molecules is attributed to poor vibrational coupling between the matrix molecules and the large molecules. This poor coupling forms a "bottle-neck" for energy transfer from the hot matrix to internal energies of the large molecules.

Johnson and Sundqvist[87,88] have applied to MALDI the pressure-pulse sputtering model, which was originally used to describe the sputtering events induced by fast-ions such as in plasma desorption. In this model a pressure gradient is set up perpendicular to the surface by the energy deposited. On exceeding a threshold value, this pressure gradient gives the molecules a net expansion velocity perpendicular to the surface. The ejection of the large molecules is the result of an additive momentum transfer from collisions with fast moving matrix molecules. The large molecules are thought to act as momentum integrators. Nevertheless, details of the mechanism for the formation of this pressure gradient are not explicitly assigned. Processes such as coulomb explosion[46], repulsive decays[89], low-energy secondary electron excitation causing soft expansion ("pop-corn")[90] and even matrix-sublimation[44,85] are possible contributors.

Studies of the effect of laser fluence on the intensity of the desorbed species, in particular the neutral macromolecules, and the quantification of the initial translational energies of the desorbed molecules / ions would provide insight into the process of momentum transfer. Methods for studying these properties have been limited by the fact that most of the experimental parameters are difficult to control, if not impossible. For instance, the momentum integration process proposed by the pressure-pulsed model[87] predicts a very different threshold behaviour for molecules of different masses. For small molecules transferring their momentum to a large molecule, the number of collisions required varies as a function of the molecular mass (i.e. $\propto(M^{5/3})$)[90] assuming a constant binding energy. Experimentally, no such dependence has been found[88] for ion yield. This, however, does not contradict the proposed model, as the experiment is for ions and the model's prediction is for total desorption yield (both neutral and ionic species). The signals in mass spectra reflect only the ionic species that are generated in the desorption / ionisation process.

One of the most influential experimental variables has been sample preparation. As has been mentioned, the commonly adopted sample preparation is simple and effective, but the resultant distributions of analyte molecules and matrix molecules are highly inhomogeneous. Given typical fluctuation in the energies of laser pulses, experiments based on monitoring of the signal intensities would suffer from large experimental uncertainties. Many investigators have studied[80,92-94] the initial kinetic energies of the desorbed species, both matrix and analyte particles, using different experimental methods. The results reported to date, however, deviate considerably from one another (see section 5.1 for detailed discussion).

1.2.5.2. Ionisation

The absence of radical molecule-ions in typical MALDI mass spectra implies that there is little or no contribution from the direct photoionisation of the analyte molecules to the molecule-ion signal observed in a typical mass spectrum. This is

consistent with the fact that very low-energy photons such as those with wavelengths at 2.94 μm and 10.6 μm can cause the same phenomenological desorption and ionisation events. At present, the ionisation of analyte molecules is still not well understood. The general consensus is that some sort of chemical ionisation such as proton transfer or cationisation is responsible for the ion formation. It has been shown that the charging pattern (intensity ratios of the singly-charged to the higher charge-state molecule-ions) varies substantially for different matrix-analyte combinations and does not depend on the number of acidic or basic moieties in a macromolecule[70]. The implication is that the charging does not depend on the usual solution-phase acid / base chemistry but rather on the detailed interactions of the matrix with the analyte. It has been suggested that the charging in typical MALDI experiments is not very efficient. This was deduced from the fact that the majority of charged species are singly protonated (for positive-ion mode) and singly deprotonated (for negative-ion mode) ion signals. The observations of near-elimination of matrix-ion signals[65-68] under specific matrix-to-analyte molar ratios (see section 4.2) for certain matrices, however, imply a very efficient charge-transfer process.

The laser desorption / ionisation of small organic molecules, including several commonly used as MALDI matrices, has been studied in detail by Ehring et al[75]. The mechanistic aspects of the ionisation of these organic molecules has been generalised in a model based on the formation of odd-electron molecule-ions, which subsequently undergo a series of chemical reactions until relatively stable molecule- or fragment-ions are formed. The authors have applied this model to explain the predominant formation of protonated or deprotonated molecule-ions in a typical MALDI experiment. Russell et al[95] have also pointed out the possible importance of the enhanced acidity of the matrix molecules upon electronic excitation.

1.2.6. Mass analysers

1.2.6.1 Time-of-flight mass spectrometry

The most common technique used to mass analyse the ions generated by MALDI is time-of-flight mass spectrometry (TOF-MS)[96,97]. The mass-to-charge (m/z) ratios are determined directly through the precise measurement of the ion arrival-time at the detector. In a simple linear time-of-flight instrument, all desorbed ions are accelerated over a short distance from their position of formation to the same energy by means of an electric field. Ions of different mass-to-charge ratios acquire different terminal velocities. Passing the ions through a field-free drift region, the ions will strike the detector in a sequence of decreasing terminal velocities (i.e. increasing mass-to-charge ratios).

$$t = L\sqrt{\frac{m}{2qeV}} \qquad (7)$$

Equation (7) describes the relationship between the mass (m) and the flight time (t). L is the length of the field-free region, q is the number of charges on the ion, e is the electronic charge and V is the accelerating potential.

Theoretically, the TOF mass analyser offers advantages over the conventional magnetic-deflection mass analyser. TOF has an unlimited mass range and very high transmission efficiency, i.e. nearly all ions produced are collected. Tens or hundreds of complete spectra can be recorded within a second. Equation (4) is not used in mass calibration, as the values for L and V in are normally not known with sufficient accuracy. Mass calibration can, however, be achieved using a simple linear equation requiring the flight times of two known mass-to-charge to determine the constant A and B in equation (8).

$$\sqrt{m/z} = At + B \qquad (8)$$

The calibration constants A and B depend on the length of the field-free path (L) and the accelerating potential (V).

The major disadvantage of TOF is the relatively low mass resolving power ($M/\Delta M$). Experimental factors, such as delayed ion formation, initial energy distributions of the ions and space charge coulomb repulsion, tend to spread ions of the same mass-to-charge ratio in both space and time. In a simple linear time-of-flight mass analyser with a 2 meter field-free path, the mass resolution is normally considerably less than 1000, depending on the ion source characteristics.

There have been a number of successful approaches for improving the mass resolution of time-of-flight mass spectrometers. The so-called "reflectron" time-of-flight instrument[98] utilises an electrostatic mirror which reflects the incident ions through an angle larger than 90°. For ions of the same mass-to-charge ratio, those having higher initial energies penetrate further into the electrostatic mirror and hence have a longer "turn-around time". With the correct setting of the electrostatic mirror potential, this additional turn-around time compensates for the time spread caused by the energy distribution. Using this approach, mass resolutions of about 10 000 have been achieved[99]. Considerable success has also been achieved through the use of impulse field focussing[100-101] and post-source pulse focussing[102] techniques.

In spite of the energy compensation obtained via ion-reflection, the first published time-of-flight mass spectra of high mass compounds obtained in MALDI had a mass resolving power ($M/\Delta M$) at full width half maximum (FWHM) of only 50. The mass resolving power in the low mass region, however, reached a value of 300-500. There have been a number of investigations into aspect of ion formation, ion transmission and ion detection, searching for reasons behind the reduction of spectral quality. In ion formation, mass-dependent initial kinetic energy distributions[94] and the pronounced effect of adduct-ion formation[69] have been found to cause substantial reduction of instrumental mass resolving power, especially in

the high-mass region. The discovery of the ion-to-small-ion conversion[103-105] phenomenon at the surface of the conversion dynode, upon the impact of high mass ions, not only explained the cause of low quality spectra but also the mysterious detection of very large molecules (above *m/z* ~ 20 000).

1.2.6.2 Fourier transform ion cyclotron resonance mass spectrometry

Fourier transform ion cyclotron resonance mass spectrometry (FT-ICR-MS)[106,107] is a technique that determines the ionic mass-to-charge ratio through the measurement of the ion cyclotron orbital frequency (ν_c) given by equation (9).

$$\upsilon_c = \frac{qeB_o}{2\pi m} \qquad (9)$$

B_o is the strength of an applied static magnetic field, q is the number of charges on the ion, e is the unit electronic charge and m is the mass of the ion. In theory, FT-ICR should be compatible with the MALDI method and would provide significantly higher mass resolution than TOF, as the ion frequency can be measured more accurately than the ion flight time. In practice, a number of factors such as initial ion kinetic energies and ion lifetimes have limited the utilisation of FT-ICR spectrometry. Recently, Wood et al[108] have estimated the theoretical ion trapping ability of FT-ICR traps of different configurations using the most probable ion ejection velocity in MALDI (760 ms^{-1})[94]. The upper mass limits for different trap configurations have been calculated to be less than *m/z* 14 000. In contrast to this calculation, Castro et al[109] have demonstrated that biopolymers with *m/z* as high as 34 000 can be observed using FT-ICR with a cubic ion trap. The mass resolving power has been found to decrease drastically in the high-mass region.

1.2.6.3. Magnetic mass analysers

Magnetic deflection mass spectrometry has long been excluded from use with ionisation techniques such as plasma desorption and laser desorption as the ions generated by these methods are in the form of discrete packets. Recently, Biemann and his colleagues[71,110] have accommodated the pulsed nature of the ions generated in MALDI in a high-mass double-focussing mass spectrometer through the use of an integrating array detector. The use of a double-focussing mass spectrometer eliminates the problems of initial energy spreads and also the peak broadening caused by the difference in flight times between secondary electrons and ions ejected from the dynode surface. Mass resolving powers of 1000 to 4500 have been achieved with ions of mass-to-charge ratios less than 15 000.

1.2.7. Accessible materials and their mass ranges

Matrix-assisted laser desorption / ionisation has been used extensively in the analysis of proteins[62,111]. Peptides and proteins with masses ranging from thousands to several hundred of thousand daltons have been successfully analysed. Both positive- and negative-ion modes[62] have been used. In positive-ion mode, protonated and cationised ions are commonly observed. In negative-ion mode, deprotonated ions are predominant. The largest functional enzyme detected has been catalase[30] of mass 236 230 daltons and the highest mass molecule desorbed has been the octamer of bovine serum albumin[31] (see section 4.3). MALDI seems to be insensitive to the hydrophilicity or the hydrophobicity of the protein[112,113], which is in contrast to fast atom bombardment[114] and plasma desorption[115]. Certain matrices such as sinapinic acid and 2,5-dihydroxybenzoic acid can selectively ionise protein molecules in the presence of high concentrations of ionic contaminants such as inorganic salts[64,67]. These matrices are also relatively non-selective in their ion generation behaviour towards proteins of different primary structure and to modifications such as phosphorylation and glycosylation[113,116].

Pure and underivatised carbohydrates[117-118] have also been analysed by the matrix-assisted laser desorption / ionisation technique. Dextrans (α-1,6-linked oligoglucan) of masses up to 10 000 daltons have been reported[118]. All ions of pure carbohydrates have resulted from cationisation rather than protonation. No negative-ion mass spectrum has yet been reported for oligosaccharides. Native and permethylated glycophingolipids were successfully analysed[119-120] in the mass range up to several thousand daltons. Typical molecule-ions were cationised and deprotonated species in the positive-ion and negative-ion modes respectively.

Oligonucleotides (both single-stranded and double-stranded) and ribonucleic acid have been analysed. Oligonucleotides up to 34-mers ($pd(T)_{34}$), i.e. relative molecular mass >10 000, have been detected[121]. Huth-Fehre et al[122] have investigated several matrix materials for the analysis of oligonucleotides using a nitrogen laser (λ=337 nm). With oligodeoxythymidylic acids as the analyte, 2,5-dihydrobenzoic acid has been found to give the best performance in terms of the extent of fragmentation and adduct-ion formation. Tang et al[121] have studied the effect of the laser wavelength on the degree of fragmentation of the desorbed oligonucleotides. Visible wavelength photons (532 nm) used in conjunction with Rhodamine-B as matrix have been found to produce less fragment-ions than shorter wavelengths (i.e. 266 nm or 355 nm). Parr et al[123] have also studied the effect of the physical and chemical nature of the analyte, using synthetic oligodeoxyribonucleotides, on the efficiency of this desorption / ionisation technique. Base composition has been found to be critical. Polynucleotides with molecular masses up to 38 000 daltons have also been reported[124]. Most of the studies have been performed under negative-ion mode. Deprotonated and matrix-adduct molecule-ions are predominant. Sodium ion substituted deprotonated ions are commonly observed when in positive-ion mode.

Analysis of synthetic polymers using matrix-assisted laser desorption / ionisation has been limited to relatively polar molecules. Water soluble polymers[125]

such as polyglycols, poly(acrylic acid) and poly(styrene sulfonic acid) have been reported. The measured molecular mass distribution and the polydispersity were in good agreement with the manufacturer's figures[125].

1.2.8. Applications

The molecular mass determination of an analyte is the primary information obtained from matrix-assisted laser desorption / ionisation mass spectra. Precise measurement of the molecular mass information[126] allows qualitative control of protein synthesis and identification of by-products[127]

The inherent properties of the MALDI technique provide gentle desorption / ionisation conditions, such that even the weak disulfide bond within a protein molecule is not cleaved under typical experimental conditions[128]. The lack of fragmentation of the analyte molecule-ions implies that the spectra obtained are very simple and easy to interpret. It is therefore well suited for mixture analysis[64,128] Nevertheless, the response of various proteins in a mixture upon laser desorption has been found to vary from matrix to matrix. Nicotinic acid, originally described by Karas et al[55], produces non-uniform responses from mixtures of proteins[64]. This leads to spectra being dominated by certain species present. Cinnamic acid derivatives, particularly sinapinic acid, have been found relatively non-selective to proteins[64], even if they have quite differ physio-chemical properties.

For other desorption / ionisation methods such as fast atom bombardment and atmospheric pressure ionisation, the analyte molecule-ion signals are very sensitive to the presence of non-protein materials particularly ionic salts[129]. The ability to tolerate a high concentration of ionic contaminants in matrix-assisted laser desorption / ionisation has led to the first application of mass spectrometry to protein analysis of crude biological extracts[64,128], such as unpurified milk and saliva.

Some biochemical techniques have been used in conjunction with the matrix-assisted laser desorption technique to increase structural information. A number of reports have been published on the use of enzymatic or chemical treatment of proteins and subsequent analysis of the reaction products. Mock et al[130] have located the position of disulfide bonds within a protein by using dithiothreital reduction reaction prior to the laser desorption studies. The carbohydrate content of glycoproteins has also been estimated[112] by comparison of the molecular mass information generated from the glycoprotein sample before and after enzymatic treatment. With the use of chemical reagents such as cyanobromide[64,130] and carboxypeptidases[127] prior to MALDI analysis, amino acid sequence information has been retrieved from the signals of the digest products. All these biochemical reactions may be processed either in a reaction vial or directly on the target. Analysis of the products can usually be performed directly out of the reaction mixture without time-consuming purification procedures.

Recently, Spengler et al[131] have demonstrated the possibility of using post-source decay of polypeptides to yield structural information. The laser-desorbed molecule-ions have been found to undergo metastable decay. The tendency towards decomposition can be enhanced by increasing the background pressure in the spectrometer, by the use of higher energy photons (e.g. 266 nm instead of 355 nm) and also by a careful selection of matrix materials.

Matrix-assisted laser desorption / ionisation has also been applied to the study of peptide-metal ion interactions[132,133]. With the use of glutaraldehyde, a cross-linking agent which traps the protein multimeric form and prevents it from dissociating during the sample preparation process, the tertiary structure of a protein in solution has been preserved and mass analysed[134].

1.3. OUTLINE OF THE PRESENT WORK

It has been pointed out (section 1.1) that only a limited number of desorption / ionisation techniques are directly applicable to synthetic polymers due to their intrinsic properties such as low polarity and high thermal sensitivity. The initial phase of the present work has been concerned with the use of field desorption (FD) to study medium-size polymer standards and an industrial polyester sample. These results are presented in chapter three. The "art" of high-temperature activation of field desorption emitters has also been studied. This has led to the establishment of empirical equations and subsequently to the automation of the growth process under computer control.

The main concern of the present work is to investigate the possible use of matrix-assisted ultra-violet laser desorption / ionisation to volatilise very large synthetic polymers (RMM of 10 000 to 100 000) for mass spectrometric studies. The potentials of this technique for synthetic polymer analysis have not been fully explored. It soon became clear that direct application of the established technique to the synthetic polymers would not give useful information. Therefore, a high proportion of the present work has been devoted to the exploration of the fundamental aspects of the desorption / ionisation process. It is believed that a better understanding of the ion formation process is essential for extending its capability to the analysis of the synthetic polymers mentioned.

In chapter two, the design and construction of the time-of-flight mass analyser within the first field-free region of a large-scale double-focussing mass spectrometer are described. Brief discussions of the laser system and the associated electronics will also be presented. Experimental aspects of the matrix-assisted laser desorption / ionisation technique examined in the present studies will be presented in chapter four. These include the effect of sample preparation methods on the sample homogeneity, the matrix-ion suppression effect in low matrix-to-analyte

molar ratios and the high degree of molecule-ion clustering in liquid matrices. Chapters five and six concentrate on examining the desorption and ionisation process in the MALDI technique. The energy content of the laser-desorbed ions has been studied, which includes the measurement of the most probable initial ion kinetic energy and also the discovery of an energy-deficit effect. Low molecular-mass peptides of different chemical properties have been used to evaluate the effect of solution pH and gas-phase proton affinity on the ionisation efficiency under typical MALDI conditions.

Finally, the possibility of applying the MALDI method to generate characteristic ions from large synthetic polymers is addressed in chapter seven. This is discussed in light of the current understanding of the desorption and ionisation processes involved. Some results concerning the analysis of small to medium size synthetic polymers are also presented.

PAGINATION ERROR

Pg 26.

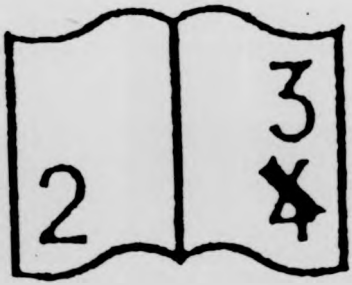

Figure 2.1
Photograph of the large-scale double-focusing mass spectrometer.

Figure 2.2
Schematic diagram of the double-focussing mass spectrometer.

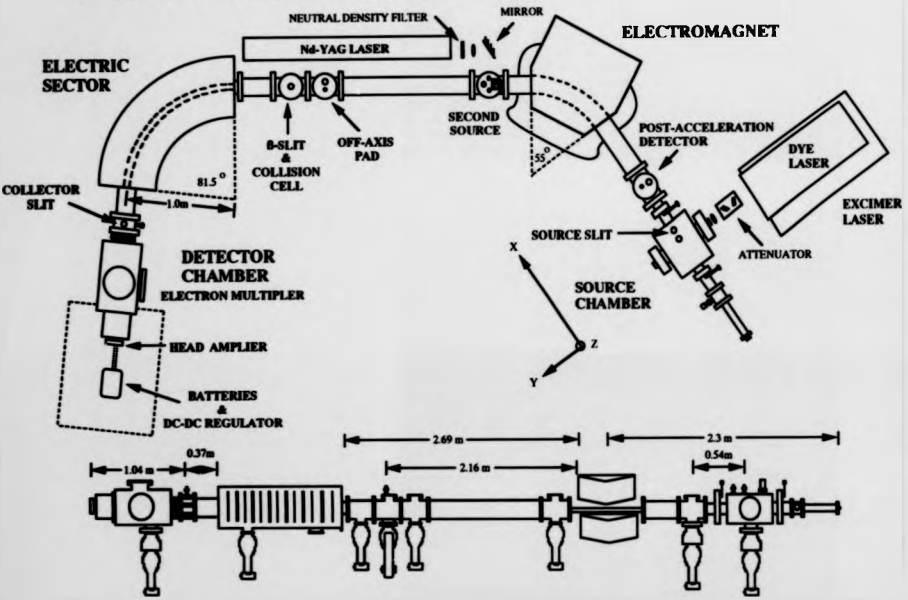

In the final sections of this chapter, the experimental methods relating to field desorption (FD) and matrix-assisted laser desorption / ionisation (MALDI) will be described.

INSTRUMENTATION

2.1. THE DOUBLE-FOCUSSING MASS SPECTROMETER

The mass spectrometer shown in Figure 2.1 has so-called reverse geometry, i.e. ions pass through the magnetic sector before the electric sector. Basically, the instrument consists of an ion source, a magnetic sector, a collision cell, an electric sector and finally a detection system. The ion source, which coincides with that of one of the time-of-flight analysers, will be described in section 2.2.2. The lens assembly used in field desorption studies was designed by Sheil[137] for use at very high acceleration potentials (up to 30 000 V).

The magnetic sector has an included angle of 55° and a theoretical radius of 78.4 cm. This electromagnet is capable of producing a 1.5 tesla magnetic field. The basic equation relating mass-to-charge ratio to other experimental parameters using a magnetic sector is given by:

$$\frac{m}{z} = \frac{B_o^2 r^2 z}{2V} \qquad (2.1)$$

B_o is the magnetic field strength in tesla, r is the radius of curvature of the ion trajectory in metres and V is the acceleration potential in volts. From equation 2.1, the upper mass limit for this instrument is ~4 200 Da when an acceleration potential of 15 000 V is used. The current for the magnet was delivered by a current-regulated power supply[138] which had a stability of ±8 mA at 80 A over 8 hours[139]. This power supply was driven by a sweep generator which could be operated in both manual or scanning mode. The magnetic field was monitored using a magneto-resistor[140]. The

output of this resistor was calibrated to provide an approximate readout of mass (± 3 Da). Accurate mass measurement would require further calibration.

The electric sector consisted of a pair of curved parallel aluminium plates of height 149.5 mm, separated by 33.5 mm. The radius of the ion path through the electric sector was 1000 mm and the sector had an included angle of 81.508°. Herzog shunts[141] were used to shape the field at the entrance and the exit of the sector; Matsuda plates[142] were used to improve the field homogeneity in the z-direction. A control signal generated from the computer through a 16 bit digital-to-analogue converter (DAC) was fed into a high-voltage differential amplifier. This produced two equal voltages of opposite polarities with a maximum value of ± 1500 V connected to the sector plates. The raw supplies to the amplifier were delivered by two 3 kV power supplies[143].

Located just in front of the focal point between the magnet and the electric sector (the β-focus) was a collision cell which was supported on the underside of a T-piece flange. The collision cell consisted of 2 cylindrical stainless steel plates of 64 mm diameter which formed the ends of a 10 mm long cavity machined from polyethylene. Slits of height 10 mm and width 2 mm were machined in these plate to restrict the out-flow of collision gas and to allow adequate transmission of the ion beam. An inert gas was allowed to leak into the collision cell from the gas-inlet via a precision leak valve[144] mounted in the supply line. The variable slit (β-slit) located at the rear side of the collision cell could be used to adjust the ion transmission.

The final image of the ion beam was adjusted by a variable collector slit located at the third focal point of the instrument. A large electrostatic lens stack focussed and accelerated the divergent beam emerging from the collector slit onto the first dynode of a 20-stage electron multiplier[145]. Two deep-cycle lead acid accumulators supplied power for the electron multiplier (-3 kV) and also for the ion counting electronics. The electronics consisted of an amplifier / discriminator and

associated logic to drive a fibre optic link. The electronics and power supplies were located within a Faraday cage mounted on the top of a large ceramic insulator. The electron multiplier, electronics and power supplies were floated at negative 30 kV in normal operation with positive ions. This so-called post-acceleration potential was derived from a 100 kV power supply[146a].

Ion counting was employed in the present detection system. The signal from the electron multiplier was amplified and then passed through a discriminator set at a pre-selected threshold level. Signals below this level were rejected to reduce background noise. Logic signals generated by the discriminator were then transferred across the high potential barrier via an optical fibre to the computer. The computer system and associated peripheral devices have been described in detail by Sheil[137].

2.2. The Laser-based time-of-flight analyser

An expanded view of the instrumental arrangement is displayed in Figure 2.3. An excimer-pumped dye laser system was situated on an optical bench perpendicular to the ion-optical axis of the time-of-flight instrument. A quartz-wedge laser-beam attenuator and an ultra-violet grade fused-silica plano-convex focussing lens were placed within the optical beam path. The source region of the time-of-flight instrument coincided with that of the double-focussing mass spectrometer. A detector was located in the first field-free region T-piece. The drift region of the time-of-flight instrument was approximately 600 mm.

2.2.1. The laser system

Pulses of photons were generated by an excimer-dye laser system. The excimer-laser used was a Lambda Physik LPX 110i[147a]. The particular excimer system employed was that of xenon-chloride which generated an ultra-violet beam at 308 nm. Table 2.1 shows the particular gas mixture used.

Figure 2.3
Photograph of the laser-based time-of-flight analyser.

Table 2.1.
Gases used in the excimer-system for producing 308 nm laser line.

Gas type	Gas	Quantity / mbar	Purity
Halogen	Hydrogen chloride	100	5% HCl / 1% H_2 / 94% He
Rare gas	Xenon	80	99.99% Xe
Buffer gas	Neon	3020	99.995% Ne
Inert gas	Helium	-	99.99% He

Total gas pressure : 3200 mbar

The inert gas (He) was used to flush the gas chamber in cases of contamination or when changing the excimer gas mixtures. A typical laser pulse had a full-width half-maximum (FWHM) of 17 ns and an energy of 150 mJ. The maximum repetition rate was 100 Hz. The output beam was steered into the dye laser using two 50 mm diameter dielectric mirrors[148a] (308 nm, 45°) which were located on an upper and a lower steering device[148b]. The upper steering device allowed independent elevation and coarse/fine azimuthal adjustment, whereas the lower steering device was only adjustable in azimuth. They were mounted onto a rack and pinion rod[148c] which allowed easy height adjustment.

The dye-laser was a high performance Lambda Physik FL3002[147b]. It consisted of an oscillator amplifier for wavelength control and pre-amplification, and an amplifier stage for power and beam quality enhancement. The oscillator consisted of a grating for narrowing the bandwidth, a dye flow-cell containing the active medium and a resonant end-mirror.

The most commonly adopted method of narrowing the bandwidth of the dye laser output makes use of the "Littrow arrangement"[149] which is shown schematically in Figure 2.4a. In this arrangement, a moderate grating angle θ of typically less than 75° can be used. The grating reflects radiation of wavelength λ only in the direction satisfying the Bragg condition:

Figure 2.4
Schematic diagrams of Littrow-type dye-laser oscillators.

2.4a : Without Lambdapure-filter

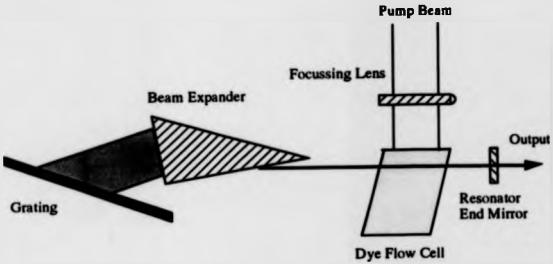

2.4b : With Lambdapure-filter

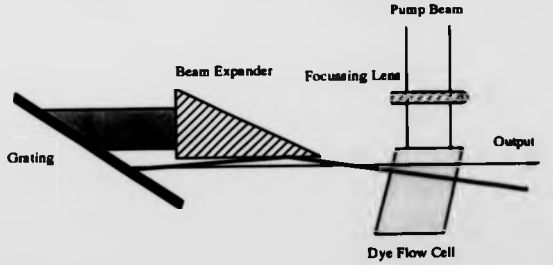

$$2d\sin|\theta| = m\lambda \qquad (2.2)$$

where m is an integer (1,2,..) and d is the spacing between lines of the grating. Wavelengths not satisfying the equation 2.2 will not be reflected back along the cavity axis and consequently have larger losses. Tuning the wavelength is accomplished by tilting the grating. Therefore only the selected wavelength will oscillate and subsequently be amplified. One of the limitations of this arrangement is that the oscillator output carries some background emission, known as amplified spontaneous emission (ASE), which originates from the oscillator itself. Consider the spontaneously emitted photons at one end of the dye flow-cell which happen to be directed along the amplifier axis or close to that direction, they will stimulate the emission of more photons leading to substantial build-up of radiation at the other end of the cell. In a conventional "Littrow arrangement", the ASE leaves the oscillator through the resonant end-mirror without being suppressed or filtered out. One of the consequences is that it may significantly deplete the upper-level population of the latter amplifier stages and thus diminish the gain available to the input signal to be amplified. The continuous build-up of this ASE, at the latter stage of the dye laser, could cause unwanted interference with the experimental conditions.

The dye laser used in this work has employed a modified "Littrow arrangement" which provides an additional automatic filtering process ("Lambdapure-filter")[147c] which is illustrated schematically in Figure 2.4b. The resonant end mirror is tilted and located slightly lower than the output beam. In this geometry, the output beam undergoes a reflection from the surface of the beam expander prism at which undesirable ASE is partially coupled out. An additional reflection from the grating before leaving the oscillator leads to a substantial reduction of ASE. Another advantage of using this configuration is that the oscillator dye-cell can also serve as a pre-amplifier by being pumped in a different region.

A beam-expanding telescope was located between the oscillator / pre-amplifier and amplifier, which matched the dye laser beam to the larger active volume in the amplifier. For the work described in this thesis, coumarin 307[150] dissolved in methanol was used as the dye solution. It has a selectable wavelength range of approximately 479 nm to 553 nm and a peak conversion efficiency of 16.3%. The concentration of the dye solutions were prepared as recommended[151], i.e. 3.4 g l^{-1} for oscillator/pre-amplifier dye-flow cell and 1.7 g l^{-1} for amplifier dye flow-cell. The output line was tuned to 532.0 nm. It was then frequency doubled into the ultra-violet region (266.0 nm) by a β-barium borate (BBO-II) second-harmonic generator crystal. The fundamental frequency was separated from the second harmonic by means a Pellin-Broca-prism separator. This consists of four Pellin-Broca prisms in which the first two are used to disperse the incoming beam according to the frequency components, and the second two recombine them into a single beam. Frequency separation is achieved by masking off the fundamental component at a position at which it is separated from the second harmonic. The output beam diameter was defined by an iris lens placed inside the dye-laser chamber. The resultant pulse energy was typically 250 to 300 μJ. A 25 mm diameter UV-grade fused silica plano-convex lens (f = 500 mm) was used to focus the output beam into the vacuum chamber through a UV-grade quartz window where it was reflected by an aluminium-coated UV-grade mirror onto the sample surface at an angle of 45°. The focussing lens was mounted onto a five-axis lens positioner[149c], which provided smooth XYZ translation plus true gimballing about two orthogonal, coplanar axes. The resulting laser spot had dimensions roughly equal to 45 μm x 125 μm. A quartz-wedge variable attenuator[148c] was used to produce an experimental fluence over a range of 0.01 J cm^{-2} to 2.0 J cm^{-2}.

2.2.2. The ion source

The sample stage was a stainless steel probe tip of 2 mm diameter mounted onto a retractable probe, which could be wound in and out of the source using a rack

and pinion assembly. The retractable probe consisted of a stainless steel cylinder fitted with a vespel rod 25.3 mm in diameter and 151.4 mm in length. This vespel rod provided insulation for the high voltage applied to the sample stage. An O-ring sealed gate valve separated the probe air-lock and the source housing to enable the former to be pre-pumped. An Edwards rotary pump[152a] was used to pump the probe air lock from atmospheric pressure down to ~0.1 torr. The pressure was monitored in the backing-line using an Edwards Pirani gauge head and Pirani-11 controller[152b]. The gauge was located in the source backing-line as the same rotary pump was also used to back the source diffusion pump[152c]. The pressure in the source housing was monitored by a Edwards ionisation gauge head and an Ion-7 controller[152d]. Another O-ring sealed gate valve separated the source chamber from the remaining vacuum system. This was essential to maintain the latter at high vacuum, when the pressure in the source chamber rose after insertion of the probe or when the source chamber was opened to atmosphere to work on the lens system.

The laser beam entered the source chamber through one of the 25 mm diameter UV-grade fused silica quartz windows located on either side of the source chamber. Electrical feedthroughs into the vacuum chamber were of the glass head type mounted in PTFE holders to increase their high voltage capabilities. The high voltages applied to the ion extraction lens were derived from Spellman HRSR series high voltage power supplies[146b]. Potential applied to the sample stage was measured precisely by an active potential divider unit coupled to one eight-digit digital voltage multimeter. Precise potential differences between two high potential supply lines, as were required in retardation experiments (see section 5.1.2.), were generated using a differential potential unit. The ion extraction lens assembly was mounted directly on the end flange of the source housing.

An electrostatic lens assembly was designed and constructed to extract and focus ions leaving the sample surface. This is illustrated schematically in Figure 2.5. This particular lens assembly was designed for laser desorption studies and

Figure 2.5
Schematic diagram of the electrostatic lens assembly (side view).

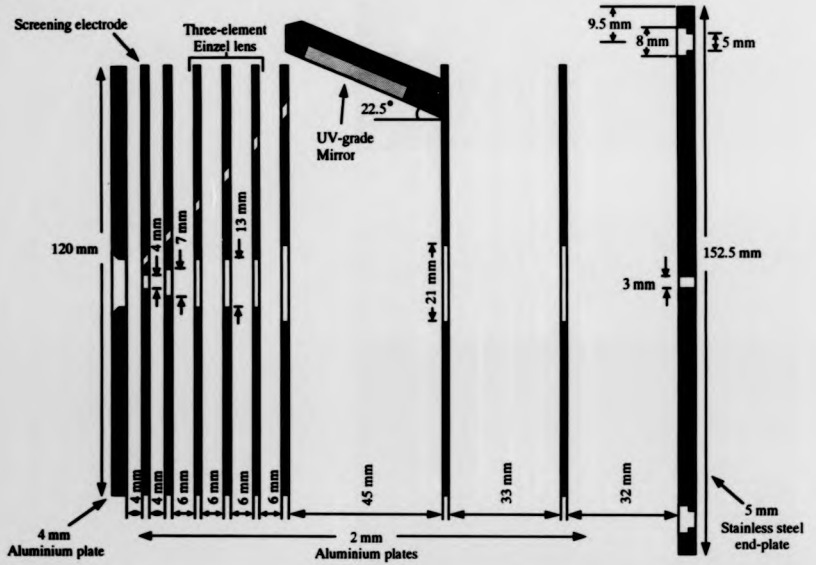

incorporated a number of features to enable the extraction and focussing of desorbed ions with large angular and energy dispersion. It comprised a screened immersion lens and a three-element Einzel lens. The design was based on 2-dimensional ion optical trajectory simulations. The simulation programs were developed by Davis[153] at the University of New South Wales and were modified to be run on the computer system presently in Warwick University. A screened immersion lens of circular aperture was used to extract the desorbed ions and also to provide the first stage ion focussing. The efficiency of such an electrode arrangement has been studied as a function of the potential of the screening electrode. Results are shown in Figure 2.6. Different geometries of the Einzel lens have been studied. Choice of a particular geometry was based on the quality of the final ion image. An Einzel lens with circular aperture was used. Some of the simulation results are presented in Figure 2.7.

The plates in the lens assembly were constructed of aluminium alloy and highly polished. Supporting rods and plate spacers were made of polyethylene ketone (PEEK). The rods acted as dowels to ensure correct alignment of the plates. Eight supporting rods were used to enable high-potential plates to be mounted on a separate set of four rods from those for the low-potential plates. The first plate of the lens assembly was specially shaped to accommodate the sample stage. This arrangement served to define precisely the region of ion acceleration and to give an accurate alignment of the sample probe with respect to the ion-optical axis. A small UV-grade aluminium coated mirror was fitted onto the lens assembly to reflect the incident laser beam onto the sample surface at an angle of 45°.

The actual lens assembly used in most of the present work is depicted in Figure 2.8 The screen electrode plate between the sample stage and the counter electrode was replaced by 2 mm spacers because of the poor machining. The aperture at the exit was enlarged from 2 mm to 5 mm to compensate for the reduction

Figure 2.6
Ion trajectory simulations of the screened immersion lens at different screening electrode potentials (sample-stage potential = 10 kV).

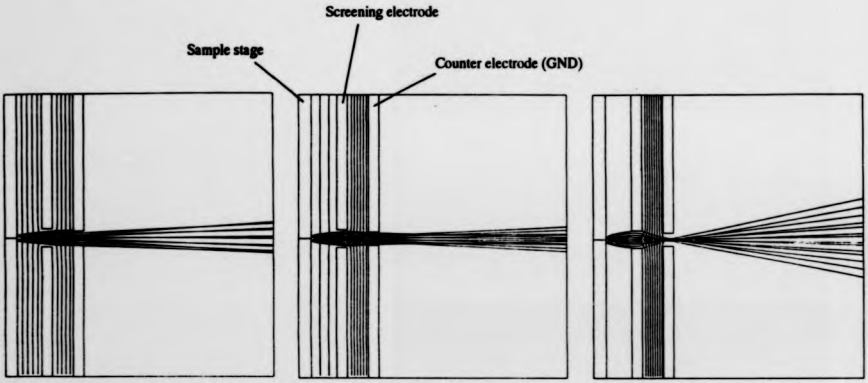

a) Screening electrode potential = 5 kV

b) Screening electrode potential = 7 kV

c) Screening electrode potential = 9 kV

Figure 2.7
Ion trajectory simulations of the electrostatic lens .

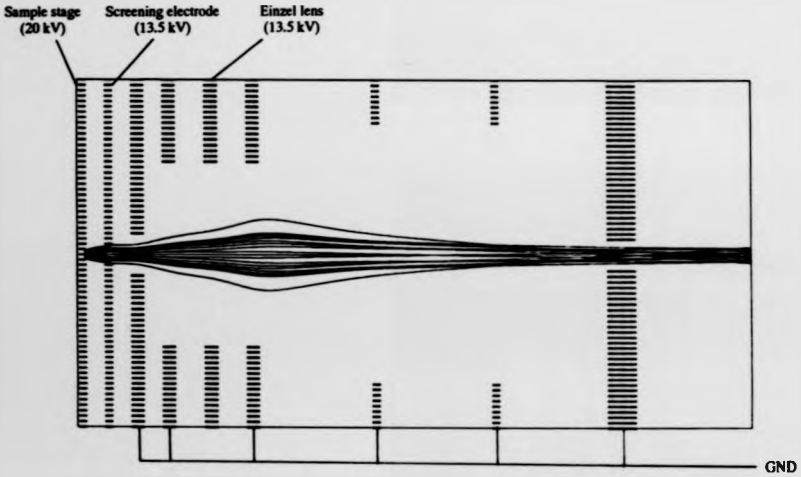

Figure 2.8
Photograph of the lens stack used in MALDI experiments.

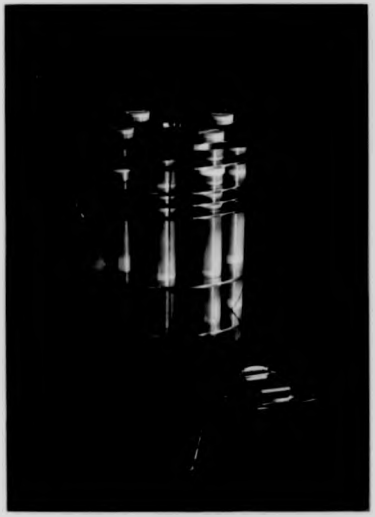

in focussing power. In practise, the desorbed ions have been found to exhibit high axial velocities[94]. Little or no change in the signal intensities was observed when the Einzel lens potential was switched off. This was possibly a consequence of the fact that the detector (described in section 2.2.3.) had a very large acceptance angle.

2.2.3. The detector system

An off-axis detector equipped with a conversion dynode was designed specifically for the present work. It is depicted in Figure 2.9 and is illustrated schematically in Figure 2.10. The conversion dynode used in this work was made of beryllium-copper alloy (Be-Cu) and was normally floated at -25 kV for detection of positive incident ions. The active component of the detector was a 20-stage electron multiplier[145]. The front plate of the electron multiplier was set at -2.5 kV. Both the conversion dynode and the multiplier were located inside two sections of a grounded stainless steel case to confine the electric fields. The whole detector assembly was mounted on the underside of the top flange of the first field-free region T-piece through four 6 mm stainless steel rods.

The incorporation of post-acceleration in the detector design was based on the fact that secondary electron emission from an electron multiplier cathode has been found to depend on the velocities of the impacting ions[154]. It has been observed that the secondary electron emission becomes a very inefficient process when the incident ion velocities fall below 10^4 m s^{-1}. The threshold velocities for electron emission were found to be ~10^3 m s^{-1} depending on the type of incident ions. Post-acceleration of the incident ions after the drift region was necessary to increase the impacting velocities of larger ions. A conversion dynode was incorporated because of the undesirability of floating an electron multipler and difficulty of coupling the analogue signals across the high-voltage barrier. The output signal of the electron multiplier was first pre-amplified by a (x10) 50 ohm high speed amplifier of in-house design and then fed to the transient digitiser through a 50 ohm input terminator. The

Figure 2.9
Photograph of the off-axis post-acceleration detector.

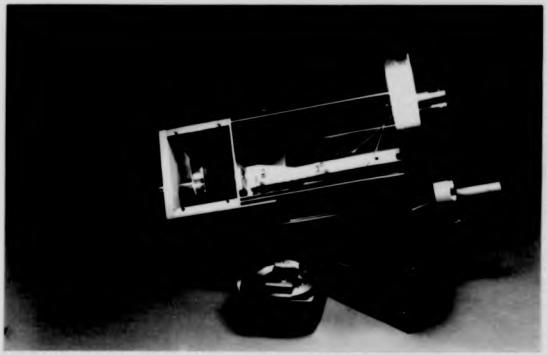

Figure 2.10
Schematic diagram of the off-axis post-acceleration detector.

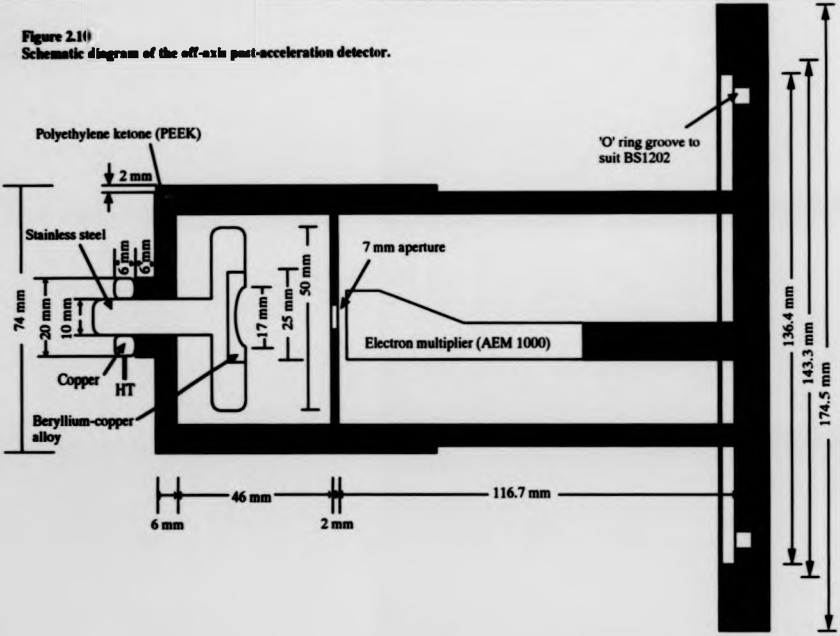

use of a conversion dynode allows the high negative potential, which is necessary for post-acceleration of the incident ions, to be kept separate from the electron multiplier. Beryllium-copper alloy used in the conversion dynode is known to have a low electron emission work-function. The dynode surface was specially shaped to improve the collection efficiency for incident ions and also focus the secondary electrons onto the electron multiplier. Figure 2.11 shows some of the simulation results.

The use of a geometry in which the particle detector is perpendicular to the ion-optical axis was essential in order to allow the interchanging of time-of-flight experiments with sector-scanning type experiments such as field desorption. The drawback of using off-axis geometry was a reduction in mass resolution due to the additional temporal spread produced by bending of ion trajectories. Recently, Spengler et al[103] have shown that ion-to-ion conversion processes on the dynode surface are the predominant mechanism for the detection of ions of masses higher than 20 000 Da. The masses of small ions emitted from the dynode surface were found to be independent of the nature of the incident ions and the surface itself. Using a tandem time-of-flight instrument, the secondary ions were found to have masses up to a few hundred daltons[103-105]. Secondary ions of both positive and negative charges have been observed during the conversion processes. The major drawback of this large-ion to small-ion conversion process is the introduction of additional temporal dispersion.

2.2.4. The computer and associated electronics

The output of the electron multiplier was first pre-amplified using a (x10) 50 ohm fast amplifier. It was then fed to the 50 ohm input of a LeCroy 175 MHz digital oscilloscope[155]. In most of the experiments, the bandwidth limit of the oscilloscope was reduced from 175 MHz to 30 MHz in order to reduce system noise and to prevent high frequency aliasing for single shot events at timebase speeds below 50

Figure 2.11
Ion trajectory simulations of the off-axis post-acceleration detector. (Incident ion energy = 5 - 15 kV)

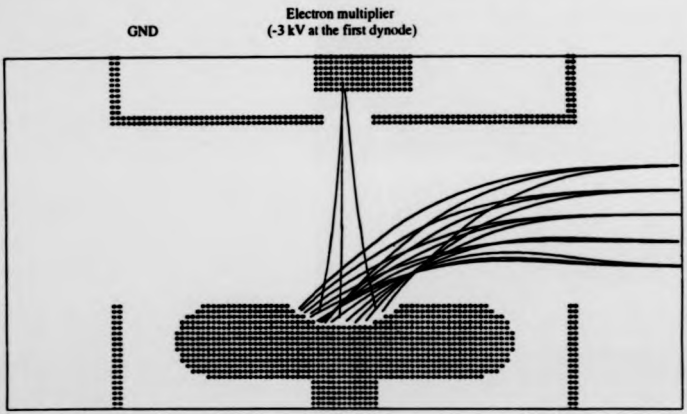

μs per division. The oscilloscope has two identical input channels. Each of them is equipped with a 100 megasample per second, 8-bit analogue-to-digital converter and a 32-kiloword acquisition memory. Up to four analog waveforms can be displayed on a 12.5 cm x 16.5 cm screen while simultaneously reporting the parameters controlling signal acquisition. Successive single-shot events can be summed and averaged. In the present work, all data acquisitions were performed through the soft-key buttons in the front panel of the oscilloscope. Data transfer from the digital oscilloscope to a computer for data storage and analysis was acheived via a serial RS-232C asynchronous interface or a parallel general purpose interface bus (GPIB) interface. The computer used was a high performance Sun-3/80 workstation[156] under a Unix environment. The interfacing ports available included two RS-232C serial ports, a small computer system interface (SCSI) port and an ethernet port. A serial asynchronous interface was initially used to perform data transfer. This communication interface was recently replaced by a high performance serial GPIB link. A GPIB-SCSI interface[157] was installed to handle data transfers between the GPIB and the small computer system interface (SCSI).

2.2.5. Computer software

The software used in this work was written in C-language under a Unix environment. The portions which were written by the author are listed in Appendix A. The software consists of a graphic display module, a remote data transfer module, a data manipulation module and finally a printing module. The graphic display module was programmed under a Sun-window environment which allows most of the operations to be performed in the main window or via different pop-up windows. The spectrum was displayed in a 400 x 600 pixel graphic window. Any portion of the spectrum could be magnified to the full display size.

The remote data transfer module transferred the data between the oscilloscope and a designated file through either a RS-232C serial link or a GPIB

parallel interface. Generally, the data were stored in a description file (*.des) and a data file (*.dat). The description file contains all information needed to interpret correctly the spectral data, whereas the data file contains the actual waveform. At the serial interface, data were transferred in hexadecimal format at a baud rate of 19 200 bit per second. At the parallel interface, data were transferred in ASCII format.

The data manipulation module contains general routines such as baseline subtraction, smoothing, peak centroiding, time-to-mass calibration and spectrum labelling. The number of channels used in smoothing can be varied from 3 to 65. The smoothing channels were weighed using coefficients generated from Pascal's triangle. Smoothing was performed bi-directionally to avoid data bias. Time-to-mass calibration could be performed using two or more peaks of known masses within the time-of-flight spectrum. Calibration was based on a simple least-square correlation procedure leading to the correlation constants A and B (Equation 1.8). These correlation constants could be stored for subsequent external calibration of spectrum obtained under identical experimental conditions. A pop-up window, which allows the analysis of a portion of the spectrum, provides information such as peak centroid, full-width half-maximum (FWHM) of the selected peak and also an integrated value of the peak area. In the printing module, the graphic window was bit-mapped into a raster file which could then be sent to the laser printer through an ethernet interface.

2.3. RAMAN MICROLINE FOCUS SPECTROMETRY[158]

Microline focus spectrometry (MiFS) (Figure 2.12), utilises a line-focussed Raman microscope coupled to a non-astigmatic spectrograph operating with a slow scanned charge-coupled device (CCD) array detector[159]. The two dimensional character of the detector results in line-scanned spectral data from the sample at each exposure. In the current instrumentation, the line focus is produced by cylindrical optics and the resultant spatial resolution is sub-micron. As configured for this work, the MiFS system produced a line-focus (up to 200 μm in length) on the

Figure 2.12
Schematic diagram of the microline focus spectrometer.

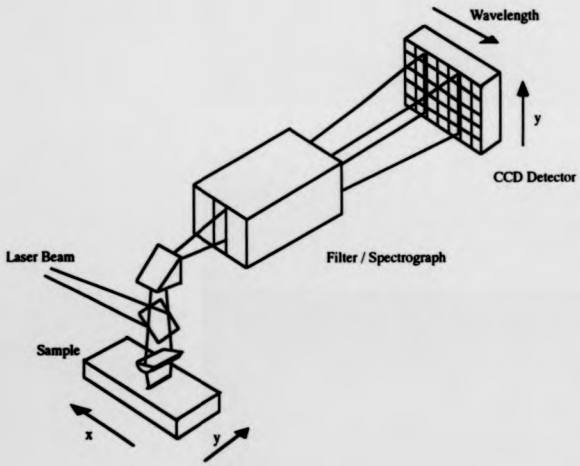

sample, or a spot focus of about 0.8-3.0 μm diameter depending upon which of the x 20 , x 40 or x 60 objectives were used[160]. The line focus has a distinct advantage for studying heat-sensitive samples as the laser power is low at any point along the line. Yet by 'binning' the spectral data in the spatial dimension on the CCD chip, good signal/noise spectra can be obtained representing the average spectrum along the line. Alternatively, sections of the spatial data can be binned to investigate certain designated regions. In this work the 514.5 nm line of an Ar^+ ion laser was used to provided a power of 10 mW in a 140 μm line focussed on the sample. With this laser power, a depth of several microns within the sample could be analysed. Exposure times between 2-15 minutes were used to give acceptable signal-to-noise ratios and Raman shifts reported are accurate to ± 3 cm^{-1}. The Raman MiFS instrument allows concurrent viewing of the focussed laser line and the sample thus allowing easy positioning of the region of interest.

EXPERIMENTAL METHODS

2.4. Field desorption (FD)

2.4.1. Sample preparation

Samples were loaded onto the emitter by dipping the emitter into either a diluted solution of sample (in methanol) or a pure sample droplet on a thin glass slide depending on the viscosity of the sample. A current of warm air was used to remove any solvent. Residue solvent in the sample would give rise to an unstable ion signal. Heavy sample loading, which might reduce the ion signal stability, was avoided by carefully dipping the loaded emitter onto a clean glass slide.

2.4.2. Emitter heating

The loaded emitter was heated by passing a regulated electrical current through the emitter inside the source chamber. This current is commonly called the emitter heating current (EHC). After raising the emitter to the desired electrical potential, the heating current was increased slowly. If the current was increased too quickly, the sample tended to come off the emitter in bursts of ions. Discharges could result which either "cleaned-off" the sample or caused the breakage of the emitter.

2.4.3. Mass calibration

Mass calibration was accomplished by co-desorbing the sample of interest with a polymer standard. Polyisoprene (Mn 1350)[161] and polypropylene glycol (Mn 2000)[162] were used in this study to calibrate different portions of the spectrum. Accurate masses of the calibrant ion peaks, typically to the first decimal place, were calculated from the known formula of the polymer standard.

2.4.4. Tandem mass spectrometry (MS/MS)

Tandem mass spectrometry (MS/MS) is a technique which employs two stages of mass analysis. There are many possible combinations of mass analysers for tandem mass spectrometry. With a reverse geometry double focussing mass spectrometer, the mass-analysed ion kinetic energy (MIKE) spectrometry technique is commonly employed. It was initially developed for the study of the unimolecular decomposition of metastable ions as they traverse the second field-free region of the mass spectrometer.

In a typical MIKE experiment, an incident ion of mass m_i and kinetic energy E_i is first selected by the magnetic field so that it will pass through the β-slit of the instrument. Some ions may undergo unimolecular decomposition to produce fragment ions of mass m_f with an energy $E_f=(m_f/m_i)E_i$. These fragment ions can then be transmitted through the electric sector and collector slit at a potential $V_{acc(f)}$ to the detector.

$$V_{esa(f)} = (m_f/m_i)V_{esa(i)} \qquad (2.1)$$

$V_{esa(i)}$ is the electric sector potential at which the incident ion is transmitted. A scan of the electric sector potential, to potentials lower than that at which the incident of parent ion is transmitted, will generate a so-called MIKE spectrum. The masses of the fragment ions can be calculated from the electric sector potentials by rearranging Equation 2.1. To increase the amount of structural information available from this technique, the decomposition of the selected molecule-ions can be enhanced by collisions with inert gas molecules. The overall process is called collisionally-activated decomposition (CAD) or collision-induced decomposition (CID). The acronym CID-MIKE is used in this thesis to distinguish this technique in which the collision process is perfomed in the second field-free region.

2.5. MATRIX-ASSISTED LASER DESORPTION / IONISATION (MALDI)

2.5.1. Sample preparation

All the chemicals used in present studies were purchased commercially and were used without further purification. Normally, the protein materials were dissolved in 0.01% trifluoroacetic acid (TFA) and deionised water to give concentrations ranging from about 1×10^{-4} mol dm^{-3} to 1×10^{-6} mol dm^{-3}.

Solid matrices, such as nicotinic acid and sinapinic acid, were either diasolved in deionised water or 40% aqueous acetonitrile to give concentrations of the order of 5 to 10 mmol dm^{-3}. Samples of different matrix-to-analyte molar ratios were made by mixing appropriate volumes of the matrix solution and protein solution. Typically, 2 µl of the mixture of matrix and the protein solution were applied to the sample stage (2 mm stainless steel tip). Samples were either dried in ambient air or under a stream of dry nitrogen (200-250 cc / min).

For liquid matrix (3-NBA) experiments, the pure liquid (0.2 - 0.5 µl) was applied to the sample stage. The protein solution (1.5 µl) was placed on top of the

matrix droplet which gave rise to matrix-to-analyte ratios of approximately 6×10^5 to 3×10^4. The water was allowed to evaporate under a stream of warm air. A visible immiscible layer developed initially but disappeared within a few minutes. At this point the liquid sample was transferred into the vacuum chamber of the mass spectrometer.

2.5.2. Extraction-field effect experiment

The ion-extraction lens was modified to suit the various studies. Figure 2.13 shows the schematic diagram of the source arrangement. The immersion electrodes and the Einzel lens arrangements were replaced by two gridded electrodes which were mounted at a distance of 18 mm and 32 mm away from the sample stage respectively. The sample stage was held at a high static potential (for positive-ion mode), and the second grid-electrode was grounded. Different extraction fields experienced by the sample surface were therefore generated by the varying the high potential applied to the counter electrode.

2.5.3. Initial velocity measurement

In addition to the two-grid source arrangement described in section 2.5.2., an additional gridded electrode was attached to the sample-probe supporting plate. Consequently, the distance of the other gridded electrodes from the additional grid were therefore 16 mm and 30 mm successively. The additional grid was used to create a field-free condition at the sample surface for ion formation, which is particularly important for the initial velocity studies. It prevented the possibility of any ion energy deficit which might cause additional shift of the ion flight time. The presence of a field-free region immediately above the sample stage also served to control the ion formation environment and hence the ionic species formed. This was particularly important as the present instrumental resolution is not sufficient to resolve individual ion peaks in the protein molecule-ion region.

Figure 2.13
Schematic diagram of the modified electrostatic lens assembly (side view).

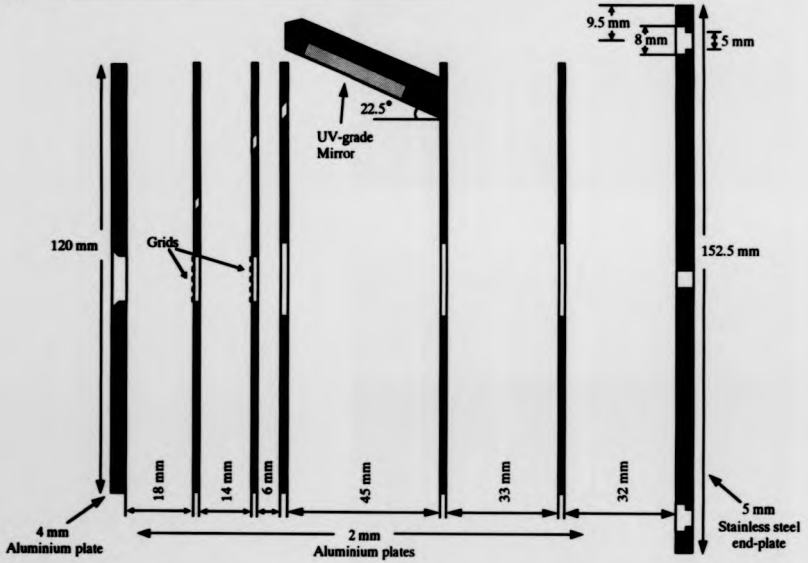

In the present source arrangement (Figure 2.14), the time-of-flight of molecule-ions of a particular species from the site of ion formation to the first-grid (T_1) and from the third-grid to the detector (T_4) are constants. The change of total ion-flight time produced by varying the high potential of the second electrode relates directly to the change of ion-flight time through the regions between grid 1 and 3 (i.e. T_2+T_3).

$$s = ut + \frac{1}{2}\left\{\frac{1}{m}\left(\frac{\Delta V}{s}\right)qe\right\}t^2 \qquad (2.2)$$

Equation 2.2 is the analytical formula to calculate the distance (d) travelled by a particle with mass m and q electronic charges in a time interval t under the influence of a potential gradient $\Delta V/s$; u is the starting velocity of the particle. Alternatively, the time-of-flight (t) for an ion to travel between two electrodes separated by a fixed distance s and at a potential difference (ΔV) can be calculated by solving the roots of this quadratic equation. T_2 and T_3 for a particular V_2 may be calculated using an arbitrary initial ion velocity.

2.5.4. Energy deficit measurement

The total kinetic energy of the desorbed ion after the full acceleration can readily be estimated using a grid-electrode to which a retardation potential Vret is applied. The lens assembly used was similar to that used in the extraction-field effect measurements. The distance of the gridded electrodes from the sample stage were 10 mm and 14 mm respectively. The sample stage was held at a static positive potential (for positive-ion mode) and the counter electrode was grounded. A positive potential (retardation potential Vret) was then applied to the third electrode. This arrangement allowed only ions with a total kinetic energy great enough to overcome the retardation potential to be transmitted. The molecule-ion signals at different retardation potentials were then monitored.

Figure 2.14
Schematic diagram of the electrostatic lens assembly used in the initial velocity measurements .

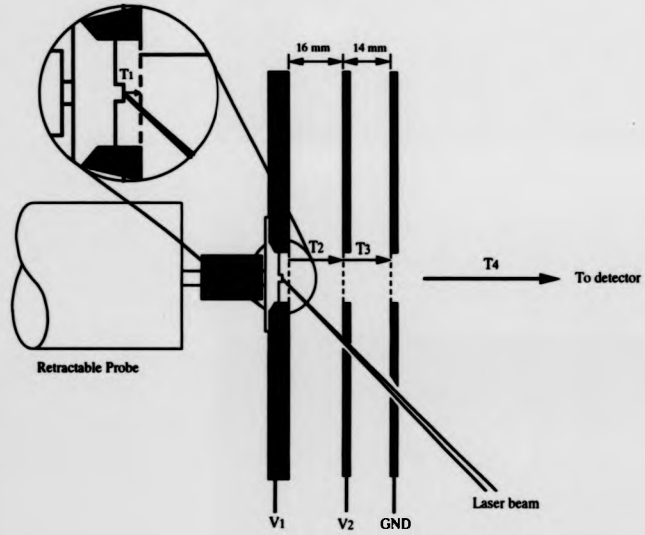

3

FIELD DESORPTION

3.1. INTRODUCTION

Field desorption (FD), first reported by Beckey[12] in 1969, is perhaps the oldest desorption / ionisation method. It remains the method of choice for analysing involatile synthetic polymers, especially those of low polarities. As has been mentioned in section 1.1., synthetic polymers consist of an "envelope" of oligomeric species differing in mass by monomeric units. Accuracy of the mass spectrometric measurement of molecular mass information for polymers depends on the desorption / ionisation method employed. Methods with high energy deposition such as fast atom bombardment and plasma desorption could lead to successive cleavage of the monomeric unit. The measured molecular mass would therefore be less than the actual value. The inherently low energy deposition of the FD technique is reflected by the production of intense molecule-ion signals and limited fragment ions. When combined with tandem mass spectrometric methods such as collision-induced decomposition, structural information can be obtained. The work presented in this chapter is intended to demonstrate the analytical capability of the FD technique using synthetic polymers of molecular masses up to 3000 Da.

3.2. ION FORMATION

Field desorption has been considered as an offspring of the closely related ionisation method - field ionisation (FI). These techniques involve ion generation from the surface of a specially prepared emitter wire under an intense electric field (10^8 - 10^9 V m^{-1}). Traditionally, the term FI refers to the ionisation of gas-phase

analytes, whereas FD involves the removal of the compound of interest from the condensed phase.

The mechanism of ion formation by FI has been explained in terms of a quantum mechanical tunnelling effect, in which electrons tunnel from analyte molecules to the surface of an emitter as a consequence of the applied electic field[7,163,164]. The mechanism of ion formation by FD is more obscure due mainly to an inadequate understanding of the interactions between high electric fields and involatile liquids or solid under high vacuum conditions. A review of the present theories of the ion formation process by field desorption has been made recently by Prokai et al[13].

Three distinct mechanisms have been proposed to explain the production of the characteristic molecule-ions under field desorption conditions. The formation of odd-electron molecule-ions ($[M]^{+\cdot}$) is generally considered to be explained by an electron tunneling mechanism, similar to that of field ionisation[165]. The high electric field strength required could be achieved at the tip of the microneedles on an activated emitter surface. Gas-phase transport (sublimation) and surface diffusion of the mobile-phase from the shanks to the tips of the microneedles, have been suggested as processes replenishing the ionisation sites. Under this model, the sample needs to be relatively volatile and non-polar. It has been suggested that the high electric field is also capable of causing surface ion-molecule reactions leading to protonated molecules ($[M+H]^+$).

To explain the formation of protonated ($[M+H]^+$) and cationised ($[M+alkali\text{-}metal]^+$) molecule-ions from polar and involatile substances, mechanisms based on the desorption of preformed ions are commonly adopted. Rollgen et al[166] observed that when strong electrolytes are deposited onto a bare emitter wire and subjected to a very high electric field, microprotrusions are formed from the sample surface. It has been suggested that field enhancement at the protrusion tips would eventually

cause desolvation and subsequent extraction of the preformed ion through successive rearrangement of molecule-molecule interactions. Derrick et al[167] have proposed a more general view of ion formation from various substances using activated emitter wire substrates. This model is based on the build-up of surface charges under typical high-field conditions. The consequence of the high electric force would be to overcome the ion-molecule and molecule-molecule interactions in the condensed phase and lead to the desorption of desolvated ions.

3.3. EMITTER ACTIVATION

The emitters used for field desorption experiments in this work were 25 μm tungsten wire covered with carbon microneedles. The tungsten wires were spot-welded across the tops of the nichrome posts of the emitter support. The length of the wire between emitter posts was 6 mm. The process of growing the carbon microneedles is referred to as activation. The emitters used in this work were activated using the high-temperature method first described by Beckey et al[12]. The procedure of activation has been studied in detail. Empirical properties of the process were extracted and formulated into an automated procedure by means of computer programs (written in Pascal). The apparatus and software programs used for activation have been described in detail elsewhere[168].

Briefly, the growth of microneedles on 25 μm tungsten wires is carried out by a pre-activation / carburisation procedure in which the emitters (five at a time) are heated in a benzonitrile atmosphere (~1 Pa) for ~ 40 minutes under a constant heating power (0.95 W per emitter wire). No high voltage is applied during this period. This heating process converts most of the tungsten into tungsten carbide[169]. After the pre-activation, the benzonitrile vapour pressure is reduced to ~ 0.5 Pa and a static electrical potential of ~15 kV is applied between the emitters and a grounded plate ~2 mm away. The heating power is then adjusted to a value which gives an average emitter surface temperature of ~1300 K. This initiates the growth of

microprotrusions on the surface of the wire. The high potential is reduced as a function of activation time. The emitter heating current is continuously monitored to fit a pre-defined power-resistance isotherm which represents the desired power-resistance relationship for the growth of microneedles. The whole process of activation takes about 50 hours. The length of the microneedles produced in this manner is approximately 60 to 90 μm, and the microneedles cover one-third of the area of the wire surface.

3.4. FIELD DESORPTION OF TRIMELLITIC ACID-BASED POLYESTERS

The increasing demands on high-temperature synthetic lubricants have led to the synthesis of special materials which combine good viscometric properties and high thermal stability. Esters of trimellitic acid, or 1,2,4-tricarboxybenzoic acid and neopentyl glycol, have been found to exhibit very good thermal stability[170]. In the present work, field desorption mass spectrometry has been used to characterise the reaction products[171] of trimellitic acid, neopentyl glycol and 2-ethylhexyl alcohol. The raw materials are shown in Figure 3.1.

3.4.1. Mass Spectra

Figure 3.2(a-d) shows field desorption mass spectra of the trimellitic acid-based esters at various emitter heating currents, i.e. EHC = 60, 93, 99 and 108 mA respectively. The emitter potential was set at 14 934 V and the detector was floated at -30 kV. Table 3.1 summarises the results obtained in Figure 3.2(a-d). It was possible to identify the molecule-ions of several species. At low EHC, a series of 2-ethylhexyl trimellitate ester clusters $(A\text{-}R)_n$ (m/z = 547, 1094, 1641, 2187 and 2733) was observed. It was found that several series of product species, where two or more trimellitic acid units are bridged by neopentyl glycol units, were desorbed at higher EHC. A linear chain-type structure of general form $AN(\text{-}A'N\text{-})_nA$ (m/z = 938, 1328, 1718, 2108, 2498 and 2889) was observed at all EHC settings. At high EHC conditions, a series of fragment ions corresponding to the loss of a neutral side-chain

Figure 3.1
Raw materials for synthesis of trimellitate esters.

Trimellitic acid

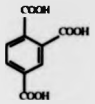

2-ethylhexyl alcohol

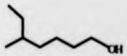

Neopentyl glycol

Figure 3.2
Field desorption mass spectra of trimellitic acid-base polyester at different emitter heating currents *EHC's*.

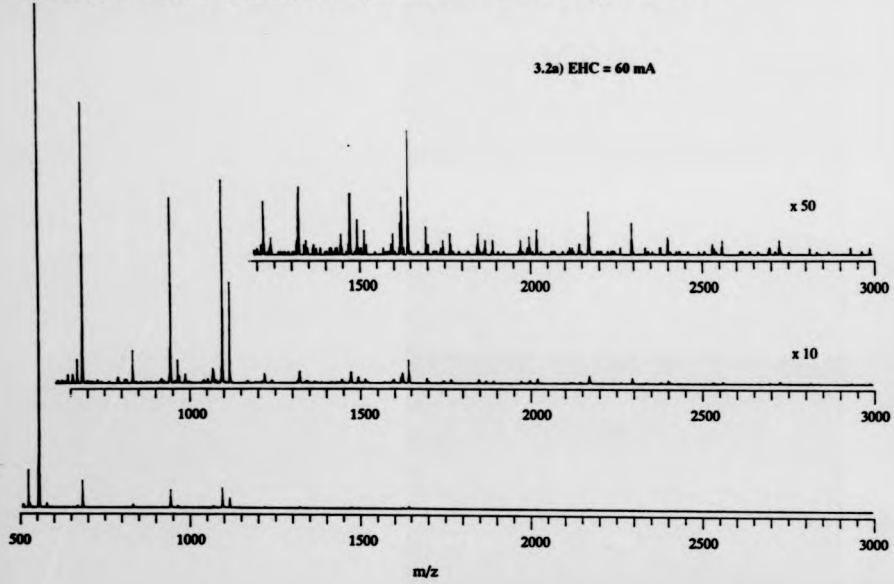

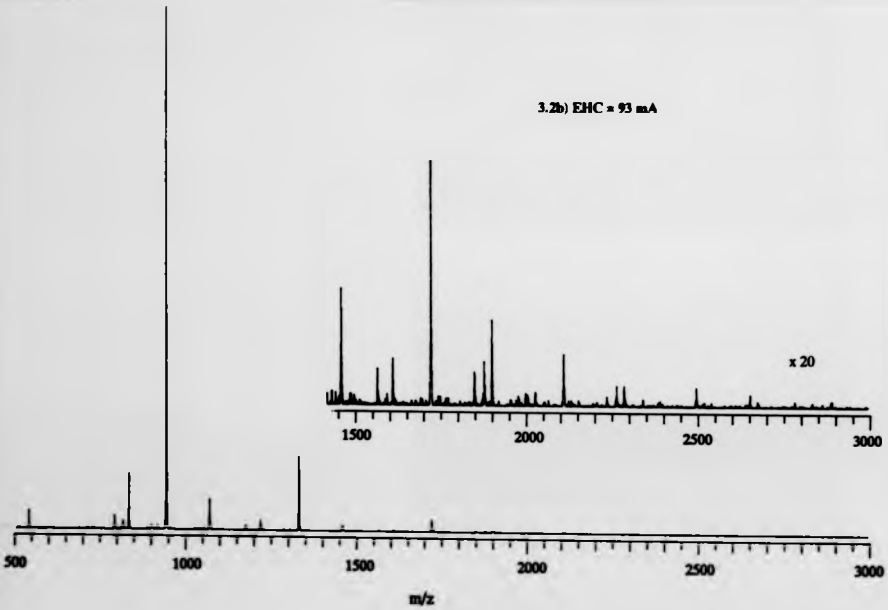
3.2b) EHC = 93 mA
x 20
1500
2000
2500
3000
500
1000
1500
2000
2500
3000
m/z

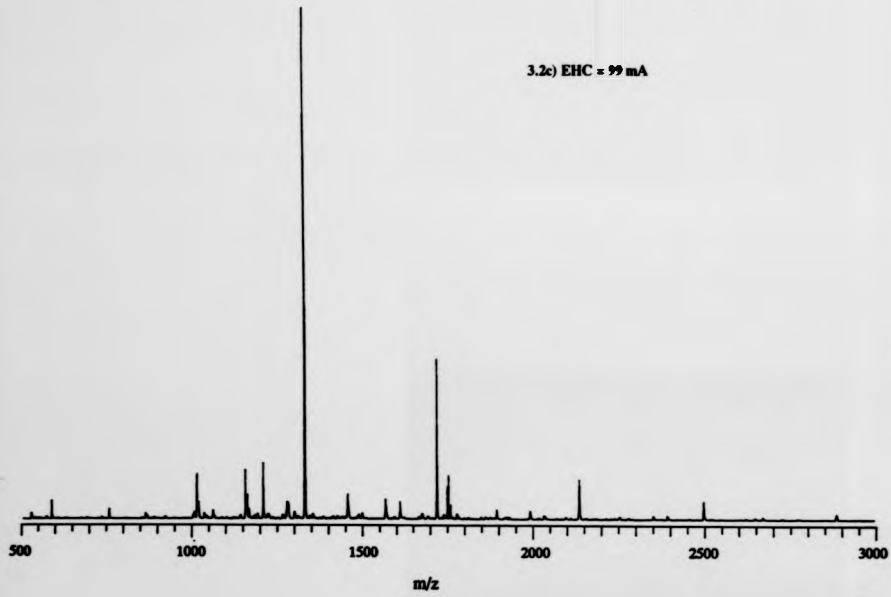
3.2c) EHC = 99 mA
500
1000
1500
2000
2500
3000
m/z

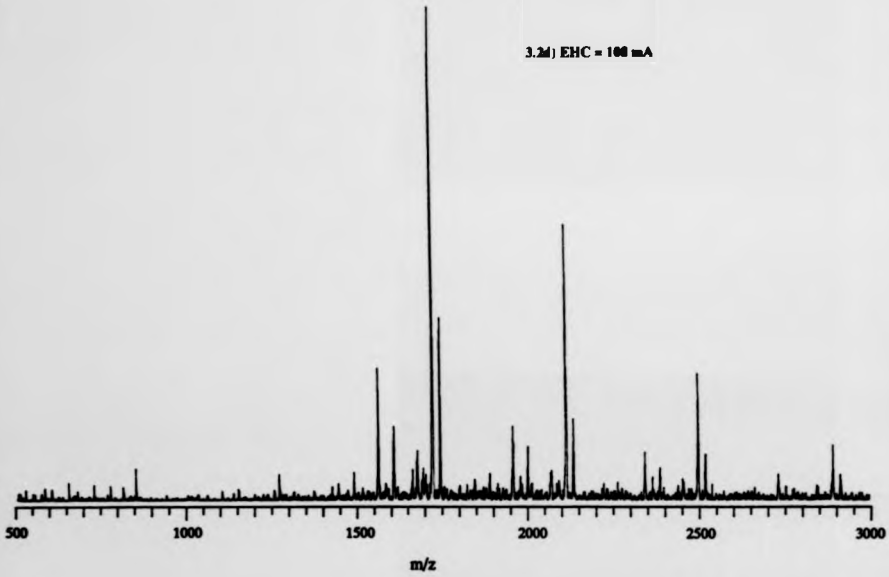
3.2d) EHC = 160 mA
500
1000
1500
2000
2500
3000
m/z

Table 3.1

Summary of the FD mass spectra of trimellitic acid-based polyesters illustrated in Figure 3.2(a-d).

m/z (Monoisotopic)	Emitter Heating Current / mA			
	60	93	99	108
	Structure assigned[#] (no. of repeating unit)			
547.4	I (1)*	-	-	-
825.4	II-f (1)	II-f (1)	-	-
937.6	II (0)	II (0)*	-	-
1093.8	I (2)	-	-	-
1215.6	II-f (2)	-	-	-
1327.8	II (1)	II (1)	II (1)*	-
1561.8	-	-	-	III (4)
1605.8	-	II-f (2)	-	II-f (2)
1640.8	I (3)	-	-	-
1718.0	-	II (2)	II (2)	II (2)[$]
1740.0	-	-	-	II+Na (2)
1952.0	-	-	-	III (5)
1996.0	-	-	-	II-f (3)
2108.2	-	II (3)	II (3)	II (3)
2130.2	-	-	-	II+Na (3)
2186.6	I (4)	-	-	-
2342.2	-	-	-	III (6)
2386.2	-	-	-	II-f (4)
2498.4	-	II (4)	II (4)	II (4)
2520.4	-	-	-	II+Na (4)
2732.4	I (5)	-	-	-
2733.0	-	-	-	III (7)
2776.4	-	-	-	II-f (5)
2888.6	-	II (5)	II (5)	II (5)
2910.6	-	-	-	II+Na (5)

[#] See Scheme 3.2. for structures

* Denotes the strongest signal in the spectrum

Table 3.1

Summary of the FD mass spectra of trimellitic acid-based polyesters illustrated in Figure 3.2(a-d).

m/z (Monoisotopic)	Emitter Heating Current / mA			
	60	93	99	108
	Structure assigned[#] (no. of repeating unit)			
547.4	I (1)[*]	-	-	-
825.4	II-f (1)	II-f (1)	-	-
937.6	II (0)	II (0)[*]	-	-
1093.8	I (2)	-	-	-
1215.6	II-f (2)	-	-	-
1327.8	II (1)	II (1)	II (1)[*]	-
1561.8	-	-	-	III (4)
1605.8	-	II-f (2)	-	II-f (2)
1640.8	I (3)	-	-	-
1718.0	-	II (2)	II (2)	II (2)[*]
1740.0	-	-	-	II+Na (2)
1952.0	-	-	-	III (5)
1996.0	-	-	-	II-f (3)
2108.2	-	II (3)	II (3)	II (3)
2130.2	-	-	-	II+Na (3)
2186.6	I (4)	-	-	-
2342.2	-	-	-	III (6)
2386.2	-	-	-	II-f (4)
2498.4	-	II (4)	II (4)	II (4)
2520.4	-	-	-	II+Na (4)
2732.4	I (5)	-	-	-
2733.0	-	-	-	III (7)
2776.4	-	-	-	II-f (5)
2888.6	-	II (5)	II (5)	II (5)
2910.6	-	-	-	II+Na (5)

[#] See Scheme 3.2. for structures

[*] Denotes the strongest signal in the spectrum

Figure 3.3
Summary of the molecule-ions of trimellitic acid-based polyesters produced by field desorption.

I : $[(A\text{-}R)_n+H]^+$ (Trimellitate ester clusters)

II : $[A\text{-}N\text{-}(\text{-}A'N\text{-})_n\text{-}A+H]^+$ (Chain-type polyesters)

III : $[(A'N)_n+H]^+$ (Ring-type polyesters)

Abbreviations :

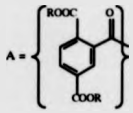

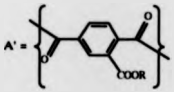

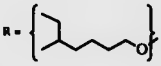

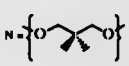

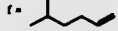

C_8H_{16} was observed. Apart from the protonated polyesters, cationised species were observed at high EHC settings. A second minor series, corresponding to molecule-ions with a ring-type structure of general form $(\text{-A'N-})_n$ (m/z 391, 781, 1172, 1562, 1952, 2342 and 2732), was observed at high EHC settings (in Figure 3.2d). It was found that fully substituted trimellitate ester and its clusters tend to be desorbed more readily than the cross-linked polyester products, especially at low emitter heating currents (EHC). High emitter heating currents were needed to promote the desorption of high-mass components. The reproducibility of field desorption mass spectra was found to depend critically on the emitter heating current.

3.4.2. Collision-induced decomposition / mass-analysed kinetic energy spectra

The detailed structures of several molecule-ions was studied using the Collision-induced decomposition / mass-analysed kinetic energy (CID-MIKE) technique. Intense molecule-ion beams were produced by field desorption of trimellitic acid-based polyester samples using a 25 μm emitter. The emitter was held at 15 000 V and was heated by an appropriate EHC. The EHC settings were selected to produce strong and long-lived signals which were necessary to improve ion counting statistics during repetitively spectral accumulations. In all the CID-MIKE experiments reported in this thesis, the signal intensities of selected molecule-ions were measured in the absence of collision gas. The collision gas pressure inside the collision cell was then adjusted to reduce the original signal intensity of the parent molecule-ion to approximately 40%. Helium was used in the present studies. The electric sector potential was scanned from 50 V to 505 V, which corresponds to a mass range of 10 - 100% of the incident molecule-ion mass.

Figure 3.4 shows the CID-MIKE spectrum of $[M+H]^+$ m/z 547.4 at an EHC of 60 mA. The parent ions correspond to the fully esterified mono-unit of trimellitic acid. Results of the analysis of this spectrum are presented in Table 3.2. Fragmentation reactions are represented in terms of the neutral fragment losses.

Figure 3.4
FD-MIKE spectrum of 2-ethylhexyl ester of trimellitic acid $[M+H]^+$ (m/z = 547.4); helium target gas, 60% parent beam attenuation, incident ion energy *Ei* = 14.9 keV.

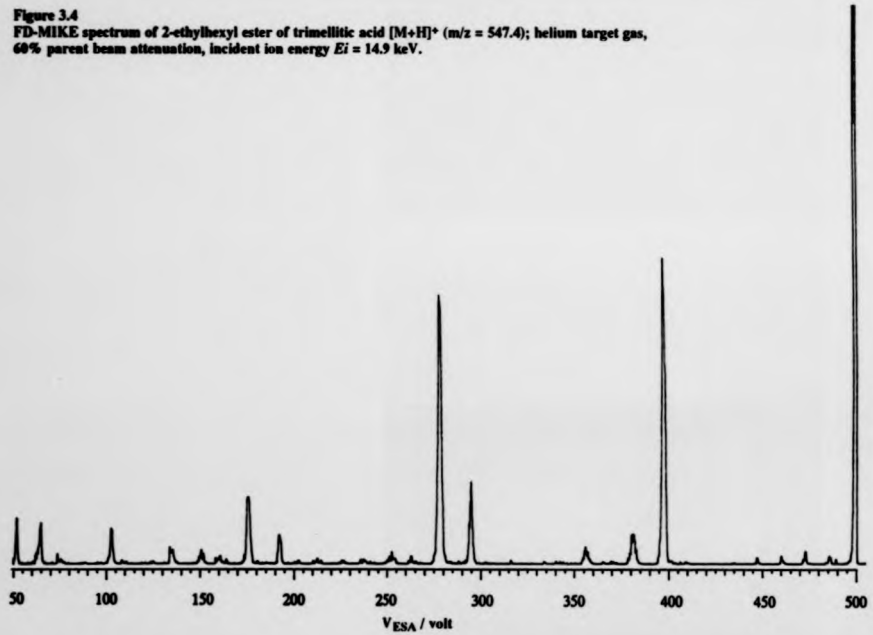

Table 3.2

Mass-analysed ion kinetic energy spectrum. Unimolecular decomposition of protonated trimellitate ester m/z 547.4 produced by field desorption (Figure 3.4).

Vesa / V	Observed neutral loss / u	Neutral fragment loss / u	Assigned mass loss / u	Reaction scheme#
500.0	-	-	-	
397.0	112.8	C_8H_{16}	112.2	a
382.0	129.2	RH	130.2	b
295.0	224.4	$2(C_8H_{16})$	224.4	a
278.0	243.1	$R\text{-}(C_8H_{17})$	242.4	c1
192.4	336.8	$3(C_8H_{16})$	336.6	a
176.0	354.7	C_8H_{16} + $R\text{-}(C_8H_{17})$	354.7	a & c1
103.0	434.6	AOH	434.6	a
65.0	476.2	$AO(CH_2)_2{=}CH_2$	475.6	-
52.0	490.5	$AO(CH_2)_3{=}CH_2$	489.7	-

See Figure 3.5 for mechanisms

Figure 3.5
Mechanisms of fragmentation for trimellitic acid-based polyesters:

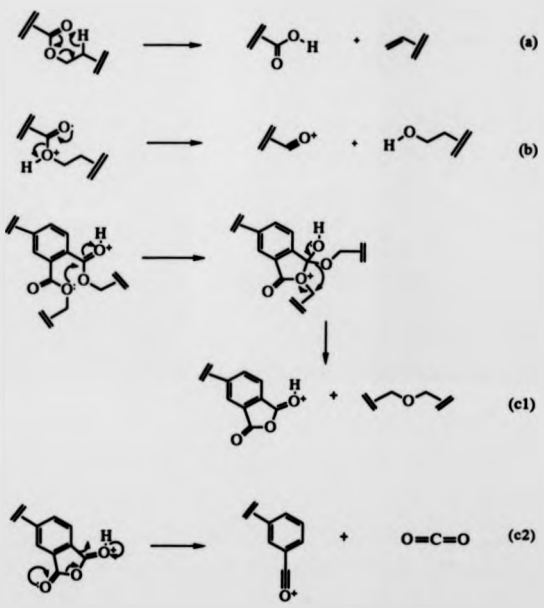

The neutral loss is calculated from the mass differences between the parent ion and the masses of the fragment ions. Figure 3.6 - 3.8 show the CID-MIKE spectra of $[M+H]^+$ m/z 937.6, 1327.8 and 1718.0 at EHC's of 93 mA, 99 mA and 108 mA repectively. These parent ions represent the homologues of the chain-type polyesters in which two or more trimellitate units are bridged by neopentyl glycol units. All the other carboxylic acid functional groups were esterified by 2-ethylhexyl alcohol. The ring-type polyesters were not studied using the MIKE technique due to their short-lived and weak signals.

Table 3.3 summarises their spectral features in term of the neutral losses. The fragmentation reaction mechanisms, involving simple C-O bond cleavages of the polymer backbone with hydrgen transfer, are proposed to account for the majority of neutral fragment loss. They are illustrated in Figure 3.5(a) and (b). The losses of neutral fragments with masses 242, 634, 1024 and 1415 have been explained by rearrangement reactions, as shown in Figure 3.5(c1). Two adjacent ester groups within an aromatic benzene ring undergo a rearrangement reaction leading to the formation of a protonated anhydride and a neutral ether fragment. The losses of neutral masses 677, 1067 and 1458 (in Table 3.3) have been attributed to the metastable decarboxylation of the anhydride products (Figure 3.5(c2)).

3.5. Conclusions

Field desorption mass spectrometry has been successfully applied to characterise an industrial polyester sample. Problems have been found in determining the average relative molecular mass from the intensities of the field-desorbed ions. Desorption and ionisation efficiencies has been found to depend closely on the molecular mass, volatility, chemical structure and experimental conditions (eg. emitter surface temperature). Generally, low-mass components tend to be desorbed more easily than high-mass components especially at low emitter heating current. High emitter heating current usually enhances both the removal of

Figure 3.6
FD-MIKE spectrum of trimellitic acid-based polyester $[M+H]^+$ (m/z = 937.6); emitter heating current *EHC* = 93 mA, helium target gas, 60% parent beam attenuation, incident ion energy *Ei* = 14.9 keV.

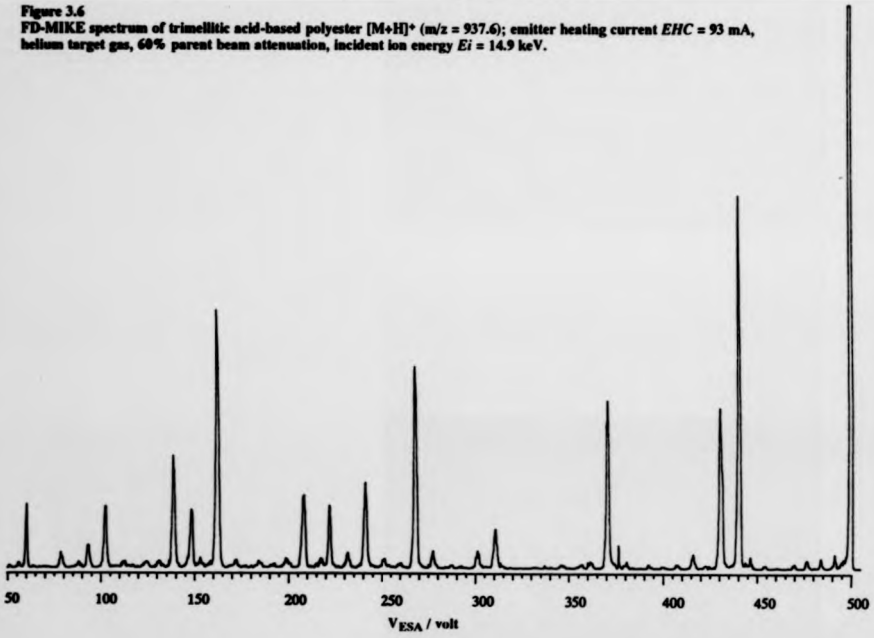

Figure 3.7
FD-MIKE spectrum of trimellitic acid-based polyester $[M+H]^+$ (m/z = 1327.8); emitter heating current *EHC* = 99 mA, helium target gas, 60% parent beam attenuation, incident ion energy *Ei* = 14.9 keV.

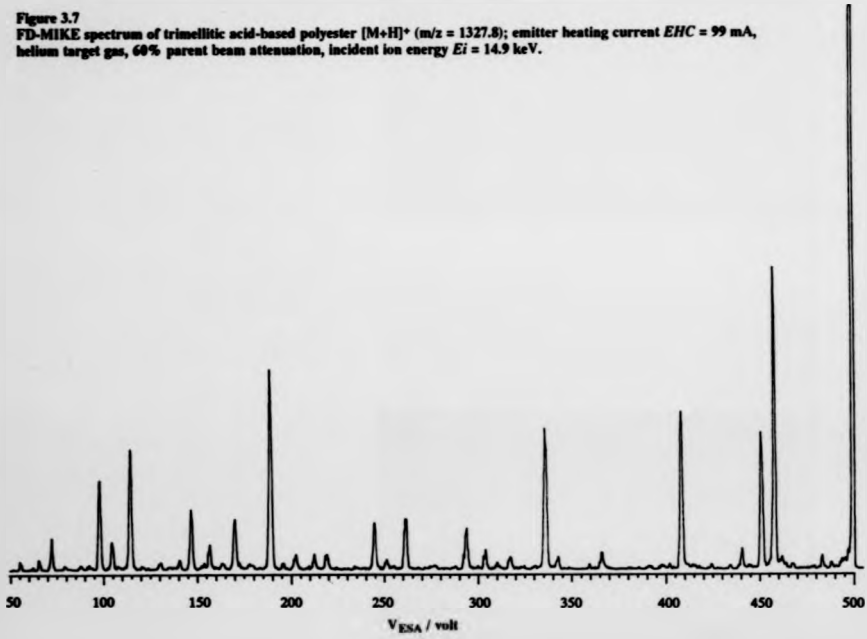

Figure 3.8
FD-MIKE spectrum of trimellitic acid-based polyester $[M+H]^+$ (m/z = 1718.0); emitter heating current *EHC* = 108 mA, helium target gas, 60% parent beam attenuation, incident ion energy *Ei* = 14.9 keV.

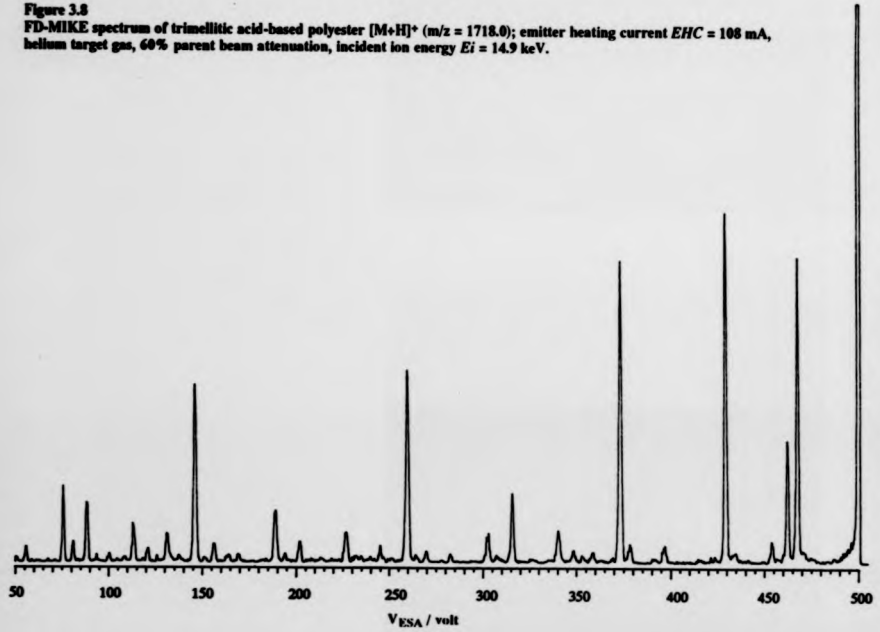

Table 3.3

Collision-induced decomposition of protonated trimellitic acid-based chain-structure polyesters produced by field desorption (Figures 3.6 - 3.8).

Parent ions (m/z)					
937.6	1327.8	1718			
Observed neutral loss / u			Netural fragment loss	Assigned mass loss / u	Reaction scheme#
111.0	111.6	112.7	C_8H_{16}	112.2	a
130.1	130.2	130.3	RH	130.2	b
242.5	242.6	243.4	R-(C_8H_{17})	242.4	c1
435.1	435.6	435.6	AOH	434.6	a
633.1	633.6	634.0	AN-(C_8H_{17})	632.9	c1
677.13	678.22	679.0	AN-(C_8H_{17}) + CO_2	676.9	c2
-	826.3	825.8	ANA'OH	825.1	a
-	1024.0	1024.5	ANA'N-(C_8H_{17})	1023.4	c1
-	1068.1	1069.2	ANA'N-(C_8H_{17}) + CO_2	1067.4	c2
-	-	1216.4	A(NA')$_2$OH	1215.5	a
		1414.7	A(NA')$_2$N-(C_8H_{17})	1413.9	c1
		1458.7	A(NA')$_2$N-(C_8H_{17}) + CO_2	1457.9	c2

See Figure 3.5 for mechanisms

low-mass components and the desorption of high-mass components. In order to generate an overall view of the relative concentrations of the various components in the sample, successive mass spectra should be accumulated as the emitter heating current is increased slowly while the polymer desorbs. The resultant summed spectrum should provide quantatively information on the relative amounts of each component within the sample and hence the averaged molecular mass information could be calculated.

The use of tandem mass spectrometry to study the structure of any component within the sample has been demonstrated. The limitation of the MIKE technique is that the instrumental geometry is unable to provide good mass resolution. The low mass resolution can be partly explained by the kinetic energy release during the decompostion of the parent ions. The mass accuracy using the CID-MIKE technique for structural elucidation is generally less than satisfactory. The peak positions were found to be somewhat displaced to lower apparent energy (or masses). This effect can be explained on the basis of collision-induced kinetic energy uptake. Mechanisms of kinetic energy release during the ion decomposition process and kinetic energy uptake during the collision process have been studied extensively[172] and they will not be discussed in details. High-resolution tandem mass spectrometry could be achieved, using additional analysers such as three / four -sector instruments and hybrid instruments.

4

MATRIX-ASSISTED LASER DESORPTION / IONISATION

4.1. SOLID MATRICES

4.1.1. Scanning electron microscopy and Raman microscopy studies

The ability to reproduce experimental results is perhaps the most important measure for the usefulness of an analytical method. For mass spectrometry, the reproducibility of mass spectral information is generally governed by the exact experimental conditions. Proper preparation of the sample seems to be a common "front-end" problem. For instance, secondary ion mass spectrometry (SIMS) requires the preparation of a very thin sample[35], typically 2 to 10 μm, to yield optinum response. Field desorption requires the use of an activated field emitter as a substrate[12]. The requirement of proper sample prearation is particularly important for techniques involving the mixing of "neat" analyte with some kind of matrix material. The homogeneity of the analyte and matrix mixture seems to govern the gaseous analyte molecule-ion formation and hence the spectral reproducibility. For plasma desorption, electrospraying[173] of a layer of matrix (such as nitrocellulose[174]) followed by a layer of protein has been found to be most effective.

For matrix-assisted laser desorption / ionisation (MALDI) using solid matrix-systems, direct drying of microlitres of the solution mixture of matrix and analyte was commonly used[61]. It was observed that the crystals, resulting from drying a small droplet of a mixture of nicotinic acid (one of the most effective matrices) and protein on a metallic target, are not evenly distributed. Strong

fluctuations in the molecule-ion signal were experienced from spot-to-spot across a sample and also between samples.

In order to optimise the sample homogeneity, several sample preparation methods have been investigated in this study. Raman microscopy and scanning electron microscopy techniques were used to assess the distribution of matrix and analyte molecules. Nicotinic acid and horse skeletal muscle myoglobin were used as matrix and analyte respectively. Doktycz et al[77] have used time-elapsed video microscopy to investigate the drying process and have claimed that the nicotinic acid and insulin molecules solidify at different times and in different spatial regimes, giving rise to a crystalline matrix phase and an isotropic analyte phase.

4.1.1.1 Results

Figures 4.1-4.6 show a series of electron micrographs and Raman scattering spectra taken from crystal deposits precipitated from solutions of nicotinic acid, myoglobin and their mixtures at different molar ratios and under different drying conditions. The sample preparation conditions are summarised in Table 4.1.

Table 4.1
Summary of conditions used in sample preparation for Raman microscopy and scanning electron imaging studies

Figure	Amount of Nicotinic acid	Amount of Myoglobin	Molar ratios [Nic/Myo]	Drying Conditions
4.1a-b	211 nmol	--	--	in air
4.2a-c	--	168 pmol	--	in air
4.3a-c	176 nmol	28 pmol	~6400	in air
4.4a-b	79 nmol	105 pmol	~750	in air
4.5a-c	176 nmol	28 pmol	~6400	under dry N_2
4.6a-c	79 nmol	105 pmol	~750	under dry N_2

i) Pure nicotinic acid (Matrix)

Figure 4.1a shows a scanning electron micrograph of a pure nicotinic acid deposit. The deposit formed from the pure nicotinic acid solution spread circularly with a diameter of ~2 mm. The nicotinic acid was in the form of fibre-like crystals which radiated inwards from the rim. A cavity was formed in the centre in which little material was deposited. Figure 4.1b shows the Raman scattering spectrum of the pure nicotinic acid deposit.

ii) Pure myoglobin (Analyte)

Figure 4.2a shows a scanning electron micrograph of the deposit formed from a solution of pure myoglobin. The deposit spread circularly with a diameter of ~2 mm. A thicker layer of material was found in the centre (diameter ~0.5 mm) and was surrounded by a thin film of material. Figures 4.2b and 4.2c show Raman scattering spectra of the pure myoglobin deposit. The differences between the spectra are attributed to the formation of different solid phases of myoglobin molecules.

The differences in scattering frequencies for nicotinic acid and myoglobin provided a basis for the investigation of the chemical composition of the crystals formed from solution mixtures of nicotinic acid and myoglobin.

iii) High matrix/analyte ratio (~6400) and drying in air

Figure 4.3a shows a micrograph of the air-dried deposit from a solution of high matrix-to-analyte ratio. The deposit shows different morphology as compared to the pure materials. Several large crystals (~50-100 μm in length) were scattered in the centre. The deposit was surrounded by a thick rim (~100 μm). Highly magnified micrographs show that the large crystals were mainly composed of a fibre-like crystal phase and were coated with a layer of amorphous material in some positions. In areas where large crystals were not found, a second type of thin crystal was observed.

Figure 4.1
Scanning electron micrograph and Raman scattering spectrum of the crystals precipitated from a solution of nicotinic acid.

4.1a : Scanning electron micrograph.

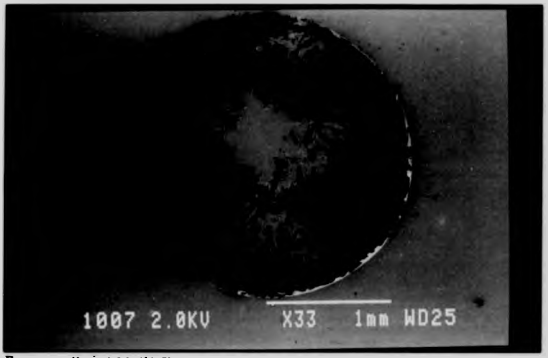

4.1b : Raman scattering spectrum.

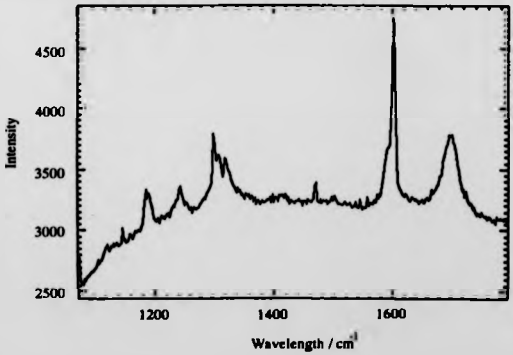

Figure 4.2
Scanning electron micrograph and Raman scattering spectra of the crystals precipitated from a solution of myoglobin.

4.2a : Scanning electron micrograph (low magnification).

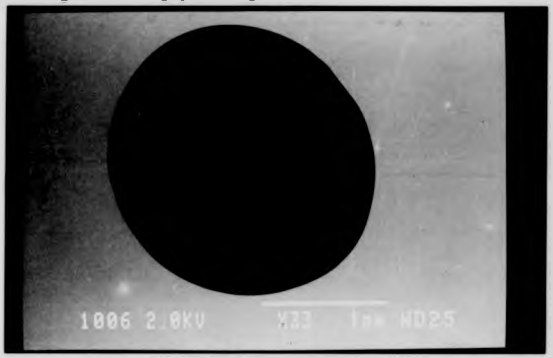

4.2b : Raman scattering spectrum (taken from the central deposit).

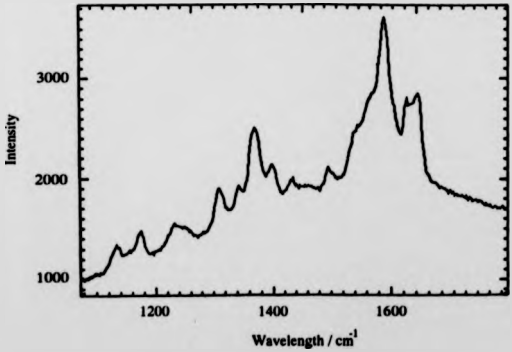

4.2c : Raman scattering spectrum (taken from the surrounding thin film).

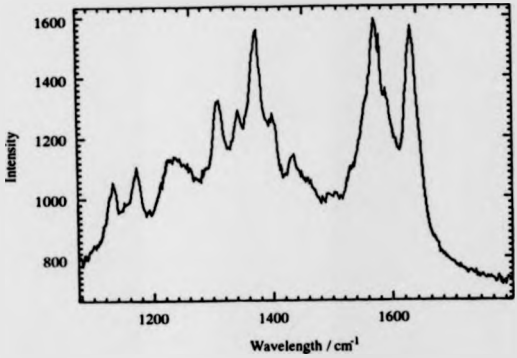

Figure 4.3
Scanning electron micrograph and Raman scattering spectra of the crystals precipitated (in air) from a solution mixture of nicotinic acid and myoglobin (molar ratio = 6400 : 1).

4.3a : Scanning electron micrograph.

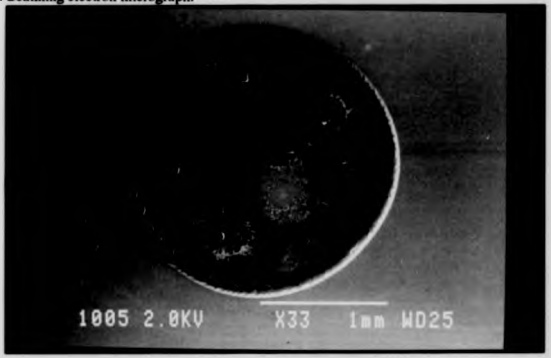

4.3b : Raman scattering spectrum (taken from a large crystal 50-100 μm).

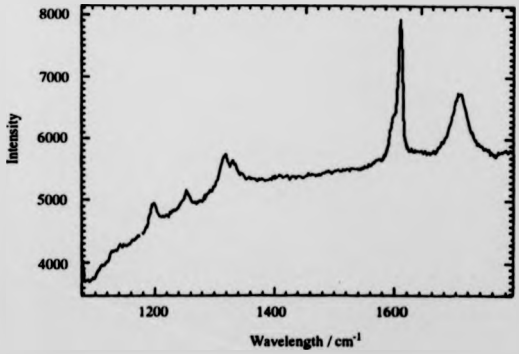

Figure 4.3b shows the Raman scattering spectrum of a large crystal. The absence of scattering frequencies 1580 cm^{-1} and 1640 cm^{-1} indicates the near absence of myoglobin. Figure 4.3c shows the Raman scattering spectrum of a thin crystal. Apart from the characteristic scattering peaks for nicotinic acid (such as 1600 cm^{-1} and 1690 cm^{-1}), the presence of intense peaks at 1580 cm^{-1} and 1640 cm^{-1} indicates the formation of a low matrix-to-analyte crystal phase. For some thin crystals, the Raman scattering spectra appeared to suggest that no nicotinic acid was present (Figure 4.3d). This discovery of the formation of different phases of crystals has an important consequence for the interpretation of MALDI results. It is tentatively suggested that the dramatic change of spectral characteristics of the MALDI mass spectra obtained from different sampling positions within a sample is caused by this phase segregation.

iv) Low matrix/analyte ratio (~750) and drying in air

Figure 4.4a shows a scanning electron micrograph of the air-dried deposit from a solution of low matrix-to-analyte ratio. The deposit comprises numerous isolated crystals (~10-20 μm in length) scattered in the centre and a thick crystalline rim on the periphery. Highly magnified micrographs show that the isolated crystal have a rock-like structure.

Figure 4.4b shows the Raman scattering spectrum of a single crystal. The presence of intense peaks at 1600 cm^{-1} and 1690 cm^{-1} and somewhat weaker peaks at 1580 cm^{-1} and 1640 cm^{-1} indicates the inclusion of a small amount of myoglobin within the nicotinic acid bulk.

v) High matrix/analyte ratio (~6400) and drying under dry-nitrogen

Figure 4.5a shows the micrograph of the deposit precipitated from a solution mixture of high matrix-to-analyte ratio under a stream of nitrogen. With the use of nitrogen purge a significant improvement of the sample homogeneity was observed.

4.3c : Raman scattering spectrum (taken from a thin crystal 10 - 20 μm).

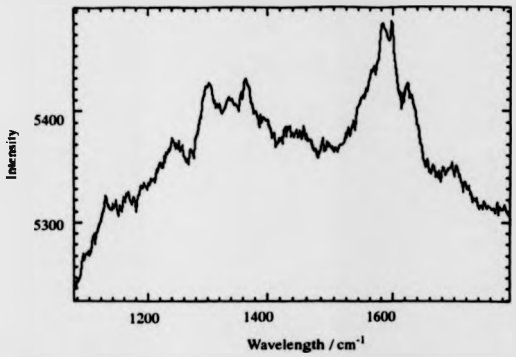

4.3d : Raman scattering spectrum (taken from another thin crystal 10 - 20 μm).

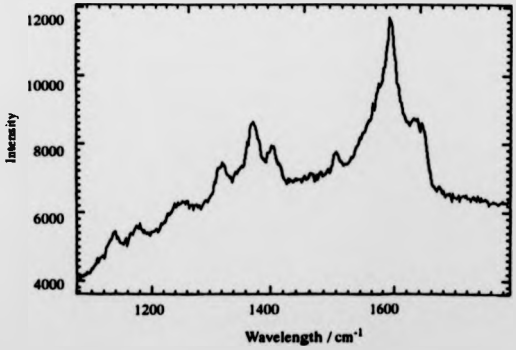

Figure 4.4
Scanning electron micrograph and Raman scattering spectrum of the crystals precipitated (in air) from a solution mixture of nicotinic acid and myoglobin (molar ratio = 750 : 1).

4.4a : Scanning electron micrograph.

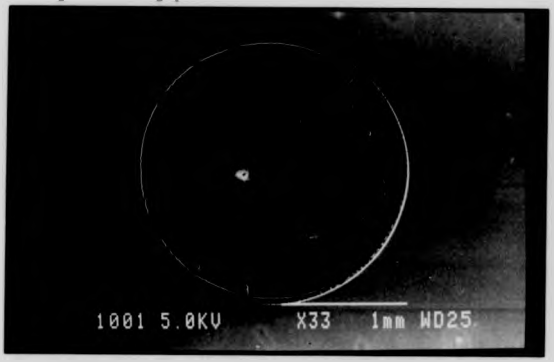

4.4b : Raman scattering spectrum.

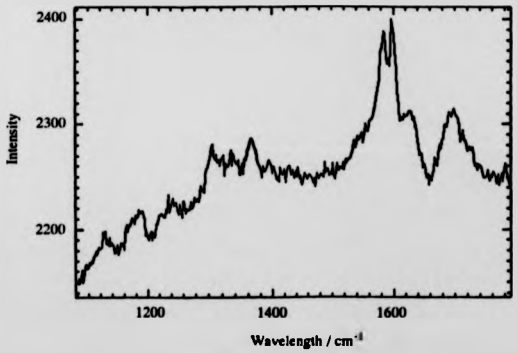

Figure 4.5
Scanning electron micrographs and Raman scattering spectrum of the crystals precipitated (under dry nitrogen) from a solution mixture of nicotinic acid and myoglobin (molar ratio = 6400 : 1).

4.5a : Scanning electron micrograph (low magnification).

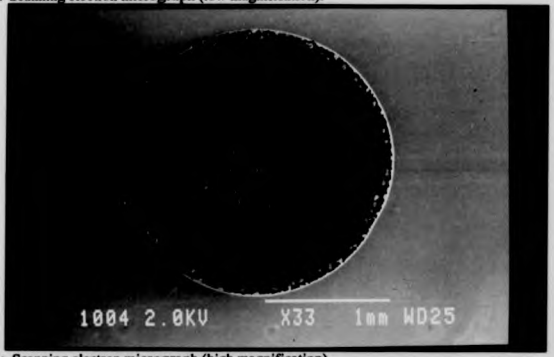

4.5b : Scanning electron micrograph (high magnification).

The aggregates had a typical dimension of roughly 20 μm in diameter and were evenly distributed across the whole sample support.

Figure 4.5c shows the Raman scattering spectrum of the aggregates. The presence of characteristic scattering frequencies at 1600 cm^{-1} and 1690 cm^{-1} (for nicotinic acid) and 1580 cm^{-1} and 1640 cm^{-1} (for myoglobin) indicates the existence of both nicotinic acid and myoglobin components.

From the highly magnified micrograph (Figure 4.5b) some fibre-like crystals were found to extend from the bases of some aggregates. The close resemblance of this sub-structure to the pure nicotinic acid crystals suggests the possible formation of two or more lattice phases within an individual aggregate. We tentatively suggest that the bases of the aggregates are composed mainly of nicotinic acid and are covered by a layer of nicotinic acid and myoglobin mixture.

vi) Low matrix/analyte ratio and drying under dry-nitrogen

Figure 4.6a shows a scanning electron micrograph of the deposit formed from a solution mixture of low matrix-to-analyte ratio under a stream of nitrogen. Again, a significant improvement of the sample homogeneity was observed using a nitrogen purge. The aggregates formed were significantly smaller and thinner (~10 μm in diameter) than those formed from high matrix-to-analyte ratio solution. The aggregates were closely and evenly distributed across the whole sample support.

Figure 4.6c shows the Raman scattering spectrum of a crystal. The spectral peaks at frequencies 1600 cm^{-1}, 1690 cm^{-1}, 1580 cm^{-1} and 1640 cm^{-1} indicate the presence of both myoglobin and the nicotinic acid.

From highly magnified micrographs (Figure 4.6b) the aggregates were found to be morphologically similar to each other. There was no evidence of any phase segregation. Nevertheless, the possibility of forming a core nicotinic acid crystal

4.5c : Raman scattering spectrum.

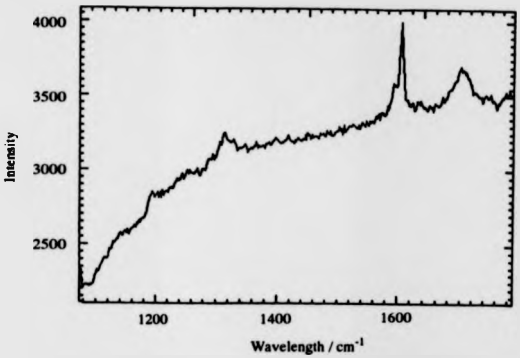

Figure 4.6
Scanning electron micrographs and Raman scattering spectrum of the crystals precipitated (under dry nitrogen) from a solution mixture of nicotinic acid and myoglobin (molar ratio = 750 : 1).

4.6a : Scanning electron micrograph (low magnification).

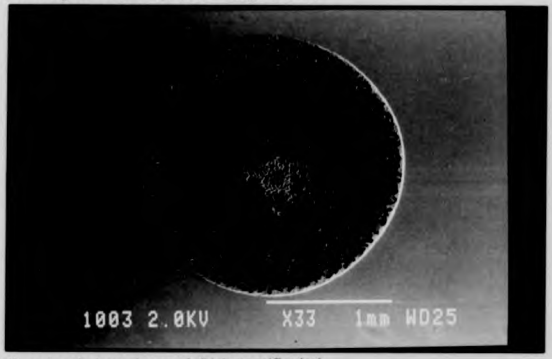

4.6b : Scanning electron micrograph (high magnification).

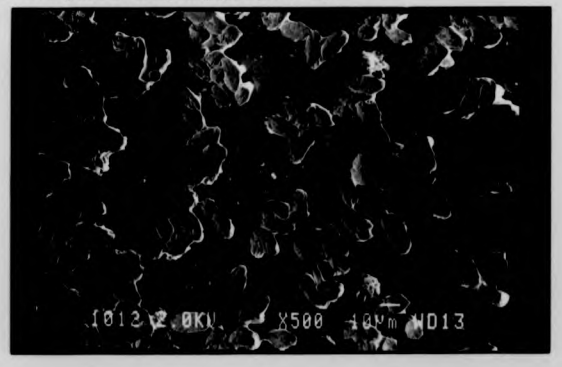

4.6c : Raman scattering spectrum.

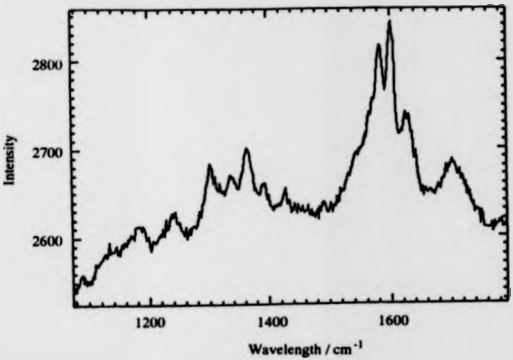

which is subsequently covered with a layer of nicotinic acid and myoglobin mixture cannot be ruled out.

4.1.1.2. Discussion and Conclusions

The complementary information obtained from the scanning electron micrographs and the Raman scattering spectra illustrated that matrix/analyte segregation had occurred spatially when solutions of high matrix-to-analyte ratio were dried in air. It was shown that this phase segregation effect could be alleviated by reducing the matrix-to-analyte ratio and by the use of nitrogen purging during the drying process. From the morphology of the aggregates formed from drying a solution of high matrix-to-analyte ratio under nitrogen purging, it was tentatively suggested that sub-structures of near pure nicotinic acid were present.

Matrix-isolation has been said to be an important criterion governing the success of an MALDI experiment[112]. Strupt et al[67] have used X-ray crystallography to study crystals developed from a saturated solution of 2,5-dihydroxybenzoic acid which contained a small amount of cytochrome-C (concentration ~ 10^{-6} mol dm^{-3}). The diffraction pattern indicated no significant perturbation of the matrix crystal lattice by the inclusion of protein molecules. The authors attributed these observations to the formation of "perfect" homogeneous crystals. Recently, Beavis et al[175] have used a biological protein strain to probe the single crystal developed from a solution mixture of sinapinic acid and insulin. Two different crystal faces were found optically within a single crystal and the protein molecules sat on only one of the crystal faces. Results from Raman microscopy and scanning electron microscopy, described in the present studies, provide information on the relative abundances of the matrix and analyte molecules within depths of several tens of micrometers. Although the Raman scattering frequencies signify some degree of matrix-analyte mixing, the results could not be used as direct evidence of matrix isolation.

Attempts to improve the sample homogeneity by using electrospray deposition were not successful. No signals corresponding to analyte molecule-ion were recorded using samples prepared by electrospray deposition. Large volumes of sample were, however, observed to be ablated even at laser fluences considerably less than those used for producing molecule-ion signal from crystals developed by drying microliters of matrix-analyte solution mixture.

4.1.2. Effect of matrix-to-analyte ratios

The effects of relative and absolute concentrations of nicotinic acid and bovine insulin have been studied. Samples of different matrix-to-analyte molar ratios were made by mixing appropriate volumes of nicotinic acid solution and insulin solution. The total protein loading, at a particular matrix-to-analyte ratio, was varied by diluting the appropriate solution mixture with deionised water.

Assuming that noise is negligible compared to the ion signal, the area of a peak in a time-of-flight spectrum can be correlated linearly with the number of incident ions. Figure 4.7 shows the intensity of the insulin molecule-ion as a percentage of the total ion intensity of the spectrum versus the molar ratio of matrix/analyte. The calculations were based on an assumption that the gain of the detector is independent of the masses of the incident ions at a mass range less than 6000 daltons. It was found that protein molecule-ion signals could be registered over a wide range of molar ratios. The relative intensity of the insulin ion seemed to drop sharply at low concentration ratios (~100 : 1).

Figure 4.8 shows the relative intensity of the insulin ion versus the total protein loading at a constant molar ratio of matrix/analyte (i.e. 588). There was a general increase in relative intensity of the protein ion as the amount of protein used was increased. At high protein loading, a sharp decline in the intensity of protein ion signal was found. Based on the supposition of matrix-isolation, the reduction of protein molecule-ion signal at high concentration of protein ($> 10^{-4}$ mol dm^{-3}) could

Figure 4.7
Intensity of bovine insulin molecule-ion relative to the total ions generated versus the molar ratio of nicotinic acid and bovine insulin.

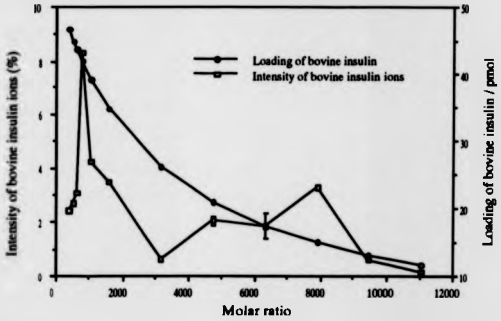

Figure 4.8
Intensity of bovine insulin molecule-ion relative to the total ions generated versus the total sample loading at a constant molar ratio (582) of nicotinic acid and bovine insulin.

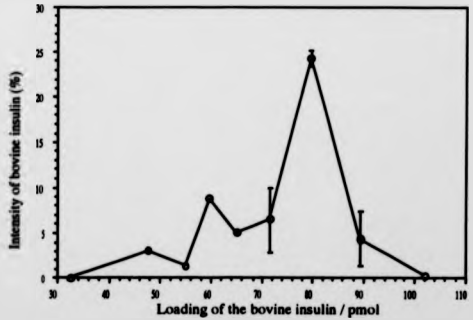

be attributed to the formation of protein aggregates which subsequently inhibited the desorption of protein molecules.

4.1.3. Matrix-ions suppression effect

In a systematic investigation of the effect of the matrix-to-analyte ratios on the analyte molecule-ion intensities, it was observed that some of the matrix-assisted laser desorption mass spectra were composed of ion signal mainly derived from the protein, even through the matrix molecules were present in large excess as compared to the analyte molecules. The existence of specific conditions under which matrix-ion formation is suppressed is of both practical and fundamental interest. One of the drawbacks of using small organic molecules as matrices has been the formation of high abundances of matrix-derived ions with masses extending up to 500 Da. This has prohibited the use of MALDI to volatilise those "difficult" substances which have molecular masses less than 500 Da. Therefore, the ability to suppress these matrix-ions might extend the application of MALDI to low molecular-mass substances. Study of the factors governing the suppression of low-mass matrix-ions might lead to a better understanding of the mechanism of molecule-ion formation from MALDI.

Two model matrices, namly nicotinic acid and sinapinic acid, were used in the present work. Bovine insulin (RMM = 5734) was the test analyte. In the case of the nicotinic acid matrix, the matrix-to-analyte ratio was found to exhibit a strong influence on the intensities of matrix-ions and analyte molecule-ions. The suppression of low-mass ion peaks in matrix-assisted ultraviolet (UV) laser desorption was found to occur at low matrix-to-analyte molar ratios[65,66]. Figure 4.9 shows a series of time-of-flight mass spectra of insulin using nicotinic acid as the matrix at different "gross" matrix-to-analyte molar ratios. The samples were prepared using the nitrogen-purging method, as described in section 4.1.1., to reduce effects caused by sample inhomogeneities. For each measurement, the laser energy

Figure 4.9
Positive-ion laser desorption time-of-flight spectra of bovine insulin (RMM = 5734) using nicotinic acid as the matrix at different matrix-to-analyte (M/A) ratios.

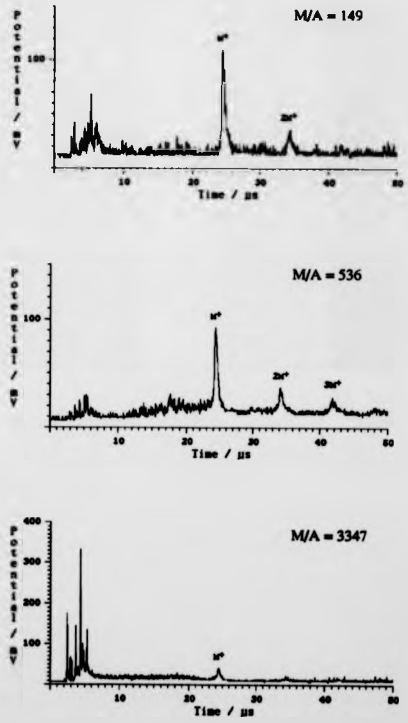

was adjusted to the threshold for ion production. This was important for observation of the matrix-ion suppression effect. The threshold fluence, which was found to vary slightly from spot to spot, was estimated to be ~ 20 mJ cm^{-2}. All spectra were recorded as an average of 20 laser shots at a single sample spot. At relatively high molar ratios of matrix-to-analyte (> 3000) a large group of low-mass ions were formed together with the molecule-ions. As the molar ratio of matrix-to-analyte was reduced, the low-mass ions due presumably to the matrix molecules were reduced, whereas the analyte molecule-ions were somewhat enhanced. At a matrix-to-analyte ratio of ~550, the protein molecule-ion peaks were maximised whereas the low-mass ions were almost eliminated. Further reduction of the matrix-to-analyte ratios led to a decrease of protein molecule-ion intensities.

In order to strengthen the conclusion that matrix-to-analyte ratio was the major factor governing the suppression effect, two other proteins namly chicken egg-white lysozyme (RMM = 14 314) and horse skeletal muscle myoglobin (RMM = 16 950) were studied. Figure 4.10 shows a series of time-of-flight mass spectra of myoglobin using nicotinic acid as the matrix at different "gross" matrix-to-analyte molar ratios. Near elimination of matrix-ions was observed at a matrix-to-analyte ratio of ~1000. The best matrix-to-analyte ratio, which maximises the protein molecule-ion signals and also gives a near elimination of low-mass ions, may therefore depend on the molecular mass of the protein in question. The best suppression spectra for bovine insulin, lysozyme and myoglobin have required matrix-to-analyte ratios of 600, 900 and 1000 respectively.

In contrast, all attempts to reproduce this suppression effect using sinapinc acid as matrix did not succeed. Figure 4.11 shows a series of time-of-flight mass spectra of insulin using sinapinic acid as the matrix at different "gross" matrix-to-analyte molar ratios. High intensities of matrix-ions, relative to those of the analyte molecule-ions, were found in the full range of matrix-to-analyte ratios (tens to

Figure 4.10.
Positive-ion laser desorption time-of-flight spectra of skeletal muscle myoglobin (RMM = 16950) using nicotinic acid as the matrix at different matrix-to-analyte (M/A) ratios.

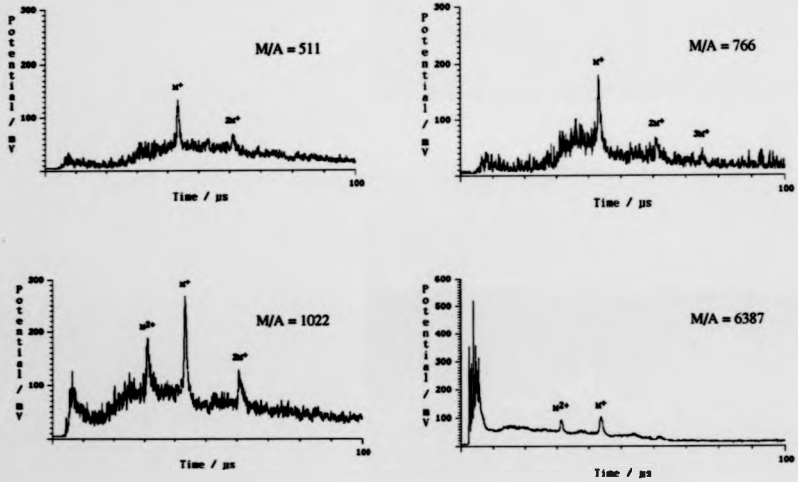

Figure 4.11.
Positive-ion laser desorption time-of-flight spectra of bovine insulin (RMM = 5734) using sinapinic acid as the matrix at different matrix-to-analyte (M/A) ratios.

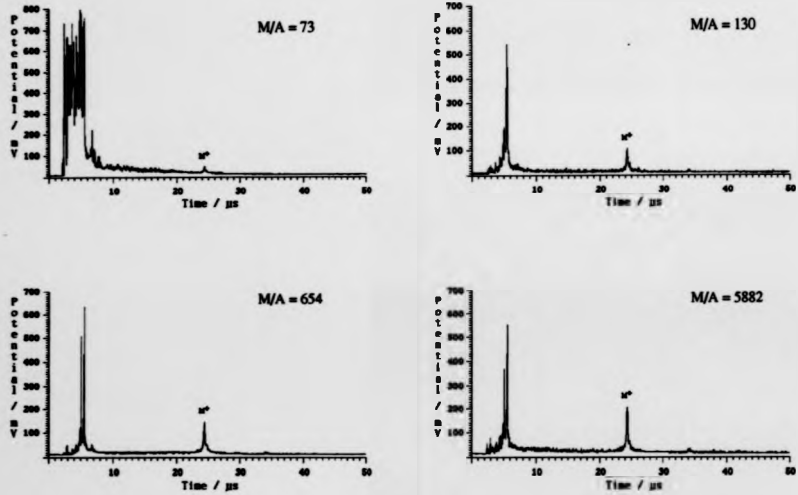

thousands). Recently, Biemann and co-workers[68] have shown that in addition to nicotinic acid, several other matrices can also exhibit matrix-ion suppression effect. Consistent with the present findings, sinapinic acid was found to exhibit no suppression effect.

The details of the ion formation process from an organic solid under MALDI conditions are not well understood. The notion of whether desorption and ionisation of analyte molecules occur simultaneously or consecutively has been controversial. The observations of matrix-ion suppression is tentatively associated with the two-step desorption / ionisation mechanism. It seems unlikely that the charge distribution between nicotinic acid and protein molecules in the solid state at the instance of irradiation would be greatly altered by a change in molar ratios, i.e. that there would be abundant matrix-ions in the solid at > 3000 : 1 for example, but none at 600 : 1. The near-absence of nicotinic acid peaks at low matrix-to-analyte ratio is therefore associated, not directly with the mechanism of desorption, but with the mechanism of charging subsequent to desorption.

As discussed in section 3.2.2., there seems to be an even distribution of matrix and analyte molecules within the sample deposit formed under nitrogen purging. With the confidence that the term "gross" matrix-to-analyte ratio reflects the chemical composition of the solid crystals, a qualitative model is proposed to explain the suppression phenomenon based on a charge supply-and-demand argument. Following the photon bombardment, some of the electronically excited nicotinic acid undergoes radiationless relaxation. A phase transition from solid into gas is induced. The relative amounts of gas phase matrix molecules and protein molecules formed depend on the crystal composition and hence upon the "gross" matrix-to-analyte ratio. Relative to the high matrix-to-analyte ratio case, the crystal of low matrix-to-analyte ratio should induce the phase transition of less charge donor (matrix molecules) and more charge acceptor (protein molecules) upon photon

bombardment. Therefore, a shift in the relative intensities of low-mass ions (i.e. matrix ions) and protein molecule ions is to be expected. The negative results obtained with sinapinic acid as the matrix material are not difficult to explain. In the optical microscopic studies of the crystals derived from sinapinic acid, Beavis et al[175] reported the formation of two crystal faces within a single crystal where the protein molecules sat only on one of the crystal faces. Since the orientations of the matrix-analyte crystals should be randomly distributed, the probability of laser-ablating pure sinapinic acid is very high. Moreover, there is no evidence to indicate a homogeneous distribution of protein molecules across the sample.

Beavis et al[69] have investigated the predominant analyte molecule-ion species resulting from MALDI of different peptides and found that proton attachment was the major mechanism of charging. After photon bombardment, any intermolecular proton transfer on or above the sample surface must depend on the relative proton affinities of the matrix and protein molecules and also on the composition of the desorbed (or about to be desorbed) sample. It has been pointed out[176] that the proton affinity of an electronically excited state of a molecule can be significantly different from that of the ground state of the molecule. Russell et al[95] have proposed that involvement of electronically excited states accounts for the predominant formation of $[M+H]^+$ ion in a typical matrix-assisted laser desorption experiment. The relevance of solution phase acid-base properties, as opposed to gas-phase proton affinities, has been studied in this work. The results and discussions will be presented in chapter six.

4.2 Liquid matrix

Over twenty organic molecules have been found to be useful as matrices[55,62,69,177] for MALDI, and almost all of these have been solids. It is believed that 3-nitrobenzyl alcohol (3-NBA) has been the only liquid matrix whose use for UV-MALDI has been reported[178]. Glycerol has been found to be useful as a

matrix for infrared (IR) MALDI[81,82], 3-Nitrobenzyl alcohol has been mixed with methanol and water (in the ratios 3:2:1)[178] and has been supported on a fibrous material. In the present work, the use of neat 3-NBA with a stainless steel substrate as a liquid matrix for UV-MALDI has been investigated.

4.2.1. Signal reproducibility

A liquid matrix system differs from the solid matrix systems in many ways. For nearly all solid matrices there is a tendency for the formation of inhomogeneous crystalline phases which cause laser desorption mass spectra to vary dramatically from one spot to another for a given sample. The molecule-ion signal also decreases with the number of laser shots for a given sample spot. Typically, a particular spot on a solid sample will be exhausted after a few shots (i.e. < 20).

For a liquid matrix, the analyte molecules will not be immobilised by the matrix lattice. Their distribution is expected to depend on the hydrophobicity or the hydrophilicity of the analyte molecules. In experiments with the liquid 3-NBA matrix loaded directly onto the stainless steel substrate, the shot-to-shot reproducibility was excellent and hundreds of shots could be used on a given spot. There was no need to select the spot irradiated. Figure 4.12(a-c) shows the positive-ion MALDI mass spectra of bovine albumin from the first, fiftieth and one hundreth laser shots on the same sample spot at a frequency of approximately one shot per second. The presumably relatively high degree of molecular mobility may allow the protein molecules to diffuse to the surface layers, replenishing the sample molecules that have been ionised or destroyed by the previous laser shot.

4.2.2. Molecular clustering

With solid matrices there seems to be a limit to the size of cluster ions easily formed from proteins, with trimers tending to be the largest clusters observed[179]. Figures 4.13 and 4.14 exhibit positive-ion MALDI mass spectra of cytochrome-C

Figure 4.12
Positive-ion laser desorption time-of-flight mass spectra of bovine serum albumin (RMM = 66 267) using 3-nitrobenzyl alcohol as the matrix.

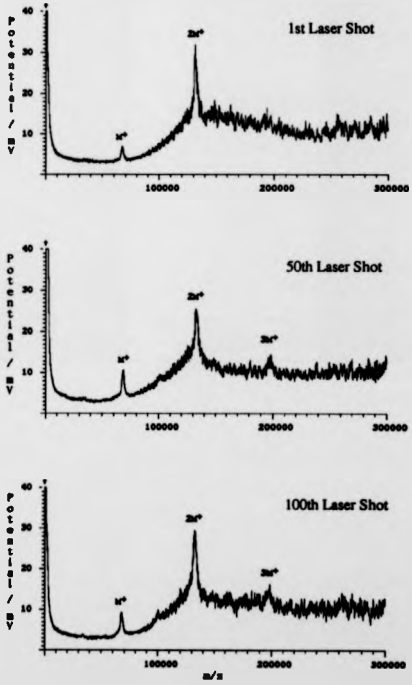

Figure 4.13
Positive-ion laser desorption time-of-flight mass spectrum of horse heart cytochrome-C (RMM = 12 354) using 3-nitrobenzyl alcohol as the matrix.

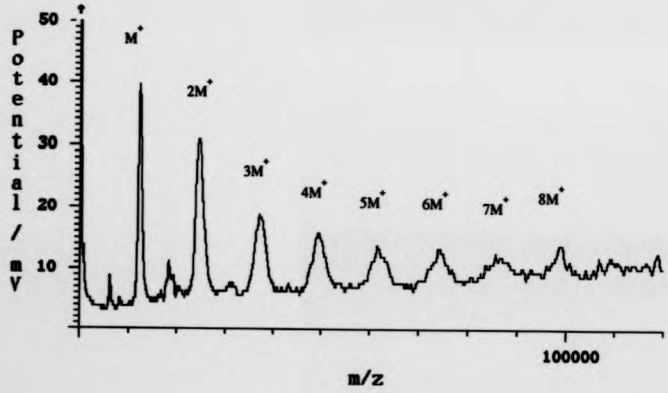

Figure 4.14
Positive-ion laser desorption time-of-flight mass spectrum of chicken-egg white lysozyme (RMM = 14 314) using 3-nitrobenzyl alcohol as the matrix.

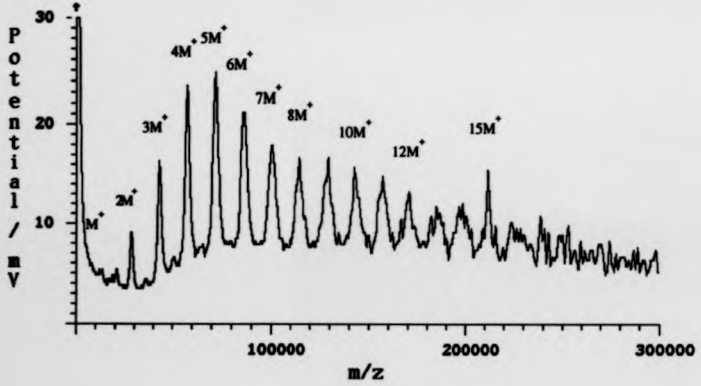

and chicken egg-white lysozyme using liquid 3-NBA as the matrix. Cluster ions extending to the 15-mer appear to have been formed in the case of lysozyme. Using liquid 3-NBA we have found that there is, at least qualitatively, a direct correlation between cluster-ion formation and the total loading of analyte (under the conditions of our experiments). As an aside, there may be a possibility of improving precision of mass measurement by using the numerous cluster peaks (c.f. electrospray[29]), although the peaks in the spectra reported here seem to be broad. To our knowledge, the largest ion measured prior to this study using MALDI was the dimer of glucose isomerase with a relative molecular mass (RMM) of 344,800[180]. Using 3-NBA liquid matrix, Figure 4.15 illustrates that cluster ions as large as the octamer of bovine albumin (calculated RMM = 530,136)[31] can be formed.

4.2.3. Effect of extraction field

The high signal stability from one laser shot to another facilitates systematic investigations of the effects of experimental factors. It was observed that there was an enhancement of the production of analyte molecule-ions using the 3-NBA matrix at relatively low extraction potentials. In order to elucidate this effect, the source lens stack described previously (section 2.2.2) was modified as decribed in section 2.5.3. Two grid electrodes were used instead of a three-element Einzel lens. With this arrangement, the field above the sample surface could be varied. Without the use of a focussing lens (Einzel lens), the desorbed ions were extracted without crossing over the ion optical axis. This was an important consideration in eliminating the possibility of ion-optical artifacts. In all experiments, the samples were held at 15 kV (V_{sam}) and the third-plate was grounded. With this arrangement, only the extraction potential ($V_{ex} = |V_1 - V_2|$) was changed when the potential of the counter-electrode was altered.

Ion-optically, the higher is the extraction potential (V_{ex}), the narrower is the angle of divergence of the extracted ion-beam or the larger is the acceptance of ions

Figure 4.15
Positive-ion laser desorption time-of-flight mass spectrum of bovine serum albumin (RMM = 66 267) using 3-nitrobenzyl alcohol as the matrix.

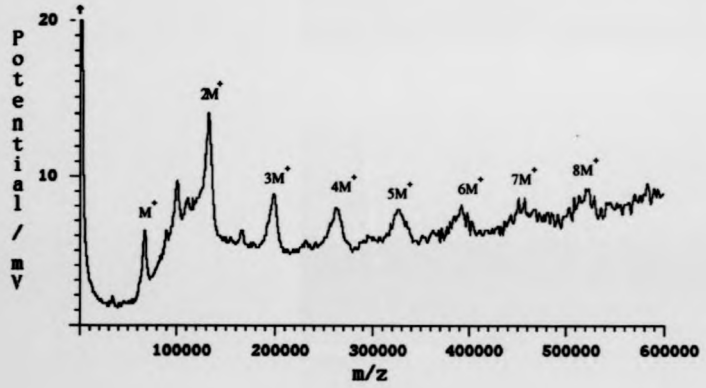

of different initial divergences and velocities. Therefore, a positive correlation between the extraction potential and the ion signal intensity is expected. Figures 4.16 and 4.17 show series of time-of-flight mass spectra of insulin and lysozyme using 3-NBA as the matrix at different extraction fields. All spectra were recorded as an average of ten shots at the same laser energy and the same sample spot. A trend of decreasing analyte molecule-ion formation at increasing extraction potential was clearly demonstrated. At very high extraction potentials (>10 kV) analyte molecule-ion formation was quenched completely. The sequence of spectra acquisition did not alter this trend, although extraction potentials at which molecule-ion formation was maximised were shifted from ~3-4 kV to ~5-7 kV. This shift could be explained by the changes of analyte concentration with time within a sample. The analyte concentration was expected to increase with time because of the continuous loss of matrix molecules through sublimation.

For the limited number of proteins tested in this study, there seemed to be a correlation between the molecular mass of the analyte and the extraction potential at which analyte molecule-ion formation was quenched. The limiting-extraction-potentials (LEP), above which protein molecule-ion formation was completely quenched, were found to be ~11 kV, ~13 kV and ~15 kV for bovine insulin, cytochrome-C, and lysozyme respectively. For bovine albumin, molecule-ions could be detected at extraction potentials greater than 20 kV.

The effect of the extraction potential on the formation of analyte molecule-ions is attributed to a greater degree of surface distortion of the sample droplet at very high extraction potential. However, this does not explain the occurrence of different limiting-extraction-potentials for proteins of different molecular masses. The possibility of the direct evaporation of charged-droplets was investigated. Significant liquid surface distortion was only observed at a field strength of ~ 3×10^6 V m^{-1}. In

Figure 4.16

Positive-ion laser desorption time-of-flight spectra of bovine insulin (RMM = 5734) using 3-nitrobenzyl alcohol as the matrix at different potentials $|V_1-V_2|$.

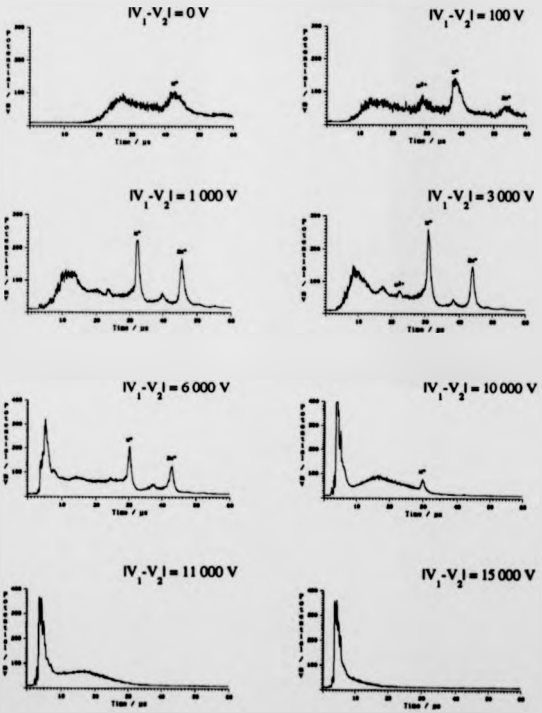

Figure 4.17
Positive-ion laser desorption time-of-flight spectra of chicken-egg white lysozyme (RMM = 14 314) using 3-nitrobenzyl alcohol as the matrix at different potentials $|V_1-V_2|$.

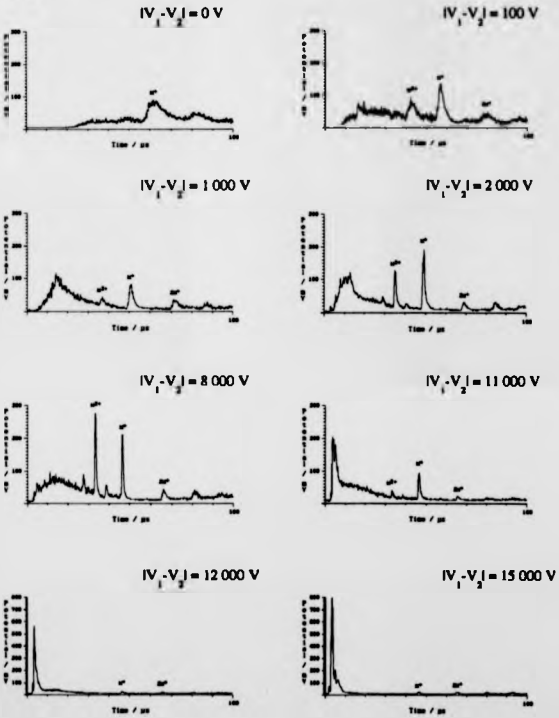

our experiments, there has been no direct evidence of the direct evaporation of charged-droplets, although the possibility cannot be excluded.

The effect of extraction field strength on the spectral characteristics for MALDI mass spectra does not contradict the proposed charge-transfer ionisation mechanism. The assumption that the desorption and ionisation of the analyte molecule are two individual steps implies the existence of a time-interval following the laser irradiation during which intermolecular interaction occurs. On reducing the extraction potential there could be a longer time interval in which the photochemically induced matrix-ions interact with the neutral analyte molecules. This proposal is consistent with the observation that matrix-ion intensities are lower at low extraction potentials. The limiting extraction potentials (LEP) for proteins of different masses could also be explained by changes in collision cross-section. The larger is the protein molecule, the larger is the collision cross-section and hence the higher is the limiting-extraction-potential for prohibiting molecule-ion formation.

5

KINETIC ENERGIES OF IONS

The generation of gaseous ions in matrix-assisted laser desorption / ionisation (MALDI) has been postulated to be a non-thermal and collective event, in which the matrix molecules play an important role. The processes of lattice disintegration and molecule-ion ejection are, however, not well understood. Studies of the initial kinetic energies and energy deficits of the matrix and analyte molecules and ions might provide insight into the dynamics of the ejection process. These properties also have an influence on the design and performance of any mass spectrometer to be used for MALDI.

A liquid matrix (3-nitrobenzyl alcohol) was used in the studies described below, because ion signals were more reproducible than those from solid matrices. Shot-to-shot reproducibility was particularly important for the experiments involving measurement of changes in ion intensities, such as the retardation-potential experiments.

5.1. MEASUREMENTS OF INITIAL VELOCITIES

5.1.1. Introduction

The initial kinetic energy (or initial velocity) distributions for both matrix and protein molecules / ions have been measured by a number of groups[76,80,92-94,119,181] and the results are summarised in Table 5.1. In general, the initial energies of ions measured using pulse-extraction techniques have been higher than those obtained through the measurements of time-shifts using high and zero extraction-fields. Initial kinetic energies of the neutral species have been found to be lower than those of the ionic species. It is, however, important to note that the initial kinetic energies and

Table 5.1
Summary of the literature results on initial kinetic energies (KE's).

Research group	Sample	Initial KE / eV	Energy Spread (FWHM)/ eV	Initial velocity / ms^{-1}
Positive-ions (UV)				
Spengler and Cotter[92]	Analyte : Tryptophan	1.0	--	--
Pan and Cotter[93]	Matrix : Nicotinic acid	0.6	0.8	1000 (700 -1300)
	Analyte : [Arg]-Vasopressin	5.6	13.5	1000 (400 - 1600)
Beavis and Chait[94]	Matrix : Sinapinic acid	1.5	1.8	1140 (825 - 1500)
	Analyte : Angiotensin	3.0	4.4	750 (485 - 1030)
	: Porcine insulin	16.7	14.5	750 (575 - 905)
	: Bovine superoxide dismutase	48.0	34.4	770 (655 - 925)
Ens and Standing[80]	Matrix : Sinapinic acid	--	--	--
	Analyte : Bovine insulin	--	50.0	--
Neutral Molecules (UV)				
Spengler et al[181]	Analyte : Tryptophan	0.4	--	--
Huth-Fehre and	Matrix : Ferulic acid	0.1	0.2	350 (200- 510)
Becker[76]	Analyte : Gramicidin-S	0.7	1.6	350 (200 - 550)
Positive-ions (IR)				
Pan and Cotter[93]	Analyte : Gramicidin-S$(+K)^+$	1.6	2.5	500 (300 - 700)

energy spreads have been found to increase with the masses of the protein ions. Converting to the scale of "velocity", it has been found that the initial velocities are similar for protein ions of different masses[94].

In this work, the initial velocities for both positive and negative protein molecule-ions produced from a liquid matrix (3-nitrobenzyl alcohol) were measured. Since the initial velocities for positive ions and neutral molecules had been found to differ from each other[76,94], it was of interest to compare the desorption velocities of negative ions with those of positive ions.

5.1.2. Experimental

The discrepancies among values obtained by different research groups can be attributed to the assumptions associated with the experimental methods. For instance, the pulse-extraction technique requires a highly reproducible ion signal. In practise, the ion signals produced from analytes embedded in solid matrices usually suffer from strong shot-to-shot fluctuation. The problem associated with signal reproducibility can be avoided by measuring the time-of-flight of the desorbed ions through a field-free path, co-axial with the ion-optical axis and located before the acceleration region. Comparing the ion flight-times under high and low extraction-fields, however, creates two different conditions for ion formation. In addition, any energy deficit associated with ions formed under high-field conditions will have an effect on the ion flight-time.

In the present study, the method of measuring ion flight-times through a field-free path co-axial with the ion optical axis was adopted. The problems with this method, discussed above, were avoided by using an additional grid-electrode placed at a very short distance from the sample stage. Maintaining this electrode at the same potential as the sample stage created a narrow field-free region with which ion generation could take place. Systematic variations of the potential at the second

grid-electrode should cause a gradual shift of the ion flight-times, depending on the initial ion velocities. The ion velocities were calculated by correlating the measured time-shifts with the values from analytical calculations.

The ion source was described in section 2.54. The sample stage was held either at +15 kV for positive-ion mode or -14 kV for negative-ion mode. The third electrode was set at ground. The electrical potential V_2 of the second grid-electrode was varied from 0 to 15 kV for positive-ion mode and 0 to -14 kV for negative-ion mode. Cytochrome-C (RMM = 12 354) was used as the analyte and 3-NBA was used as the matrix. A total of 10 pmol cytochrome-C was placed onto a 2 µl droplet of 3-NBA. The volatile solvent was allowed to evaporate by warming with an air gun before inserting into the spectrometer.

5.1.3. Results

Figures 5.1 and 5.2 show a series of positive-ion and negative-ion time-of-flight spectra of cytochrome-C at different potentials ($|V_1-V_2|$). V_1 is the sample-stage potential and V_2 is the potential applied to the second grid-electrode (see Figure 2.10). The molecule-ion flight-times were found to increase on decreasing the potential difference $|V_1-V_2|$. Using 3-NBA as the matrix, the relative intensities of the protein molecule-ion and its multiple-charged ions depend on the concentration of the protein in the 3-NBA droplet. The higher is the concentration of the protein, the higher are the intensities of the oligomers and the lower are the intensities of the multiple-charged ions. The spectral appearance for a particular sample is therefore expected to change progressively with the time of analysis, due to the evaporation of the 3-NBA. As a result, the relative ion signals in Figure 5.1 and 5.2 do not reflect only the changes in $|V_1-V_2|$.

Tables 5.2 and 5.3 and Figure 5.3 present results of three different sets of experiments. The negative-ions had longer flight-times than the corresponding positive-ions, because of differences in total ion-energy and responses to post-

Figure 5.1
Positive-ion laser desorption time-of-flight mass spectra of cytochrome-C at different potentials $|V_1-V_2|$ using 3-nitrobenzyl alcohol as the matrix.

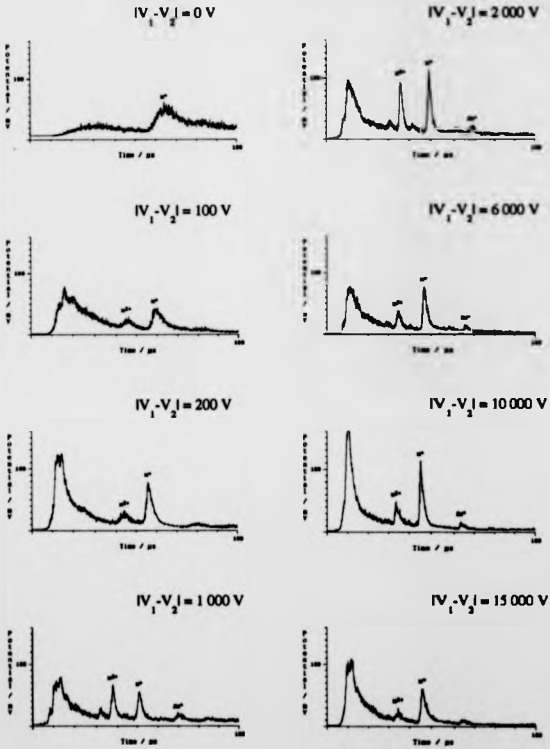

Figure 5.2
Negative-ion laser desorption time-of-flight mass spectra of cytochrome-C at different potentials $|V_1 - V_2|$ using 3-nitrobenzyl alcohol as the matrix.

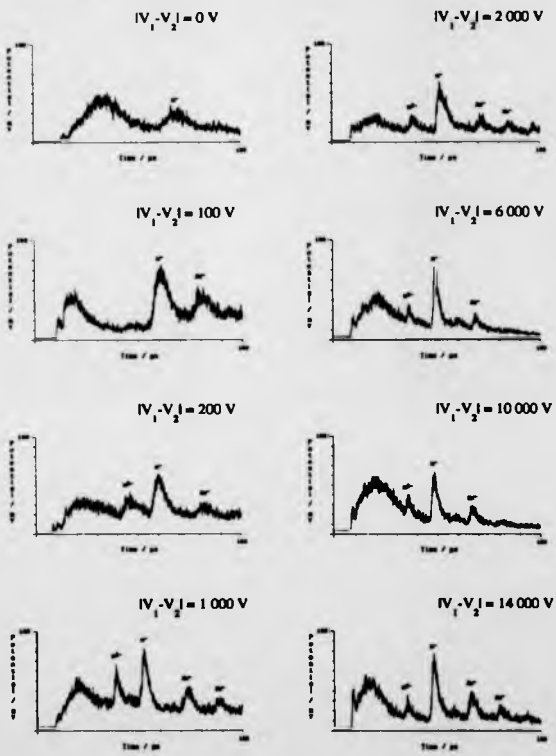

Table 5.2
Flight times of positive cytochrome-C molecule-ions at various potential differences $|V_1-V_2|$.

$\|V_1-V_2\|$ / volt	Time-of-flight / μs				Confidence limits (95%)
	Set 1	Set 2	Set 3	Average	
0	64.66	64.58	64.89	64.71	±0.40
20	62.31	62.32	62.25	62.29	±0.09
40	58.74	60.17	58.02	58.98	±2.72
60	57.94	57.06	57.85	57.62	±1.20
80	57.12	59.29	59.62	58.68	±3.37
100	58.80	58.41	59.51	58.91	±1.39
120	58.00	58.46	58.16	58.21	±0.58
140	58.06	57.99	57.55	57.87	±0.69
160	56.72	56.81	56.54	56.69	±0.34
180	56.19	57.13	56.75	56.69	±1.17
200	56.02	56.15	56.04	56.07	±0.17
220	55.47	55.30	55.00	55.26	±0.59
720	54.53	53.79	52.81	53.71	±2.14
1183	51.09	50.66	50.97	50.91	±0.55
2215	49.53	49.53	49.45	49.50	±0.11
4169	48.00	48.04	48.04	48.03	±0.06
6197	46.92	46.80	47.19	46.97	±0.50
8214	46.37	46.27	46.66	46.43	±0.50
10189	46.01	45.62	45.55	45.73	±0.62
12179	46.44	46.20	46.28	46.31	±0.30
14070	46.25	46.07	46.13	46.15	±0.23
15000	45.66	45.62	46.27	45.85	±0.91

Table 5.3
Flight times of negative cytochrome-C molecule-ions at various potential differences $|V_1-V_2|$.

$\|V_1-V_2\|$ / volt	Time-of-flight / μs				Confidence limits (95%)
	Set 1	Set 2	Set 3	Average	
0	70.01	68.17	67.92	68.70	±2.84
20	66.43	64.47	64.34	65.08	±2.91
40	64.97	64.72	64.08	64.59	±1.14
60	61.94	63.12	62.49	62.52	±1.47
80	61.88	60.06	62.30	61.41	±2.96
100	62.52	60.58	60.44	61.18	±2.89
120	59.69	59.65	58.72	59.35	±1.36
140	58.69	58.59	59.50	58.93	±1.24
160	59.03	59.41	59.52	59.32	±0.64
180	58.55	58.82	58.74	58.70	±0.34
200	59.27	60.11	58.88	59.42	±1.56
220	58.18	57.10	57.07	57.45	±1.57
740	54.65	54.65	54.65	54.65	±0.00
1234	53.25	52.46	52.26	52.66	±1.30
2191	51.47	51.57	51.89	51.64	±0.55
4218	49.69	49.63	49.55	49.62	±0.17
6263	48.93	49.18	49.06	49.06	±0.31
8228	48.26	48.27	48.39	48.31	±0.18
10223	48.34	48.63	48.48	48.48	±0.36
12203	48.18	47.93	48.10	48.07	±0.32
14000	48.08	48.06	47.90	48.01	±0.25

Figure 5.3
The effect of the potential difference between V_1 and V_2 on the flight times of cytochrome-C molecule-ion.

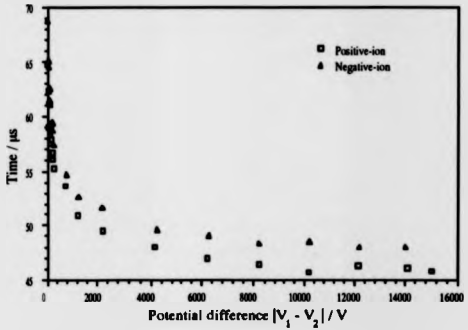

acceleration. Referring to the schematic diagram of the source lens (in Figure 2.10), T_1 and T_4 were assumed to be independent of the potential at the second grid-electrode under the present experimental conditions employed. The changes in the ion flight-times with changes in $|V_1-V_2|$ (Figure 5.1 and 5.2) are caused by the changes in T_2 and T_3.

Using the Equation 2.2 (section 2.5.3.), theoretical values of the ion flight-times ($T_2 + T_3$) at different potentials $|V_1-V_2|$ can be calculated for a particular initial velocity. When an appropriate value of u which corresponds to the initial ion velocity V_{ini} is used in calculating T_2 and T_3, there should be a unity correlation between the experimental times and the calculated values. Plotting the experimental times versus the calculated values should give a straight line with a gradient of one. The initial ion velocities V_{ini} were obtained using the above arguments.

The velocity u was systematically varied and used to calculate ($T_2 + T_3$) at different potentials $|V_1-V_2|$. The experimental times were correlated with each set of the results of these calculations. If the velocities u used in calculations are less than the initial ion velocity, the rate of change of the calculated values of $T_2 + T_3$ will be lower than that of the experimental times. The gradients of these correlation plots will therefore be less than unity. On the contrary, if u are higher than the initial ion velocity, the rate of change of the calculated values of $T_2 + T_3$ will be higher that that of the experimental times. The gradients of these correlation plots will be higher than unity. The gradients of these correlation plots together with their 95% confident limits were plotted against the corresponding velocity in Figures 5.4a and 5.4b for the positive-ion and negative-ion respectively. The initial ion velocities were identified at gradient values of one and were found to be 840 ± 70 ms^{-1} and 750 ± 40 ms^{-1} for the positive and negative molecule-ions of cytochrome-C respectively.

Figure 5.4
Dependence of the gradients of plots of experimental flight times against calculated values on initial velocity

a) Positive-ion

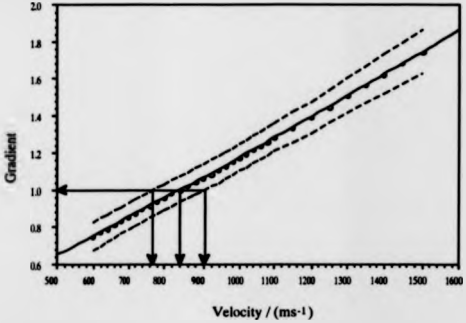

b) Negative-ion

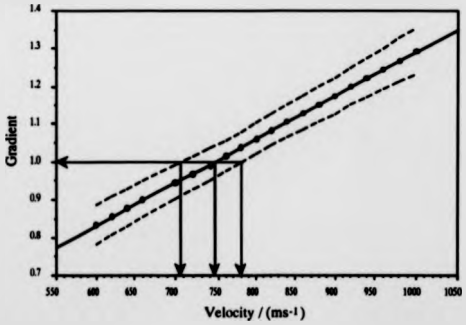

Figures 5.5a and 5.5b show the correlation plots of the experimental and the calculated flight times for the positive and negative molecule-ions of cytochrome-C. The error bars represent the 95% confident limits for each data point.

5.1.4. Discussion and conclusions

Huth-Fehre and Becker[76] reported that the initial velocities of the neutral matrix and protein molecules were around ~300-400 ms^{-1}. These figures are significantly lower than those found for the ionic species. Similarly, the initial velocity of the positive-ion[92] of tryptophan (kinetic energy = 1 eV or ~1000 ms^{-1}) was found to be higher than that of neutral molecules[181] (kinetic energy = 0.4 eV or ~600 ms^{-1}). These comparisons suggest that coulombic repulsive forces or space-charge effects may play a role in the overall desorption.

In the experiments described here, both the positive and negative cytochrome-C molecule-ions were generated under conditions of zero electric field. It has been found that molecule-ions of both polarities were formed with the same initial velocities within the experimental uncertainties. Recently, threshold laser fluences for the production of analyte molecule-ions using 3-NBA as the matrix have been measured[182]. The reported thresholds were identical for the positive and negative ions. These results were taken to imply that a cloud of neutral molecules and ions (both positive and negative) were generated upon laser irradiation. The existence of both positive and negative charges within such an expanding plume would imply that columbic repulsion is not a major contributor to the observed initial velocities.

Figure 5.5
Correlation between the experimental ion flight times and the calculated values for cytochrome-C (RMM - 12 3354).
(The error bar represent the 95% confident limits)

a) Positive-ion (Initial velocity = 840 ms^{-1})

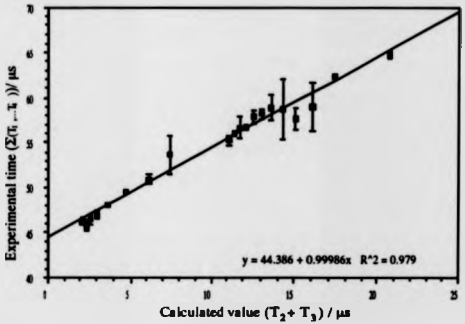

b) Negative-ion (Initial velocity = 750 ms^{-1})

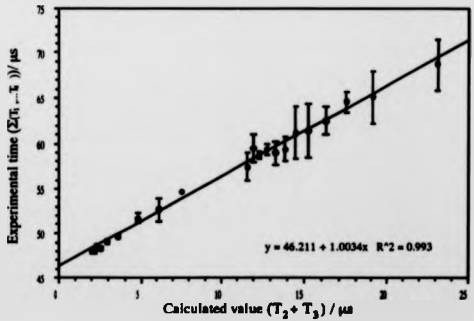

5.2. Measurements of Energy Deficit

5.2.1. Introduction

The energy deficit ΔE of a singly-charged ion formed in laser desorption / ionisation can be defined as $\Delta E = e(V_{sam}-V_{acc})$ (assuming zero initial ion kinetic energy). V_{sam} is the potential applied to the sample stage and V_{acc} is the potential through which the ion is actually accelerated prior to analysis. The enegy deficit is an important quantity as it must be related to the distance from the sample surface at which the ion is formed, whether in a condensed phase or in free space. The value at V_{acc} can be determined by using a grid-electrode to which a retardation potential V_{ret} is applied. In the experiments to be described, molecule-ion signals were monitored as a function of the retardation potential. There appears to have been no report in the literature concerning the existence of energy deficits associated with MALDI. The lack of such information might be a consequence of the inability to produce reproducible molecule-ion signals from different laser shots using solid matrices.

In this investigation, the effects of the masses of the analyte ions and of the sample-stage potential on the magnitudes of energy deficits were investigated. Bovine insulin (RMM = 5 734) and chicken egg-white lysozyme (RMM = 14 314) were used as analytes. The sample loadings were ~125 pmols, in each case. Liquid 3-NBA was employed as the matrix to achieve satisfactory reproducibility of molecule-ion signals. Sample-stage potentials of +3 000 V and +5 000 V were used. Caesium iodide was employed as a reference standard.

5.2.2. Experimental

The lens arrangement used was described in section 2.5.5. The sample stage was maintained at a static positive potential (for positive-ion mode) and the counter electrode was grounded. A positive retardation potential V_{ret} was then applied to the third electrode. This arrangement allows only ions with kinetic energies greater

than the retardation potential to be transmitted. Time-of-flight mass spectra were measured at different retardation potentials. Each of the time-of-flight mass spectra was recorded as an average of 10 single laser-shot spectra.

5.2.3. Results

5.2.3.1. Effect of analyte mass

Figure 5.6 shows a series of time-of-flight mass spectra of bovine insulin at various retardation potentials. There was no observable insulin molecule-ion signal at retardation potentials close to the sample-stage potential (i.e. 3 000 V). The insulin molecule-ion signal appeared when the retardation potential was reduced to 2 960 V. The signal intensity increased gradually with successive reduction of the retardation potential. The insulin molecule-ion signal ceased to increase at retardation potentials below −2 880 V.

The time-of-flight mass spectra of chicken egg-white lysozyme are shown in Figure 5.7. A gradual increase of lysozyme molecule-ion signals was observed on reduction of the retardation potential. Compared to the case of insulin, the lysozyme molecule-ion signal ceased to increase at a lower retardation potential, i.e. −2 700 V. Figure 5.8 show a series of caesium-ion Cs^+ time-of-flight spectra. Caesium-ion signal was clearly observed, even at retardation potentials above 3 000 V. The signal ceased to rise at retardation potentials below −2 900 V.

Tables 5.4-5.6 summarise the results obtained in the insulin, lysozyme and caesium iodide experiments respectively. Two separate series of experiments were performed. The total molecule-ion signal of an individual spectrum was calculated by multiplying the peak height and the full-width half-maximum (FWHM) of the ion signals (M^+) after proper signal smoothing. The results from the two series were averaged, and normalised with respect to the highest signal.

Figure 5.6
Time-of-flight mass spectra of bovine insulin at different retardation potentials (Vret). (sample-stage potential = 3 000 V)

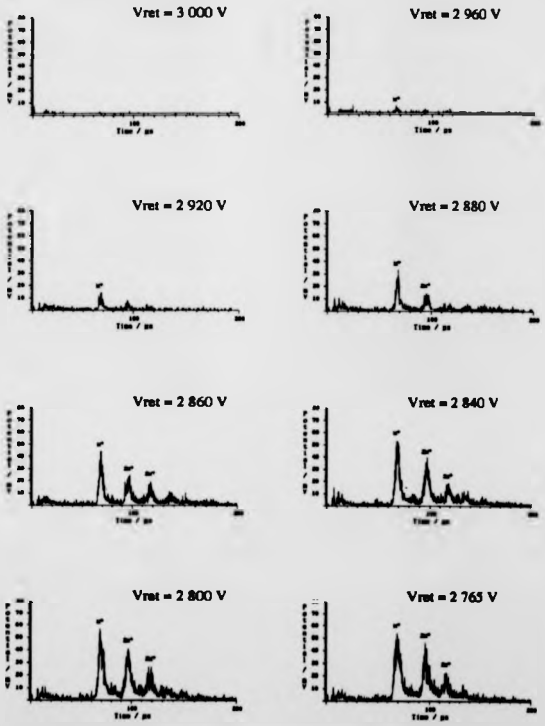

Figure 5.7
Time-of-flight mass spectra of chicken egg-white lysozyme at different retardation potentials (Vret). (sample-stage potential = 3000 V)

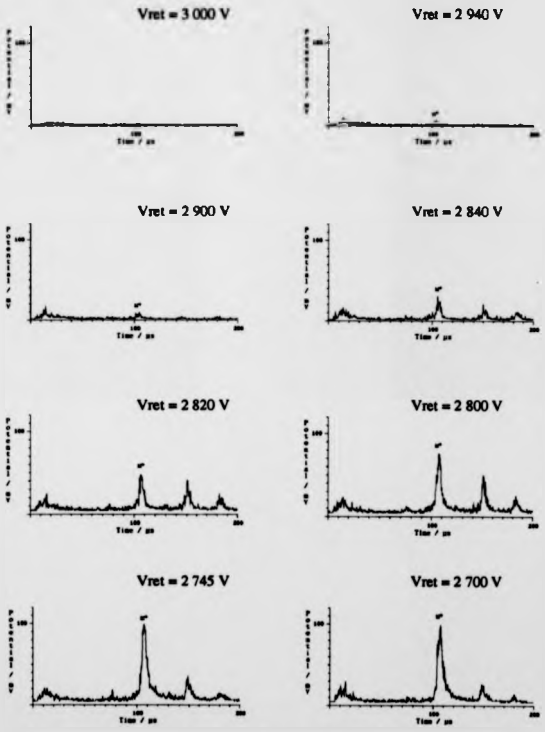

Figure 5.8
Time-of-flight mass spectra of caesium-ion at different retardation potentials (Vret). (sample-stage potential = 3 000 V)

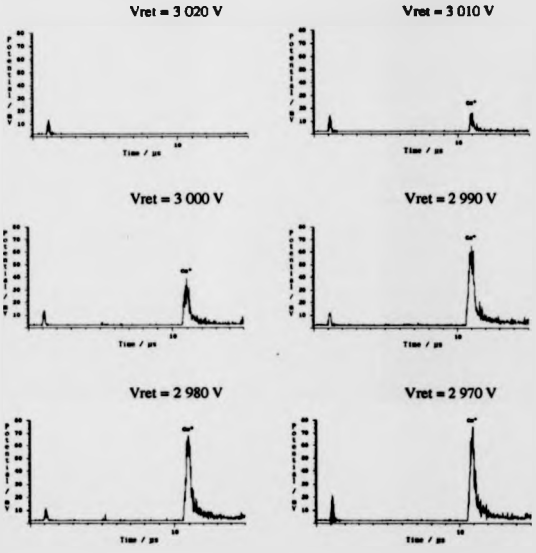

Table 5.4
Dependence of the insulin molecule-ion signals on the retardation potential (sample-stage potential = 3 000 V)

	Insulin molecule-ion signal				
Retardation Potential / V	Data 1	Data 2	Average	Normalised Value	Smoothed Value
3000	0.00	0.00	0.00	0.00	--
2980	3.03	6.28	4.65	1.78	1.94
2960	7.02	15.51	11.27	4.31	5.19
2940	21.76	35.49	28.63	10.96	11.00
2920	41.79	51.14	46.46	17.79	17.77
2900	49.57	78.66	64.12	24.54	25.67
2880	79.31	111.74	95.52	36.56	36.92
2860	128.66	133.94	131.30	50.26	52.26
2840	184.58	198.35	191.46	73.29	70.11
2820	202.79	223.02	212.91	81.49	82.39
2800	221.57	269.08	245.33	93.90	90.64
2780	243.04	232.96	238.00	91.10	94.24
2765	261.26	261.26	261.26	100.00	--

Table 5.5
Dependence of the lysozyme molecule-ion signals on the retardation potential (sample-stage potential = 3 000 V)

	Lysozyme molecule-ion signal				
Retardation Potential / V	Data 1	Data 2	Average	Normalised Value	Smoothed Value
3000	0.00	0.00	0.00	0.00	--
2980	4.05	0.00	2.02	0.39	0.22
2960	0.00	0.00	0.00	0.00	0.42
2940	16.22	0.00	8.11	1.56	1.59
2920	13.39	20.56	16.97	3.27	3.19
2900	23.53	24.49	24.01	4.62	5.05
2880	45.28	37.54	41.41	7.97	7.69
2860	55.35	48.88	52.11	10.03	11.68
2840	92.54	113.29	102.91	19.81	21.23
2820	174.79	201.91	188.35	36.25	38.22
2800	319.42	323.69	321.56	61.89	59.65
2780	393.46	407.62	400.54	77.09	76.71
2765	458.83	447.06	452.95	87.17	87.96
2750	450.96	588.26	519.61	100.00	94.44
2735	464.55	505.92	485.23	93.38	96.19
2720	478.15	525.61	501.88	96.59	95.58
2705	496.44	504.04	500.24	96.27	94.72
2690	415.99	524.60	470.29	90.51	89.48
2678	396.26	446.95	421.60	81.14	--

Table 5.6
Dependence of the caesium-ion signals on the retardation potential (sample-stage potential = 3 000 V)

Retardation Potential / V	Caesium-ion signal			Normalised Value	Smoothed Value
	Data 1	Data 2	Average		
3030	0.00	0.00	0.00	0.00	--
3020	0.00	0.00	0.00	0.00	2.85
3010	2.82	2.19	2.50	13.32	16.95
3000	8.06	8.34	8.20	43.57	49.09
2990	20.91	16.58	18.74	99.57	87.44
2980	17.89	19.35	18.62	98.93	99.30
2970	21.20	16.45	18.82	100.00	--

Figure 5.9 displays the normalised ion signals of insulin, lysozyme and caesium-ions as a function of the retardation potentials. The fitted curves shown in Figure 5.9 were derived through 7-point smoothing of the interpolated data (i.e. at an interval of 5 V). Data interpolation, prior to the 7-point smoothing, is essential in order that the data set has fixed voltage-intervals. Kinetic energy distributions for these molecule-ions at an sample-stage potential of 3 000 V were obtained by differentiating the curves (Figure 5.9). The results are summarised in Table 5.7 and displayed in Figure 5.10. Caesium-ions were found to have a relatively well-defined energy distribution (FWHM = 20 eV), whereas the energy distributions of insulin and lysozyme molecule-ions were found to spread over relatively large ranges of energy (FWHM ~ 90 eV). The mean energy deficit found in the case of the caesium-ion was ~ 5 eV. For insulin and lysozyme molecule-ions at a sample-stage potential of 3 000 V, the mean energy deficit were ~ 145 eV for insulin and ~ 190 eV for lysozyme molecule-ion.

5.2.3.2. Effect of the sample-stage potential

Figure 5.11 shows a series of time-of-flight mass spectra of bovine insulin (sample-stage potential = 5 000 V) at various retardation potentials. There was no observable signal for the insulin molecule-ion at retardation potentials above 4950 eV. The insulin molecule-ion signal appeared and progressively increased when the retardation potential was reduced to below 4940 V. The signal ceased to rise at a retardation potential of −4675 V. Table 5.8 summarises the results.

In Figure 5.12, the normalised ion signals of insulin molecule-ion are plotted against the apparent energy deficit (i.e. $V_{stage} - V_{ret}$). Results from insulin experiment at an sample-stage potential of 3 000 V are shown for comparsion. The fitted curve for 5 000 V data was derived from the 9-point smoothing of the interpolated data (5 V per division). The kinetic energy distributions for insulin molecule-ions at sample-stage potentials of 3 000 V and 5 000 V were calculated by differentiating the fitted-

Figure 5.9
The effect of retardation potential on the caesium, insulin and lysozyme molecule-ion signals. (sample-stage potential = 3 000 V)

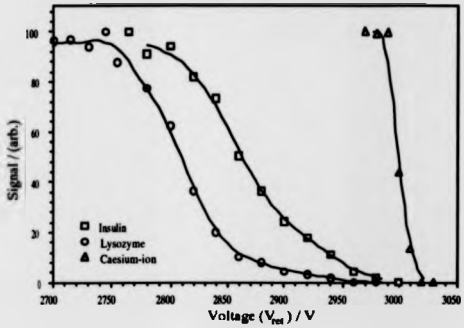

Figure 5.10
The energy distributions of caesium, insulin and lysozyme molecule-ions.
(sample-stage potential = 3 000 V)

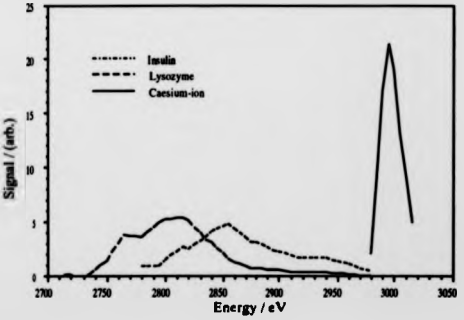

Table 5.7
Energy distribution of the caesium-ion, insulin and lysozyme molecule-ions at a sample stage potential of 3 000 V.

	Relative Intensity / (arb.)		
Energy / eV	Insulin	Lysozyme	Caesium-ion
3010	--	--	9.207
3000	--	--	19.120
2990	--	--	16.967
2980	0.526	0.014	2.008
2970	0.726	0.028	--
2960	1.073	0.112	--
2950	1.374	0.256	--
2940	1.681	0.406	--
2930	1.691	0.404	--
2920	1.699	0.389	--
2910	1.882	0.435	--
2900	2.253	0.552	--
2890	2.689	0.649	--
2880	3.185	0.699	--
2870	3.637	0.883	--
2860	4.424	1.342	--
2850	4.561	2.131	--
2840	4.169	3.158	--
2830	3.261	3.963	--
2820	2.502	5.096	--
2810	2.259	5.380	--
2800	1.472	5.291	--
2790	0.910	4.483	--
2780	0.871	3.612	--
2770	--	3.748	--
2760	--	2.958	--
2750	--	1.368	--
2740	--	0.582	--
2730	--	-0.502	--
2720	--	0.098	--
2710	--	-0.289	--
2700	--	-1.315	--
2690	--	-2.177	--

PAGINATION ERROR

P138

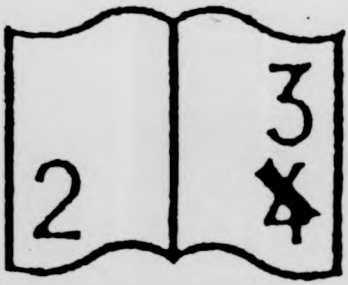

Table 5.8
Dependence of the insulin molecule-ion signals on the retardation potential (sample-stage potential = 5 000 V)

Retardation Potential / V	Insulin molecule-ion signal				Normalised Value	Smoothed Value
	Data 1	Data 2	Data 3	Average		
5000	0.00	0.00	0.00	0.00	0.00	--
4980	0.00	0.00	0.00	0.00	0.00	0.00
4960	2.83	0.00	0.00	0.94	0.31	0.68
4940	6.28	4.602	4.01	4.96	2.45	2.14
4920	3.11	9.09	10.77	7.66	3.79	4.87
4900	17.35	13.38	23.90	18.21	9.01	8.35
4880	21.44	15.80	34.84	24.03	11.88	12.26
4860	26.21	26.20	45.37	32.59	16.12	17.35
4840	46.24	35.15	68.93	50.11	24.78	23.40
4820	57.95	44.19	70.68	57.61	28.49	31.01
4800	79.51	64.35	106.48	83.45	41.27	40.56
4780	89.83	85.18	137.46	104.16	51.51	52.43
4765	127.27	95.17	151.93	124.79	61.71	61.77
4750	135.15	120.00	178.93	144.69	71.55	72.09
4735	176.35	145.00	189.17	170.17	84.15	80.20
4720	202.40	130.18	178.50	170.36	84.24	88.77
4705	204.21	175.73	226.75	202.23	100.00	92.59
4690	215.84	168.40	185.27	189.84	93.88	--
4675	224.04	165.29	161.41	183.58	90.78	--

Figure 5.12
The effect of retardation potential on the insulin molecule-ion signals at different sample-stage potentials. (V_{sam})

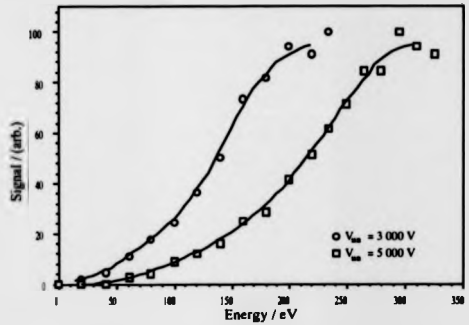

Figure 5.13
The energy distributions of insulin molecule-ions at different sample-stage potentials (V_{sam})

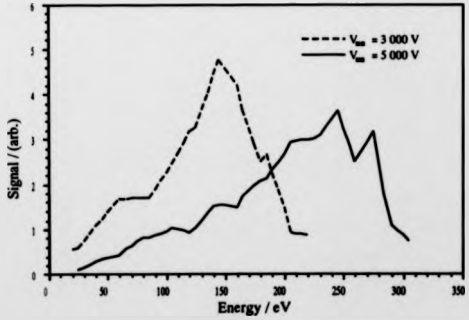

curves. The results are tabulated in Table 5.9 and plotted in Figure 5.13. The energy spreads for the insulin molecule-ion increased from 90 eV to 120 eV (FWHM) and the mean energy deficit increased from 150 eV to 250 eV, on increasing the sample-stage potential from 3 000 V to 5 000 V.

5.2.4. Discussion and conclusions

The process of laser ablation of a caesium-ion from a solid sample has been described using a thermal evaporation model[183]. The energy loss observed here (~5 eV) for the caesium-ion, extracted by a static field of 2.5×10^5 Vm^{-1}, is tentatively attributed to the potential drop across the crystal sample. For the protein molecule-ions, the factors causing the large energy deficits are not understood. Taking a constant initial velocity of 800 ms^{-1}, the initial kinetic energies would be higher for lysozyme molecule-ions (17.2 eV) than that of insulin (6.9 eV). For a constant sample-stage potential, the kinetic energies of the lysozyme molecule-ions after the full acceleration were, however, found to be lower than those of the insulin molecule-ions. The energy deficits found experimentally were roughly 160 eV for insulin and 210 eV for lysozyme molecule-ions at an sample-stage potential of 3 000 V, and 260 eV for insulin molecule-ion at an sample-stage potential of 5 000 V.

The effect of the analyte molecule-ion mass on the energy deficit can be considered by comparing the mass ratio of the analyte molecules to the corresponding energy deficit ratio. For a constant sample-stage potential of 3 000 V, a 2.50-times increase in the analyte mass (i.e. lysozyme / insulin) has resulted in ~1.32-times increase in the energy deficit. The effect of the sample-stage potential on the energy deficit can also be considered by comparing the sample-stage potential ratio to the corresponding energy deficit ratio. For insulin molecule-ions, an increase in the sample stage potential of 1.67-times (i.e. 5 000 / 3 000). has caused a similar increase in the energy deficit (~1.64-times).

Table 5.9
Energy distribution of the insulin molecule-ions at a sample-stage potential of 5 000 V.

Energy / eV	Relative Intensity / (arb.)	Energy / eV	Relative Intensity / (arb.)
4970	0.136	4820	2.072
4960	0.273	4810	2.298
4950	0.347	4800	2.661
4940	0.421	4790	2.958
4930	0.642	4780	2.991
4920	0.796	4770	3.081
4910	0.851	4760	3.445
4900	0.936	4750	3.253
4890	0.990	4740	2.504
4880	0.935	4730	2.942
4870	1.191	4720	2.468
4860	1.513	4710	1.081
4850	1.521	4700	0.844
4840	1.492	4690	--
4830	1.844		

Although the origin of the energy deficits for the desorbed analyte molecule-ions in matrix-assisted laser desorption / ionisation is not well understood, several factors can be suggested. Potential drops across the sample droplet would certainly cause an energy deficit, however the differences in the energy deficits for analyte-ions of different masses at the same sample-stage potential could not readily be accounted for. Delay in molecule-ion generation is another possibility. If charge-transfer between matrix-ions and desorbed macromolecules took place after a delay time following the desorption process, the analyte molecule would presumably become charged at a distance above the sample surface due to the initial velocities of the matrix and analyte molecules. The formation of analyte molecule-ions above the sample surface would lead to an energy deficit which would be proportional to the extraction field. For the retardation experiments using a 3 kV sample-stage potential (extraction field ~ 2.5×10^5 Vm^{-1}), the distances from the surface at which the molecule-ion formation would have to occur would be ~0.66 mm for insulin and ~0.86 mm for lysozyme. For the retardation experiments using a 5 kV sample-stage potential (extraction field ~ 4.17×10^5 Vm^{-1}), the distance from the surface at which the insulin molecule-ion formation would have to occur would be ~0.59 mm. Taking a constant initial ion velocity of 800 ms^{-1}, the delay times of ion formation would be 0.83 μs and 1.08 μs for insulin and lysozyme respectively at 3 kV sample-stage potential, and 0.74 μs for insulin at 5 kV sample-stage potential.

Metastable decay of the molecule-ions formed in MALDI has been reported[71,184]. As the parent ion decays, part of its kinetic energy will be lost as the translational energy of the neutral fragment. The resulting ion (daughter-ion) will then suffer from an energy deficit. Reports in the literature have concerned metastable decay of protein-ions in MALDI through losses of small neutral fragment(s) such as water or ammonia. For the lysozyme molecule-ion, loss of an ammonia molecule after the full acceleration through 3 kV will give rise to an energy loss of only ~4 eV. In order to account for the large energy deficits observed here,

the neutral fragment losses would have to be at least ~300 Da and ~1000 Da for the fully accelerated insulin and lysozyme molecule-ions respectively. Losses of such large fragments would be expected to require considerable amounts of internal energy within the analyte molecule-ions. Nevertheless, this possibility cannot be excluded. It is emphasised that to date independent experimental data on the subject of metastable decay in MALDI experiment is available only in the cases of solid matrices.

Another possibility is that gaseous matrix-analyte cluster-ions could be formed during the desorption process and subsequent evaporation of matrix molecules could occur. Analogous to the metastable decay, this process would produce analyte molecule-ions with energy deficits after acceleration. The notion of forming matrix-analyte cluster-ions does not violate the experimental observations. A larger energy deficit for lysozyme molecule-ions as compared to the insulin molecule-ion would be consistent with their capacities to accommodate small molecules, such as matrix molecules. Energy deficits arising in this way would also be expected to increase in proportion to the sample-stage potential.

6

CHARGING PROCESSES

6.1. INTRODUCTION

Many research groups have studied the charging processes in MALDI[75,95,185], but the mechanism of ion formation is still not well understood. The problem lies mainly with the difficulties in understanding the complex matrix-to-analyte interactions. Empirically, analytes of different hydrophilicity and hydrophobicity have been analysed successfully using MALDI. Both acidic and basic organic molecules have been found to be effective as matrices in UV-MALDI. In the present study, the relationships of the ground-state solution-phase acidity and gas-phase proton affinity on the ionisation efficiency of matrix-assisted laser desorption / ionisation have been studied.

The matrices, sinapinic acid and thiourea (Figure 6.1), were selected for study on the basis that these two matrices were unlikely to exhibit the same specific matrix-peptide interactions. The ionisation of a peptide is likely to be associated with the availability of protonation or deprotonation sites, i.e. acidic or basic amino acid residues, hence the peptides were selected on the basis of their amino acid compositions. Table 6.1 gives the amino acid compositions of the peptides studied. The amino acids are arranged in descending order of their standard solution acidities. The group of six peptides used in the present study consisted of two acidic, two neutral and two basic peptides. These subdivide into two groups of three peptides, one of which has molecular masses of roughly 1000 and the other of above 3500 daltons. The possible effects of competition between peptides of different acidities on ionisation probabilities were assessed by investigating equal molar mixtures of pairs of peptides.

Figure 6.1
Structures of sinapinic acid and thiourea.

Sinapinic acid (RMM = 224.14)

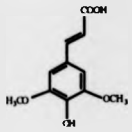

Thiourea (RMM = 76.12)

Table 6.1
Amino acid compositions and relative acidities of the peptides used to probe the relevance of solution acid/base properties to understanding MALDI. (* is used to indicate the number of amino acid within the peptide)

Compound Name		Epidermal-F (Acidic)	LHRH (Neutral)	Lys--Arg (Basic)	Pro-Kin-C (Acidic)	Insulin-B (Neutral)	Vaso-Int-Pep (Basic)
Molecular Weight		1376.5	1182.3	1006.2	3354.7	3495.5	3467.1
Catalogue No.		E1886	L7134	L 4772	P2303	I6383	V9129
	pKa						
Aspartic acid	2.77	***			**		*
Glutamic acid	3.24	*	*	*	******	**	
Cysteine	5.02					2*(SO_3H)	
Pheylalanine	5.40				**	***	
Asaparagine	5.41				*	*	***
Glutamine	5.65				**	*	*
Tyrosine	5.66	*	*		*	**	***
Serine	5.68		*		*	*	*
Methionine	5.74				**		*
Tryptophane	5.89		*				
Valine	5.96	**			*	***	*
Glycine	5.97		**	*	**	***	
Leucine	5.98	*	*		****	****	***
Alanine	6.01	*			**	**	*
Isoleucine	6.02	*			*		*
Threonine	6.16					*	**
Proline	6.30	*	*	*	*	*	**
Histidine	7.59		*	*	*	**	
Lysine	9.82			**		*	****
Arginine	10.76		*	**		*	****
-NH_2		*	*		*		*

Epidermal-F : Epidermal Growth Factor Receptor
Pro-Kin-C : Protein Kinase-C fragments (530-558)

LHRH : Luteinising Hormone Releasing Hormone
Vaso-Int-P : Vasoactive Intestinal Peptide

Lys--Arg : Synthetic peptide

Information as to the gas-phase proton affinities is not currently available for most of the useful matrices. The effect of gas-phase proton affinity on the ionisation efficiencies was investigated by varying the nature of peptide molecules. Table 6.2 gives the amino acid composition of the peptides selected. The amino acids are arranged in descending order of gas-phase proton affinities[186]. As with the acid/base experiment, six peptides, comprising two sets of three peptides of different molecular masses, i.e. ~1000 and 3500 daltons, were selected. Peptides used in the acid/base experiments, were also used in the proton affinity experiments, if they possessed the appropriate amino acid residues.

6.2. Experimental

The standard lens assembly described in section 2.2.2. was employed. The sample probe was held at +18 kV with respect to the grounded counter electrode. Since the molecular masses of the peptides used in this study were relatively low, an on-axis electron multiplier was used to improve the mass resolution.

Matrices were purchased from Aldrich Chemical Company[165]. Apart from glucagon, all peptides were supplied by Sigma Chemical Company[187]. Glucagon was purchased from Boehringer Mannheim U.K.[188]. Sinapinic acid was dissolved in a 2 : 3 mixture of acetonitrile and deionised water; as thiourea was dissolved in deionised water. The solution concentration was 0.05 mol dm^{-3} in each case. Each peptide was dissolved in deionised water to give a concentration of 2×10^{-5} mol dm^{-3}. No acid or base was added to change the pH. The experiments were divided into two sets: the first was laser desorption / ionisation of single peptides, and the second involved mixtures of two peptides, i.e. equi-molar mixtures of a low-mass and a high-mass peptide. For single-peptide experiments, samples were prepared by mixing 10 µl of the matrix and 10 µl of the peptide solution in a sample vial. 2 µl of the resulting mixture were applied to a 2 mm diameter sample probe-tip and dried under a stream of warm air. A peptide loading of 10 pmol was, therefore, used. For two-peptide

Table 6.2

Amino acid compositions and relative proton affinities (P.A.) of the peptides used to probe the relevance of gas-phase proton transfer to understanding MALDI. (* is used to indicate the number of amino acid within the peptide)

Compound Name	Buccalin (Low P.A.)	LHRH (Medium P.A.)	Lys--Arg (High P.A.)	Insulin-B (Low P.A.)	Glucagon (Medium P.A.)	Vaso-Int-P (High P.A.)
Molecular Weight	1053.2	1182.3	1006.2	3495.5	3482.8	3467.1
Catalogue No.	B 4528	L7134	L 4772	I6383	11423823-01	V9129
Glycyl	•••	•	•	•••	•	
Alanyl	•			••	•	•
Cysteinyl				$2^*(SO_3H)$		
Seryl	••	•		•	••••	•
Aspartyl	•				•••	•
Valyl				•••	•	•
Leucyl	••	•		••••	••	•••
Threonyl				•	•••	••
Isoleucyl						•
Phenylalanyl	•			•••	••	
Methionyl	•				•	•
Tyrosyl		•		••	••	•••
Glutamyl		•	•	••		
Asparaginyl				•	•	•••
Tryptophyl		•			•	
Prolyl		•	•	•		••
Glutaminyl				•	•••	•
Lysyl			••	•	•	••••
Histidyl		•	•	••	•	
Arginyl		•	••	•	••	••••
$-NH_2$	•	•				•

LHRH : Luteinizing Hormone Releasing Hormone Vaso-Int-P : Vasoactive Intestinal Peptide Lys--Arg : Synthetic peptide

experiments, samples were prepared by mixing 5 µl of each peptide solution with 10 µl of the matrix solution in a sample vial. 2 µl of the resulting mixture were applied to a 2 mm diameter sample probe-tip and dried under the same conditions. A total sample loading of 5 pmol of each peptide was, therefore, used.

6.3. Results

The spectra presented were averaged over 20 single laser-shots to reduce effects of signal fluctuation and to improve the signal-to-noise ratio. Special attention was paid to maintaining constant experimental conditions, in particular the sample preparation method and the time which the samples spent in the vacuum prior to the analysis. It was known that the intensity of a peptide molecule-ion signal would depend strongly on the laser fluence and also on the sampling position. Thus in each case, the laser fluence was carefully adjusted to optimise the molecule-ion signal at a particular sample position. The problem of variation in the peptide signal from one sample position to another was alleviated by taking a number of spectra at various sample positions. For the samples containing two peptides, the signals of both peptide molecule-ions were optimised. Individual spectra presented in this thesis have been selected as being representative of the sample in question. To facilitate comparisons, the raw spectra are presented with time-scales rather than mass-scales. No background subtraction or data smoothing was performed on the data. To facilitate comparisons, some of the time-of-flight spectra appear in more than one Figure.

6.3.1. Single-peptide systems

6.3.1.1. Relationship of solution-phase acidity to the ionisation efficiency of MALDI

Figures 6.2 and 6.3 show the positive-ion laser desorption time-of-flight mass spectra of the peptides shown in Table 6.1, using sinapinic acid as the matrix. In the case of the low-mass peptides (~1000 daltons), the peptide molecule-ion signal is

Figure 6.2
Positive-ion laser desorption time-of-flight spectra of low-mass peptides (~1000 daltons) using sinapinic acid as the matrix.

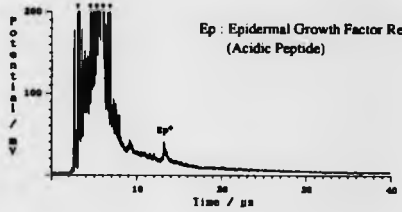

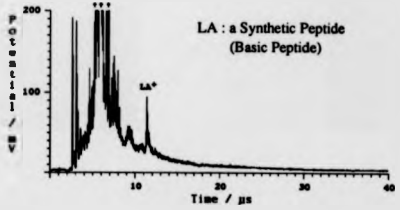

Figure 6.3
Positive-ion laser desorption time-of-flight spectra of high-mass peptides (~3500 daltons) using sinapinic acid as the matrix.

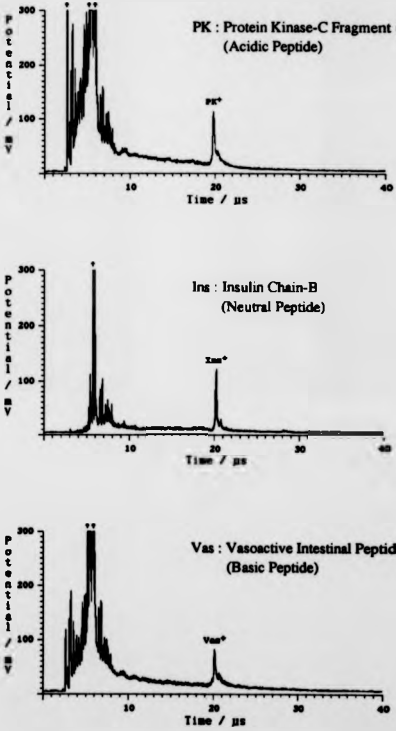

stronger for the basic peptide than for the acidic peptide (Figure 6.2). The molecule-ion signal intensity for luteinising hormone releasing hormone (LHRH) (not shown) was similar to that of epidermal growth factor receptor (Ep). In the case of the high-mass peptides (~3500 daltons), a slight decrease in the molecule-ion signal intensity was observed for the basic peptide as compared to the acidic or neutral peptides (Figure 6.3).

Figures 6.4 and 6.5 show the corresponding sets of time-of-flight mass spectra using thiourea as the matrix. For the low-mass peptides (Figure 6.4), the molecule-ion signals obtained using the thiourea matrix were nearly twice the intensity of those obtained using the sinapinic acid matrix in absolute terms. Comparing the peptide molecule-ion signals with thiourea, the basic peptide exhibited a higher sensitivity than the acidic peptide (as was the case when sinapinic acid was used). In the case of the thiourea matrix, the signal intensity for the neutral peptide was very high. For the high-mass peptides (Figure 6.5), the molecule-ion signals obtained using the thiourea matrix were similar to those obtained using sinapinic acid in absolute terms. There was no observable enhancement of sensitivity on moving from sinapinic acid to thiourea. Comparing the relative molecule-ion signal intensities when using thiourea as the matrix, there was little discrimination observed in the ionisation efficiency between peptides of different acidities.

6.3.1.2. Relationship of gas-phase proton affinity to the ionisation efficiency of MALDI

Figures 6.6 and 6.7 show the positive-ion laser desorption time-of-flight mass spectra of peptides of different proton affinities using sinapinic acid as the matrix. For the low-mass peptides (Figure 6.6), the peptide molecule-ion signal was stronger for high proton affinity peptides than low proton affinity peptides. The molecule-ion signal intensity for the luteinising hormone releasing hormone (LHRH)

Figure 6.4
Positive-ion laser desorption time-of-flight spectra of low-mass peptides (~1000 daltons) using thiourea as the matrix.

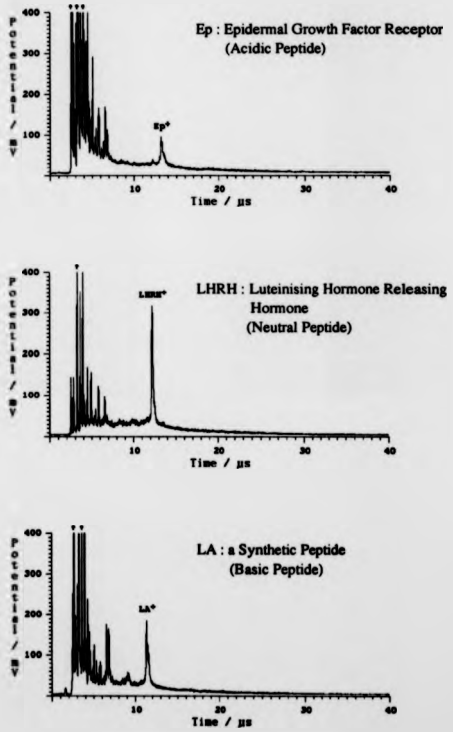

Figure 6.5
Positive-ion laser desorption time-of-flight spectra of high-mass peptides (~3500 daltons) using thiourea as the matrix.

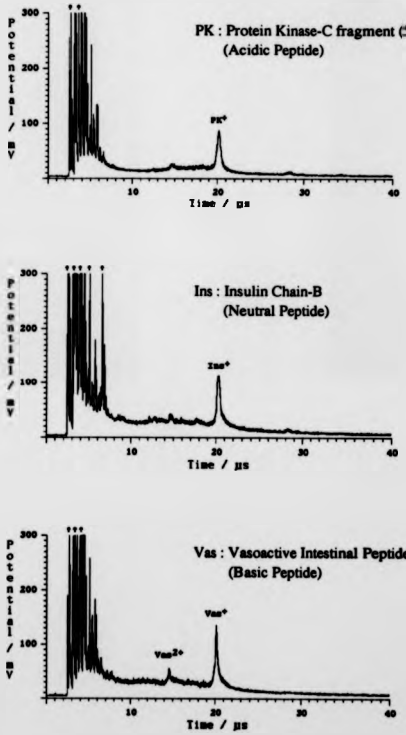

Figure 6.6
Positive-ion laser desorption time-of-flight spectra of low-mass peptides (~1000 daltons) using sinapinic acid as the matrix.

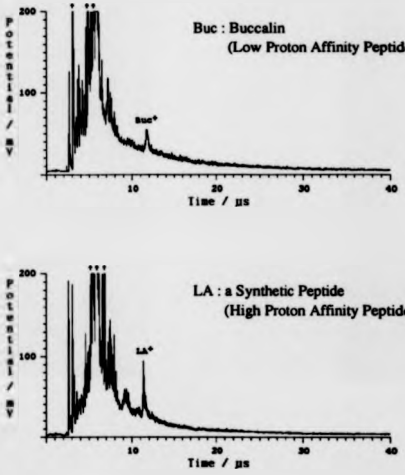

Figure 6.7
Positive-ion laser desorption time-of-flight spectra of high-mass peptides (~3500 daltons) using sinapinic acid as the matrix.

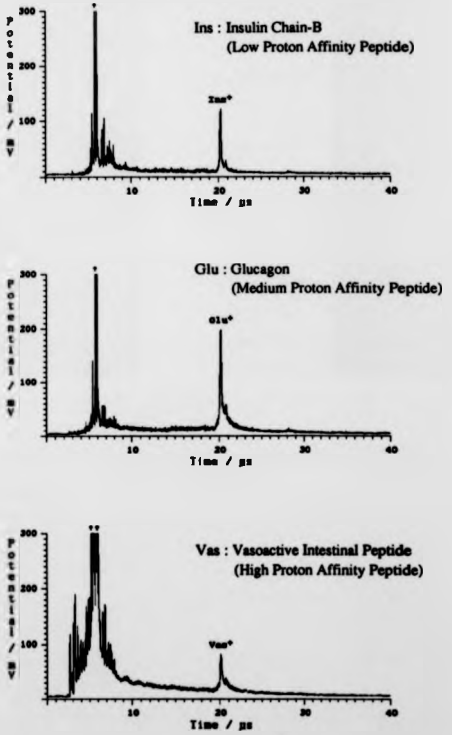

(not shown) was similar to that of buccalin. Among the high-mass peptides (Figure 6.7), the medium proton affinity peptide (glucagon) had the strongest molecule-ion signal, whereas the peptide of highest proton-affinity (vasoactive intestinal peptide) gave the weakest molecule-ion signal.

Figures 6.8 and 6.9 show the corresponding set of time-of-flight mass spectra using thiourea as the matrix. For the low-mass peptides (Figure 6.8), the highest proton-affinity peptide exhibited a higher sensitivity than the low proton-affinity peptide (as was the case when sinapinic acid was used). The medium proton-affinity peptide (LHRH) gave the highest sensitivity. For the high-mass peptides (Figure 6.9), there was little or no discrimination in the ionisation efficiency among peptides of different proton affinities using thiourea as the matrix.

6.3.1.3. Discussion

From the above results, it is concluded that the intensity of the peptide molecule-ion depends largely on the specific combination of matrix and peptide. For the low-mass peptides, the basic peptide and high proton-affinity peptide gave stronger molecule-ion signals than the acidic peptide and low proton-affinity peptide respectively. It is, however, important to realise that these observations could be due in some part to characteristics of the particular commercial samples. For instance, all attempts to analyse glucagon samples supplied by Sigma Chemical Company failed, whereas the same peptide supplied by Boehringer Mannheim U.K. gave an excellent molecule-ion signal under identical experimental conditions. The notion that basic or high proton-affinity peptides can be ionised more efficiently in positive-ion mode is further dispelled by the strong dependence of signals for the neutral or medium proton-affinity peptide (luteinising hormone releasing hormone) on the identity of the matrix. Moreover, thiourea, which is a less acidic matrix than sinapinic acid, seemed to generate stronger peptide molecule-ion signals in general (compare Figure 6.2 with Figure 6.4, and Figure 6.6 with Figure 6.8). This might

Figure 6.8
Positive-ion laser desorption time-of-flight spectra of low-mass peptides (~1000 daltons) using thiourea as the matrix.

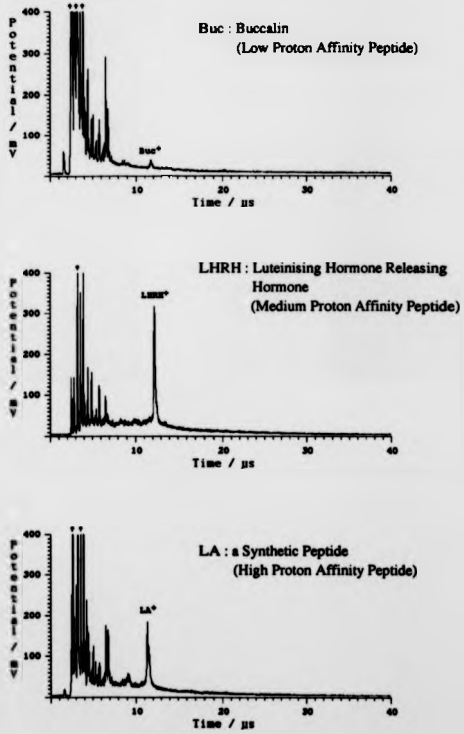

Figure 6.9
Positive-ion laser desorption time-of-flight spectra of high-mass peptides (~3500 daltons) using thiourea as the matrix.

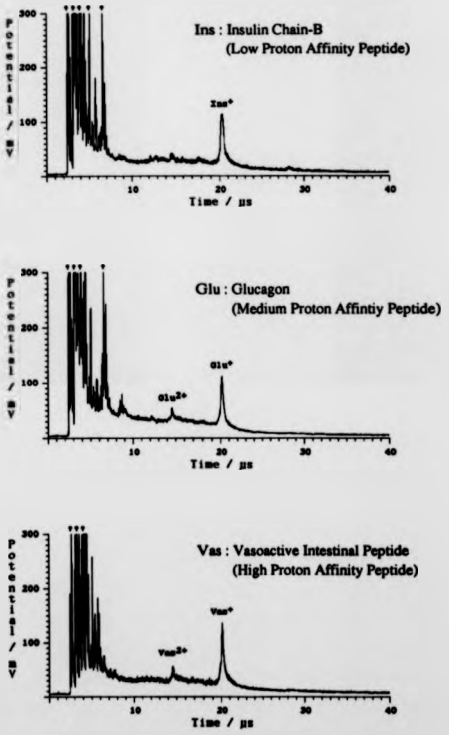

imply a larger cross-section for proton transfer with the thiourea matrix than with the sinapinic acid matrix.

For the high-mass peptides, there is little or no dependence of the peptide molecule-ion signal on the chemical nature of the peptides. An important finding is that thiourea matrix produced uniform responses from peptides of different chemical properties, in contrast to sinapinic acid matrix.

It is also interesting to note that there was a higher tendency for peptides to form doubly-charged molecule-ions with thiourea as the matrix (Figures 5 and 9), as compared with spectra (Figures 3 and 7) using the sinapinic acid matrix. This is inconsistent with the notion[185] that a more acidic matrix gives a higher ionisation cross-section and stronger multiply charged molecule-ion signals. As an aside, the temporal profiles of the molecule-ion peaks were considerably broader when the thiourea matrix was used instead of the sinapinic acid matrix.

6.3.2. Two-peptide systems

As has been mentioned, the information which was deduced on the basis of absolute molecule-ion signal intensity could be affected by the peptide activity within the commercial sample. This problem could be avoided by using a two-peptide system, i.e. a mixture of equal molar amounts of two peptides with different chemical properties. The logic of this is that any effect of acid/base properties or proton affinities on the ionisation process would result in an enhancement of ionisation for one peptide and suppression of ionisation for the other peptide. The importance of acid/base properties and proton affinities can therefore be assessed by comparing the relative molecule-ion intensities of the two peptides observed from the single-peptide systems to the one observed from the two-peptide system. In order to facilitate comparisons, the two single-peptide spectra have been presented together with the corresponding peptide-mixture spectrum.

6.3.2.1. Relationship of solution-phase acidity to the ionisation efficiency in MALDI

Figures 6.10 to 6.11 show spectra obtained using sinapinic acid as the matrix. Figure 6.10 shows the spectra of epidermal growth factor receptor (Ep) (acidic peptide), vasoactive intestinal peptide (Vas) (basic peptide) and their equi-molar mixture. The relative molecule-ion signals in the time-of-flight spectrum of the peptide mixture were similar to the ratio of the signals in the two single-peptide spectra. This observation implies that there is no competition between these peptides as regards acquisition of charge. Figure 6.11 shows the spectra of a basic peptide (the synthetic peptide (LA)), an acidic peptide (protein kinase-C fragment (PK)) and their mixture. In this case, the molecule-ion signal of PK was suppressed in the presence of the basic peptide (LA).

Figures 6.12 to 6.14 show the corresponding time-of-flight spectra obtained using thiourea as the matrix. Without going into the details of each comparison, the preferential molecule-ion signal enhancement and suppression effects observed in the case of sinapinic acid matrix were not observed with thiourea. The ratios of the molecule-ion yields in the spectra of the individual peptides were qualitatively reproduced in the corresponding peptide-mixture spectra. This implies that the ionisation process in matrix-assisted laser desorption / ionisation (MALDI) cannot be correlated with the solution-phase acid/base properties of the peptides using thiourea as the matrix.

6.3.2.2. Relationship of gas-phase proton affinities to the ionisation efficiency of MALDI

Figures 6.15 to 6.16 show the results obtained with pairs of peptides using sinapinic acid as the matrix. In contrast to the results obtained in the study of acid/base effect, the time-of-flight spectra of the peptide mixtures gave rise to peptide ratios similar to those derived by corresponding single-peptide spectra. Figures 6.17 to 6.19 show the results obtained using thiourea as the matrix. These

Figure 6.10
Positive-ion laser desorption time-of-flight spectra of two individual peptides and their mixture using sinapinic acid as the matrix.

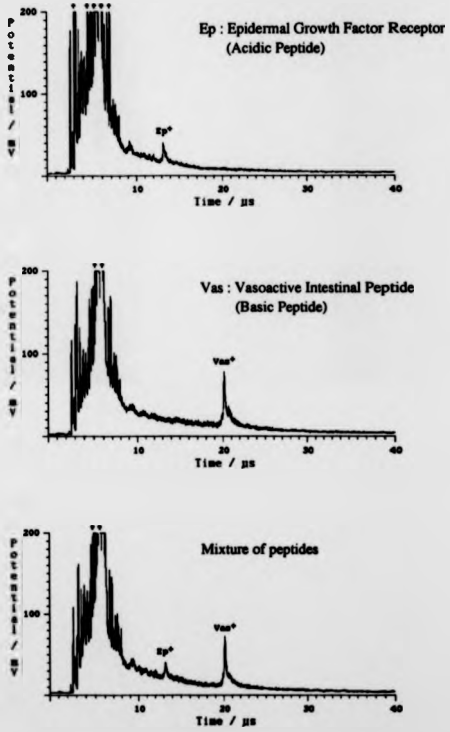

Figure 6.11
Positive-ion laser desorption time-of-flight spectra of two individual peptides and their mixture using sinapinic acid as the matrix.

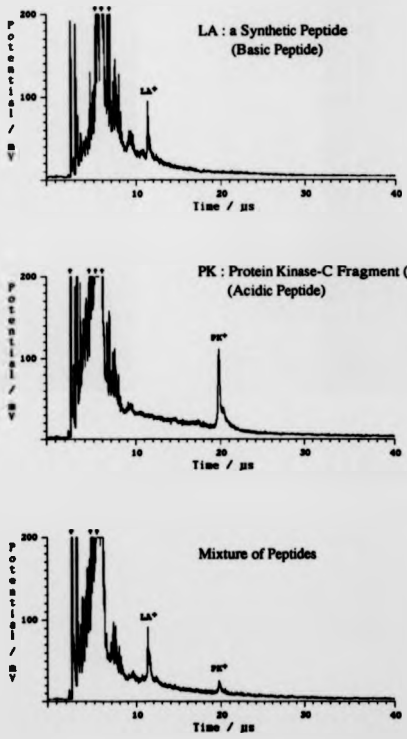

Figure 6.12
Positive-ion laser desorption time-of-flight spectra of two individual peptides and their mixture using thiourea as the matrix.

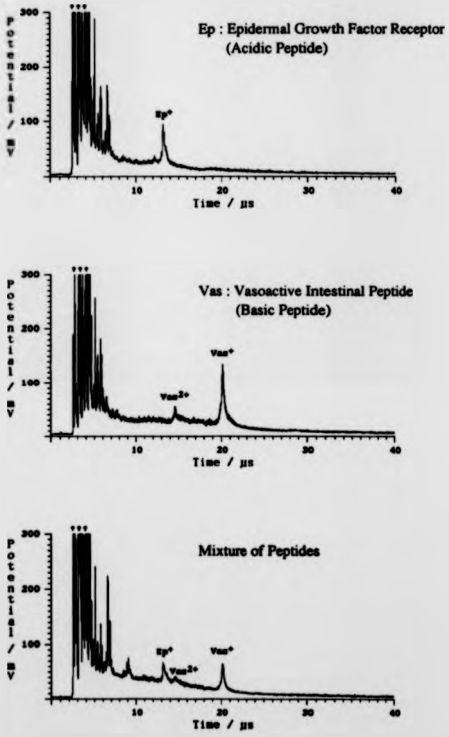

Figure 6.13
Positive-ion laser desorption time-of-flight spectra of two individual peptides and their mixture using thiourea as the matrix.

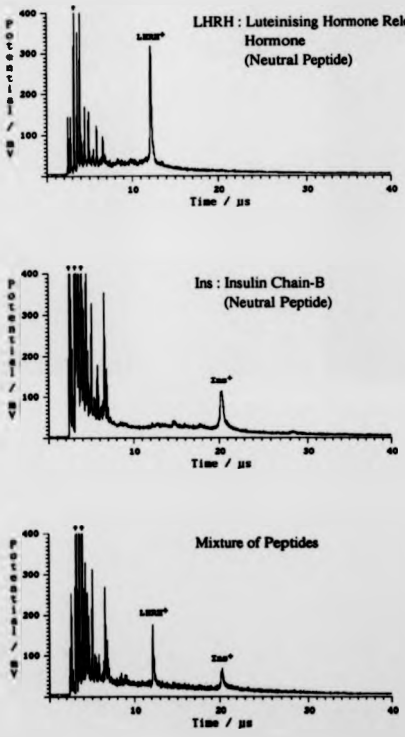

Figure 6.14
Positive-ion laser desorption time-of-flight spectra of two individual peptides and their mixture using thiourea as the matrix.

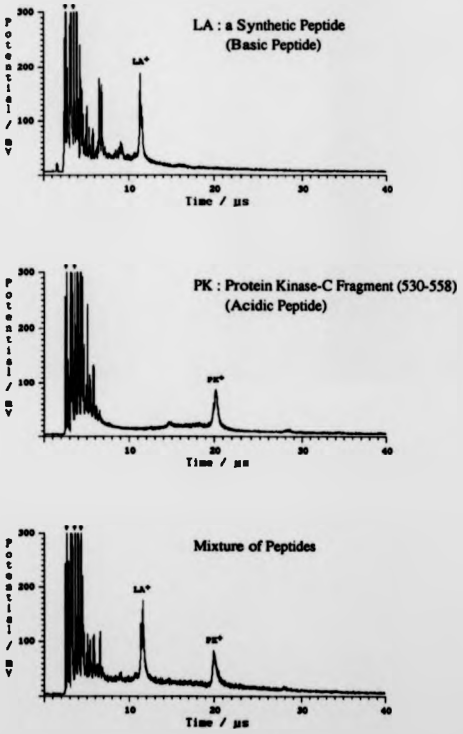

Figure 6.15
Positive-ion laser desorption time-of-flight spectra of two individual peptides and their mixture using sinapinic acid as the matrix.

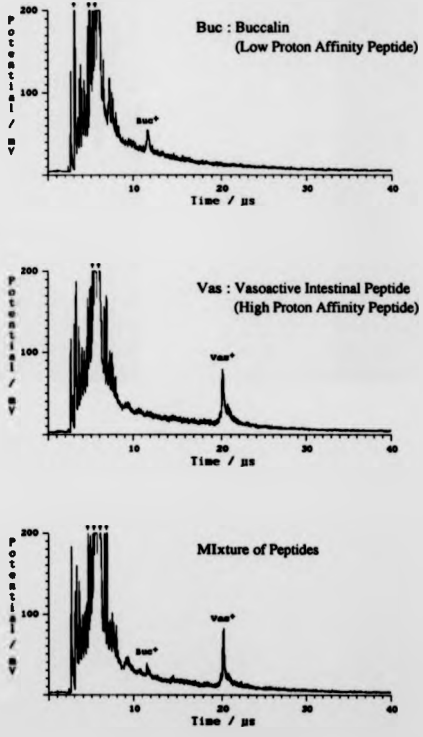

Figure 6.16
Positive-ion laser desorption time-of-flight spectra of two individual peptides and their mixture using sinapinic acid as the matrix.

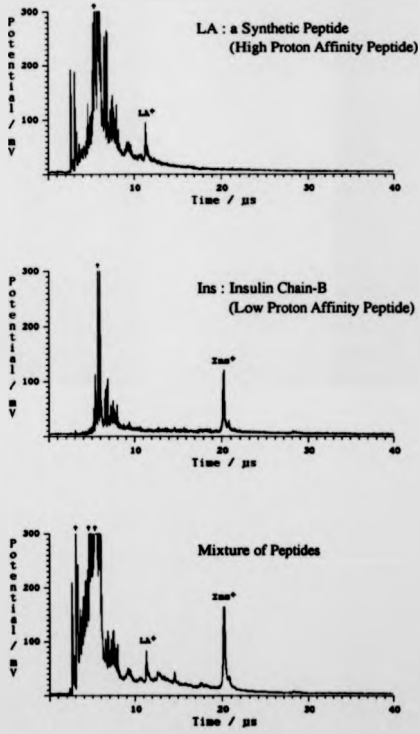

Figure 6.17
Positive-ion laser desorption time-of-flight spectra of two individual peptides and their mixture using thiourea as the matrix.

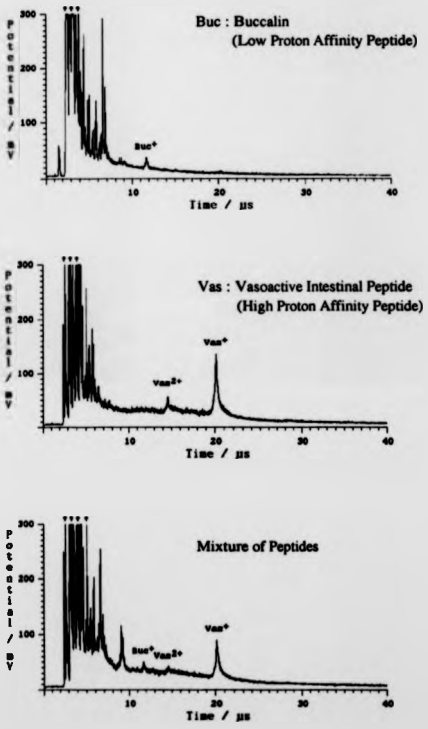

Figure 6.18
Positive-ion laser desorption time-of-flight spectra of two individual peptides and their mixture using thiourea as the matrix.

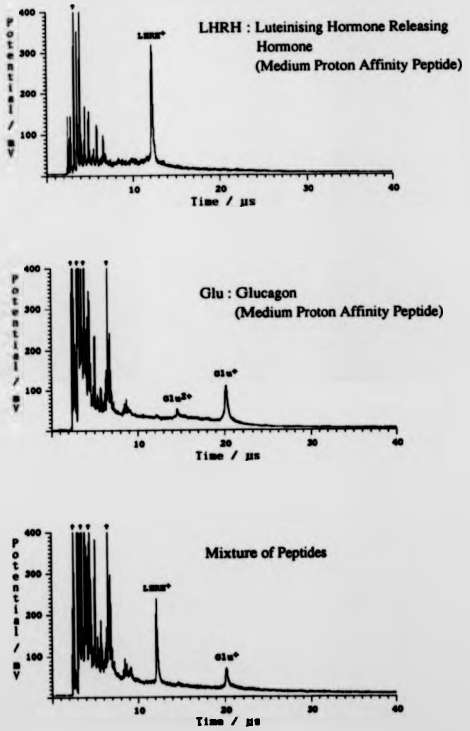

Figure 6.19
Positive-ion laser desorption time-of-flight spectra of two individual peptides and their mixture using thiourea as the matrix.

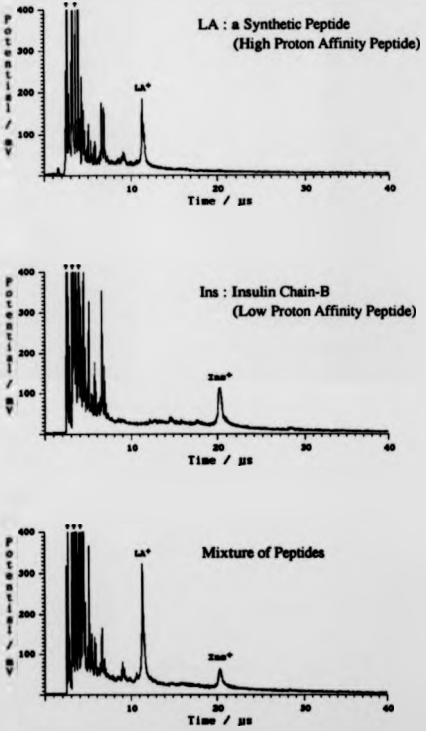

time-of-flight mass spectra of peptide mixtures again exhibit peptide ratios similar to those derived by corresponding single-peptide spectra. The only exception is shown in Figure 6.19. The response of the high proton-affinity peptide (synthetic peptide (LA)) seemed to be enhanced in the presence of the low proton-affinity peptide (Insulin chain-B (Ins)).

6.3.2.3. Discussion

It has been found that the ionisation process in matrix-assisted laser desorption / ionisation seems not to depend on the chemical properties of the peptide. It is tentatively suggested that the signal enhancement and suppression observed in Figures 6.11 using sinapinic acid as the matrix, were caused by specific matrix-peptide interactions rather than the formation of preformed ions in the solid crystals. This explanation is supported by the fact that these effects were not present in the corresponding experiments using thiourea as the matrix. The absence of these competitive effects in the proton-affinity experiments with the sinapinic acid matrix implies that such effects are not caused by gas-phase processes. It is tentatively suggested that specific matrix-peptide interaction may lead to an inhomogeneous distribution of peptide within the matrix crystal during sample preparation.

6.4. Discussion

In a typical matrix-assisted laser desorption / ionisation experiment, direct photoionisation of the analyte molecules is considered unlikely, because the laser fluences typically used are low and the concentrations of matrix molecules which are highly absorptive at the laser wavelength are high. This non-occurrence of direct photoionisation is consistent with the absence of radical analyte molecule-ions in MALDI spectra[69,71]. Most of the laser energy is expected to be absorbed by the matrix molecules resulting in a localised electronic excitation. It is generally believed

that some kinds of chemical or photo-chemical processes are responsible for the formation of protonated analyte molecules. From the present experimental results, it is concluded that the analyte solution-phase acid/base properties and gas-phase proton affinity have no direct relationship or influence on the analyte ionisation efficiency in typical matrix-assisted laser desorption / ionisation experiments. These conclusions have importance for the evaluation of the proposed ionisation mechanisms.

6.4.1. Ion-pair formation

The ion formation process of organic acids in ultra-violent laser desorption has been explained in term of ion-pair formation[189]. Analogous to the precusor model[190], which was originally proposed to explain the secondary ion emission in secondary ion mass spectrometry (SIMS) experiments, this mechanism involves the formation of a precusor of the finally emitted ion on the sample surface. Carboxylic acids and amino acids are known to crystallise from solutions in head-to-head lattice structures[191] and thus serve as precusors for the intermolecular proton transfers. The overall process for such a proton transfer can be written as :

$$2BH_{(s,g)} \xrightarrow{h\nu} BH_2^+{}_{(g)} + B^-{}_{(g)} \qquad (1)$$

This reaction can also be referred to as intermolecular proton transfer reaction or a disproportionation reaction. The overall energetics of ion-pair formation has also been considered theoretically[189]. Figure 6.20 illustrates the energy correlation diagram for the ionisation of an amino acid dimer. Assuming the most stable ground-state form of the dimer is the head-to-tail configuration, the minimum of the potential energy surface correlates with two uncharged amino acids at infinite separation (curve A). Therefore, a simple thermal process will cause the adiabatic separation of the amino acid pair resulting in two uncharged molecules. Curves B and C, which involve the formation of one and two zwitterions respectively, require more energy to sustain charge separation without solvation or association. Curve D corresponds to

Figure 6.28
Energy correlation digram for the ionisation of an isolated amino acid dimer.

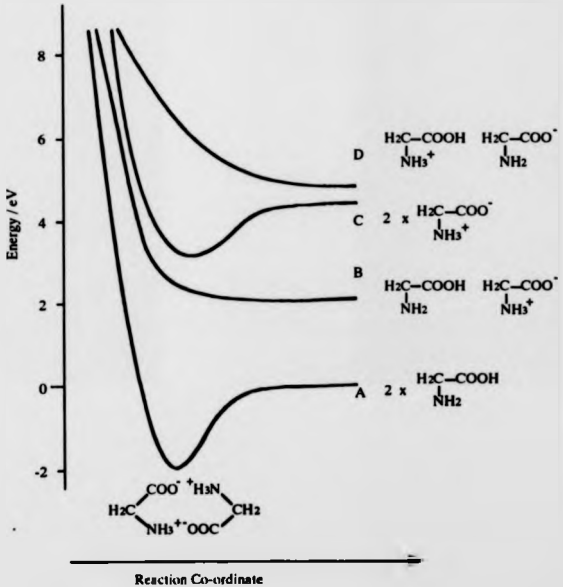

the separation of two ions corresponding to the protonated and deprotonated amino acids. This curve is also repulsive at the normal bonding distance. The photon energy at a wavelength of 266 nm is 4.6 eV; at 337 nm the energy is 3.7 eV. Absorption of one photon could not produce ions useful for mass spectrometry. Two or more photon absorption could, however, raise the system to curve D leading to the ion-pair formation.

This intermolecular proton transfer reaction has been applied[185] in an attempt to explain the ionisation of peptides in matrix-assisted laser desorption / ionisation. In this case, a proton is believed to transfer from a neutral matrix molecule to a neutral peptide molecule resulting in the simultaneous formation of a protonated-peptide and deprotonated-matrix molecules.

$$Matrix_{(s,g)} + Peptide_{(s,g)} \rightarrow [Matrix\text{-}H]^{\bullet}_{(g)} + [Peptide+H]^{+}_{(g)} \quad (2)$$

The energetics of the proton transfer process would be essentially the same as those of the amino acid dimer described. The relevance of the present work to this ionisation mechanism rests on the formation of the prerequisite solid-state precursor. Under the standard sample preparation method used in the present work, certain preferential matrix-analyte interactions could be expected to form in the crystallised sample. Peptides with predominantly acidic amino acid residues would be expected to bind better to a basic matrix than to an acidic matrix. Therefore, some general influence of the acid/base properties of the peptides and matrices is expected. The negative results obtained in the present study imply that intermolecular proton transfer is not the dominating charge-transfer process leading to the formation of the protonated analyte molecules in MALDI.

6.4.2. Random proton transfer reactions

Another ionisation model involves the laser-induced production of acidic and basic species which undergo subsequent ion-molecule reactions with the co-

desorbed neutral analyte molecules to form protonated and deprotonated molecule-ions. The steps in this mechanism are :

$$M_{(s)} + Peptide_{(s)} \xrightarrow{-----nh\nu---->} M_{(g)} + Peptide_{(g)} \qquad (3)$$

$$M_{(g)} + Peptide_{(g)} \xrightarrow{----------} [M\text{-}H]^-_{(g)} + [Peptide + H]^+_{(g)} \qquad (4)$$

$$M_{(g)} + Peptide_{(g)} \xrightarrow{----------} [M+H]^+_{(g)} + [Peptide - H]^-_{(g)} \qquad (5)$$

In this model, proton transfer reactions of the peptide proceed in the gas-phase after volatilisation. The extent of the proton transfer reaction is expected to be governed by the gas-phase proton affinity of the analyte for a particular matrix. Preferential charging is also expected for co-desorbed peptides possessing different amino acid residues. In the experiments reported here, it was however, demonstrated that there appears not to be a general trend for the chemical composition of a peptide to influence the ionisation efficiency. It is concluded that random gas-phase proton transfer reactions are not the dominating charge-transfer process in MALDI leading to the formation of the protonated analyte molecules.

6.4.3. Excited-state acid-base chemistry

Excited-state chemistry has been suggested[55,95] to play an important role in the analyte charging process. Since electronic excitation is usually accompanied by a modification of charge density within a molecule, acid-base properties of molecule in an excited state vary considerably from those of the ground state. The importance of excited-state chemistry on the ionisation processes in a typical MALDI experiment is, however, determined significantly by the lifetime of the excited-state of the matrix molecule. The rate of internal relaxation in the higher excited states (S_3-S_2 or S_2-S_1) of a typical aromatic molecule is usually within the picosecond range, which is likely to be much faster than any chemical processes involving the first-excited state. In addition, the fluorescence of first-excited state molecules is likely to take place on a time-scale comparable to charge transfer processes (~10 ns). The first-excited state

matrix molecules may, therefore, participate in some kinds of charge transfer processes which lead to the ionisation of the desorbed analyte molecules.

The effect of electronic excitation on the solution-phase acidity of the organic molecules has been studied very extensively. These studies have utilized absorption data and fluorescence data in conjunction with the Forster cycle[176] (see Figure 6.21) to determine changes in pK in excited singlet and triplet states. Ireland et al[192] have generalised the enhanced acid-base properties of organic molecules upon electronic excitation in term of various functional groups. Table 6.3. shows some of the important functional groups and their associated pK changes upon electronic excitation. Molecules with negative ΔpKa values become stronger acids in the first excited state and those with positive ΔpKa values are stronger bases. Beauchamp et al[193] have investigated gas-phase excited state proton affinities of different mono-substituted benzenes and have shown that gas-phase studies correlate with the solution phase studies using the Forster cycle.

The role of electronic excitation of the matrix molecules can be visualised as an amplification of the ground-state acid/base or gas-phase proton transfer chemistry. For certain aromatic compounds, such as phenol and aniline, electronic excitation would lead to an increase in the tendency to donate a proton. On the other hand, with other compounds such as benzoic acid and nitrobenzene electronic excitation would result in an increase in the tendency to abstract a proton. Therefore, a preferential formation of either protonated or deprotonated molecules is expected for a particular matrix material. For several model matrices, such as nicotinic acid, 2,5-dihydroxybenzoic acid and cinnamic acid derivatives, the positive-mode and negative-mode analyte molecule-ion signals are of comparable intensities. Even taking account of the excited-state chemistry, the ultimate mechanism of the charging process should still be affected by the chemical properties of the analyte molecules. The absence of any general preference of ion formation from peptides of different chemical compositions and the absence of competition effect on the ion

Figure 6.21
Forster's relationship of enthalpy changes associated with electronic transitions.[5]

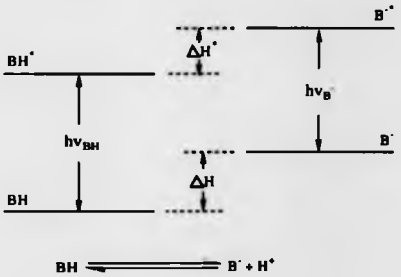

$$\Delta H^* - \Delta H = Lh(\nu_{B^-} - \nu_{BH})$$

L = Avogadro number
h = Planck's constant
ν = frequency / cm^{-1}
ΔH = enthalpy of deprotonation in ground state
ΔH^* = enthalpy of deprotonation in first excited state

Table 6.3

p*K*-change on excitation for the dissociation reaction of various functional groups.[192]

Reaction	$pK(S_1)$- $pK(S_0)$	Example
- OH <=> - O^- + H^+	Negative	1-Naphthol $pK(S_1)$ = 2.0; $pK(S_0)$ = 9.2
- NH_3^+ <=> - NH_2 + H^+	Negative	2-Naphthylamine $pK(S_1)$ = -1.5; $pK(S_0)$ = 4.1
- CO_2H <=> - CO_2 + H^+	Positive	1-Naphthoic acid $pK(S_1)$ = 7.7; $pK(S_0)$ = 3.7
- $CO_2H_2^+$ <=> - CO_2H + H^+	Positive	1-Naphthoic acid $pK(S_1)$ = 2.0; $pK(S_0)$ = -7.7
-NO_2H^+ <=> - NO_2 + H^+	Positive	Nitrobenzene $pK(S_1)$ = -11.3; $pK(S_0)$ = 2.3
$C_5H_5NH^+$ <=> C_5H_5N + H^+	Positive	Acridine $pK(S_1)$ = 10.6; $pK(S_0)$ = 5.5
>C=OH^+ <=> >C=O + H^+	Positive	Xanthone $pK(S_1)$ = 1.0; $pK(S_0)$ = -4.1

formation between peptides of distinct different chemical properties imply that the ionisation mechanism is not chemical specific, i.e. not associated with the acid/base chemistry.

6.4.4. Photoionisation and photochemistry

Ultra-violet laser desorption of small organic molecules have been investigated extensively. It is generally found that radical cations / anions (i.e. odd-electron species) are formed in the UV-laser desorption of non-polar[194] or weakly polar molecules[195]. Formation of protonated or deprotonated molecules (i.e. even-electron species) is usually associated with polar molecules[189]. Ehring et al[75] have studied the UV laser desorption mass spectra of a wide range of polar organic molecules and found that radical molecule-ions can also be formed. For some organic molecules such as tyrosine and tryptophan, which form only even-electron ions at room temperature, radical molecule-ions appear in addition to the protonated molecules at low temperatures (~90 K). It should be noted that the typical ionisation energy for polar organic molecules in the gas phase falls in the range 7.5 to 9 eV. Photoionisation of the matrix molecule could, therefore, be achieved through resonant two-step absorption of two single photons, or by sharing the energy of two singly excited molecules. It is known that there is a high tendency for radical cations or radical anions to undergo proton transfer reactions leading to the formation of uncharged free radicals. Under the matrix-assisted laser desorption / ionisation conditions, there are several possible reactions :

$$Matrix^{+\cdot}_{(g)} + Matrix_{(g)} \longrightarrow [Matrix + H]^{\cdot}_{(g)} + [Matrix - H]^{+}_{(g)} \qquad (6)$$

$$Matrix^{+\cdot}_{(g)} + Matrix_{(g)} \longrightarrow [Matrix - H]^{\cdot}_{(g)} + [Matrix + H]^{+*}_{(g)} \qquad (7)$$

$$Matrix^{-\cdot}_{(g)} + Peptide_{(g)} \longrightarrow [Matrix + H]^{\cdot}_{(g)} + [Peptide - H]^{-}_{(g)} \qquad (8)$$

$$Matrix^{+\cdot}_{(g)} + Peptide_{(g)} \longrightarrow [Matrix - H]^{\cdot}_{(g)} + [Peptide + H]^{+*}_{(g)} \qquad (9)$$

Only the protonated and deprotonated molecules (matrix or peptide) could therefore be detected in mass spectrometry. The present experimental results do not falsify this ionisation model. The chemical specificity of the analyte molecules should impose very little influence on the extent of proton transfer reaction from highly reactive radical cations or radical anions. This model is further supported by the matrix-ion suppression effect (see section 4.1.3). It is tentatively suggested that the tendency for the transfer of proton between the photo-ionised matrix molecules and the co-desorbed analyte molecules is higher than that of the photo-ionised matrix molecules and the co-desorbed matrix molecules. If analyte molecules are present in high concentration, a preferential enhancement of analyte molecule-ion signal or suppression of matrix molecule-ion signal is thus expected. It was indeed observed that the matrix-ion suppression effect is associated with the gross matrix-to-analyte ratios. Successful matrix-ion suppression could only be registered using relatively low matrix-to-analyte ratios.

6.5. Conclusions

It has been shown that sinapinic acid, which is one of the most commonly used matrices, somtimes shows higher ion signals for some peptides than for others, whereas thiourea shows a much more even response to most of the peptides tested. The uneven response of the sinapinic acid matrix is tentatively attributed to specific peptide interactions rather than any competition in proton transfer reactions. In summary, there is no evidence supporting a general influence of either acid/base chemistry or gas-phase proton affinity of peptides on the charging processes in matrix-assisted laser desorption / ionisation. The charging processes in matrix-assisted ultra-violent laser desorption / ionisation is rationalised in terms of the formation of matrix radical-ions and subsequent proton transfer reaction between these radical ions and the co-desorbed neutral matrix and analyte molecules.

7

CONCLUDING REMARKS

7.1. Conclusions

The objective of the work described in this thesis was to investigate the process by which gaseous ions are formed in ultra-violet matrix-assisted laser desorption / ionisation (UV-MALDI). Given a better understanding of the ion-formation process, it was hoped to be able to extend MALDI to analysis of non-polar polymers. The experimental results presented in this thesis emphasise that there are many factors which will affect the efficiency of the desorption / ionisation of analyte molecules. For a solid matrix, the method in which the matrix and the analyte molecules are mixed and crystallised is very important. In the case of nicotinic acid as the matrix, the use of a dry-nitrogen purge has been an efficient method of producing a homogeneous solid sample in terms of the matrix and analyte distributions. The analyte molecule-ion intensity has been found to be very sensitive to the laser fluence. The facility for fine control of the attenuation of the laser power is, therefore, essential to optimise analyte signals. For a liquid matrix, the method of sample preparation is less critical. High loadings of analytes (> 100 pmol) have been found to lead to production of analyte molecular clusters.

Initial ion velocities of approximately 800 ms^{-1} have been found for both positive and negative analyte molecule-ions when using a liquid matrix. Experimental evidence has shown that both positively and negatively charged molecules are present in the ablated microvolume. This fact would point to a model involving molecular ejection through a mechanical propelling force, rather than an electrical or coulombic force. Several mechanical models have been proposed. The radiationless internal conversion of the electronic excitation energy into vibrational

energy of the matrix molecules might produce sudden heating and expansion, leading to evaporation or sublimation[44]. Alternatively, the electronic excitation of the matrix molecules might lead to rapid cleavage or rearrangement reactions and expansion due to the loss of volatile fragments[84] such as water and carbon dioxide. Nevertheless, the important fact is that translational motion of the analyte molecules is excited, but not their internal motions.

The discovery of a matrix-ion suppression effect in experiments with solid matrices and the field-effect on the spectral characteristics when using a liquid matrix strongly suggest a consecutive process for desorption and ionisation of the analyte molecules. (i.e. a gas-phase charging mechanism for analyte molecules). It is proposed that there is a time-interval following the lattice disintegration in which the analyte molecules 'scavenge' charges at some distance above the sample surface. This proposal is supported by the mass-dependent energy deficit for analytes of different molecular masses. Certain factors affecting the charging of analyte molecules have been studied. Using a solid matrix, it has been shown that the solution-phase acid / base properties and gas-phase proton affinities of the analytes (peptides) do not correlate with the ionisation efficiencies of the analyte molecules in a typical matrix-assisted laser desorption / ionisation experiment. These observations favour an ionisation model as proposed by Ehring et al[75], in which photoionisation and photochemistry of the matrix molecules play an important role in MALDI.

7.2. MALDI OF NON-POLAR POLYMERS

Figure 7.1 shows the MALDI time-of-flight mass spectra of poly(propylene glycol) 1025 and poly(ethene glycol) 1450, using sinapinic acid as the matrix (λ = 266 nm). Series of molecule-ion peaks were observed in both cases, corresponding to the polymer envelopes of these polymers. Figures 7.2 and 7.3 show the MALDI time-of-flight spectra of poly(propylene glycol) 2000 and poly(acrylic acid) 3700.

Figure 7.1
Positive-ion MALDI mass spectra of low molecular-mass polyglycols, using sinapinic acid as the matrix.

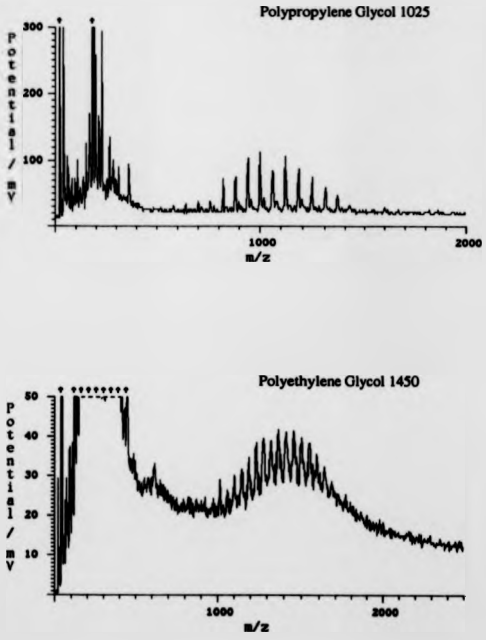

Figure 7.2
Positive-ion MALDI mass spectrum of poly(propylene glycol) 2000, using 2,5-dihydoxybenzoic acid as the matrix.

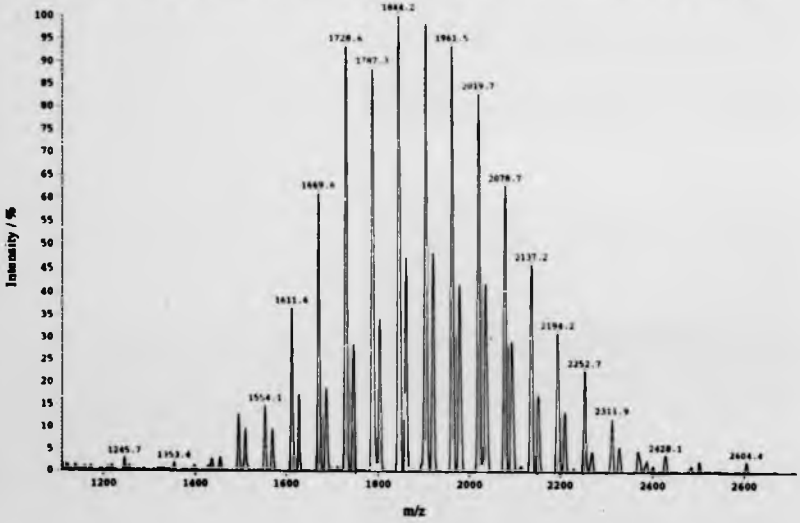

Figure 7.3
Negative-ion MALDI mass spectrum of poly(acrylic acid) 3700, using sinapinic acid as the matrix.

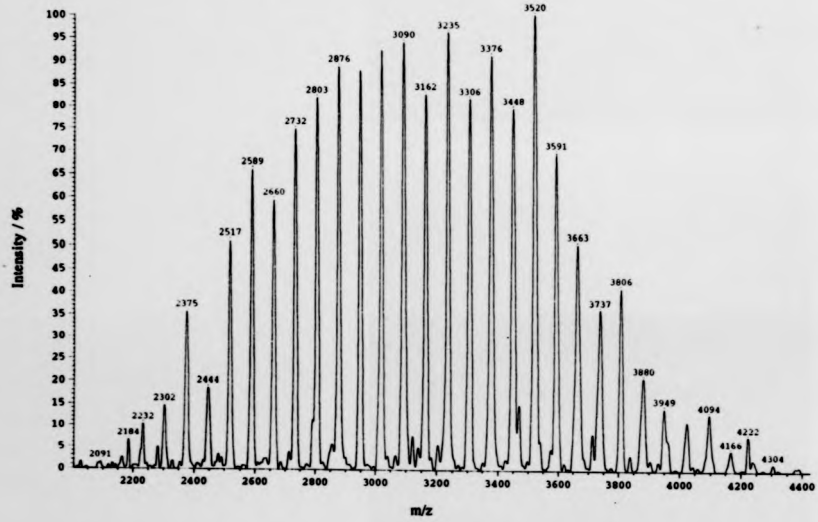

They were obtained using a commercial MALDI instrument[196]. The laser was a nitrogen laser operating at a wavelength of 377 nm. Figure 7.2 shows the positive-ion MALDI spectrum of poly(propylene glycol) 2000 using 2,5-dihydroxybenzoic acid as the matrix. Two distinct polymer envelopes were observed, corresponding to Na^+ and K^+ cationised polymers. Figure 7.3 shows the negative-ion MALDI spectrum of poly(acrylic acid) 3700 using sinapinic acid as the matrix. Other water-soluble polymers, such as poly(styrene sulfonic acid) have also been reported[125]. Attempts to analyse non-polar polymers, such as poly(isoprene) and poly(styrene), did not succeed. It is supposed that the desorption of the analyte is by and large mechanical, and hence should not be affected by the chemical nature of the analyte molecules. It is,therefore, supposed that the main difficulty arises in the ionisation of the desorbed non-polar molecules. Figure 7.4 shows a qualitative energy diagram of the supposed charging processes. It is suggested that there is a proton transfer process between photoionised matrix radical-ions and the co-desorbed analyte molecules. The observed matrix-ion suppression effect is, therefore, readily explained if it is supposed that a sufficiently high abundance of desorbed analyte molecules per unit volume will quench most, if not all, of the matrix radical-ions. The resulting mass spectrum, thus, exhibits little or no signal originating from the matrix molecules. However, if a non-polar analyte is used, the matrix radical-ions will, it is suggested, react preferentially with the co-desorbed matrix molecules, leaving the non-polar molecules uncharged. This can be rationalised on the basis of the extremely low proton-donating and proton-accepting tendencies of non-polar materials which would prohibit essential proton transfer reactions.

It is well known that the best way to ionise a non-polar molecule is to give or take away an electron from the molecule concerned. Direct implantation of energy into the target molecules leads, however, to the onset of competitive degradation processes. In order to take advantage of the matrix technique, the use of an aprotic matrix which has no labile proton is proposed. An aprotic matrix, in principle, should

Figure 7.4
A qualitative energy diagram of the charge transfer processes in matrix-assisted ultraviolet laser desorption.

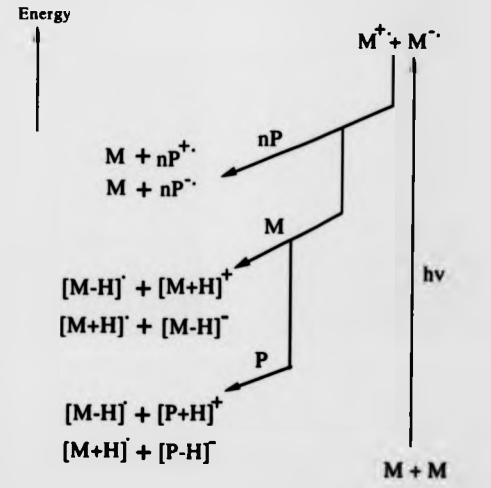

preclude the matrix-matrix proton transfer reactions and enhance the electron transfer reaction.

REFERENCES

1. T. Graham, *Phil. Trans. Roy. Soc. (London), Ser. A*, 1861, **151**, 183.

2. J.M. Evans, *Polym. Eng. Sci.*, 1973, **13**, 401.

3. K. Weber and M. Osborn, *J. Biol. Chem.*, 1969, **224**, 4406.

4. U.K. Laemmli, *Nature (London)*, 1970, **227**, 680.

5. M.S.B. Munson and F.H.Field, *J. Am. Chem. Soc.*, 1966, **88**, 2621.

6. B. Munson, *Anal. Chem.*, 1977, **49**, 722A.

7. M.G. Ingram and R.J. Gomer, *J. Chem. Phys.*, 1954, **22**, 1279.

8. P.L. Robert and H.-R. Schulten, *Anal. Chem.*, 1989, **61**, 61.

9. R.G. Bray, R.M. Hochstrasser and J.E. Wessel, *Chem. Phys. Lett.*, 1974, **27**, 167.

10. E.W. Schlag and H.J. Neusser, *Acc. Chem. Res.*, 1983, **16**, 255.

11. R.P. Lattimer, R.E. Harris, C.K. Rhee and H-R. Schulten, *Rubber Chem. Technol.*, 1988, **61**, 639.

12. H.D. Beckey, *Int. J. Mass Spectrom. Ion Phys.*, 1969, **2**, 500.

13. L. Prokai, Field Desorption Mass Spectrometry, Marcel Dekker, New York, 1990, 9.

14. M.L. Vestal, *Int. J. Mass Spectrom. Ion Phys.*, 1983, **46**, 193.

15. K.L.Busch and R.G. Cooks, *Science*, 1982, **218**, 247.

16. F. Lafortune, R. Beavis, X. Tang, G. Standing and B.T. Chait, *Rapid Comm. Mass Spectrom.*, 1987, **1**, 114.

17. M. Barber, R.S. Bordoli, G.J. Elliot, R.D. Sedgwick and A.N. Tyler, *J. Chem. Soc. Chem. Commun.*, 1981, **7**, 325.

18. C.J. McNeal and R.D. Macfarlane, *J. Am. Chem. Soc.*, 1981, **103**, 1609.

19. M. Barber, R.S. Bordoli, G.J. Elliott, R.D. Sedgwick, A.N. Tyler, B.N. Green V.C. Parr and J.L. Gower, *Biomedical Mass Spectrom.*, 1982, **9**, 11.

20. M. Barber, R.S. Bordoli, G.J. Elliott, R.D. Sedgwick and A.N. Tyler, *Anal. Chem.*, 1982, **54**, 645A.

21. R.D. Macfarlane and D.F. Torgerson, *Science*, 1976, **191**, 920.

22. C.J. McNeal, *Anal. Chem.*, 1982, **54**, 43A.

23. M. Karas and F. Hillenkamp, A. Benninghoven (ed.), Ion Formation from Organic Solids, Springer series in Chemical Physics, **25**, Springer-Verlag New York, 1983.

24. M.A. Posthumus, P.G. Kistemaker, H.L.C. Meuzelaar and M.C. Ten Noever de Brauw, *Anal. Chem.*, 1978, **50**, 985.

25. M. Barber and B.N. Green, *Rapid Commun. Mass Spectrom.*, 1987, **1**, 80.

26. M. Karas and F. Hillenkamp, *Anal. Chem.*, 1988, **60**, 2299.

27. K. Tanaka, H. Waki, Y. Ido, S. Akita, Y. Yoshida and T. Yoshida, *Rapid Commun. Mass Spectrom.*, 1988, **2**, 151.

28. M. Yamashita and J.B. Fenn, *J. Phys. Chem.*, 1984, **88**, 4451.

29. B. Fenn, M. Mann, C. K. Meng and S.F. Wong, *Mass Spectrom. Rev.*, 1990, **9**, 37.

30. M. Karas, U. Bahr and F. Hillenkamp, *Angew. Chem. Int. Ed. Engl.*, 1989, **6**, 760.

31. T-W.D. Chan, A.W. Colburn and P.J. Derrick, *Org. Mass Spectrom.*, 1992, **27**, 53.

32. R.P. Lattimer and G.E. Hansen, *Macromolecules*, 1981, **14**, 776.

33. R.P. Lattimer and H-R. Schulten, *Int. J. Mass Spectrom. Ion Proc.*, 1985, **67**, 227.

34. I.V. Bletsos, D.M. Hercules, J.H. Magill, D. van Leyen, E. Niehuis and A. Benninghoven, *Anal. Chem.*, 1988, **60**, 938.

35. H. Feld, A. Leute, R. Zurmuhlen and A. Benninghoven, *Am. Chem. Soc.*, 1991, **63**, 903.

36. C.F. Ijames and C.L. Wilkin, *J. Am. Chem. Soc.*, 1988, **110**, 2687.

37. K.D. Cook, *Mass Spectrom. Rev.*, 1986, **5**, 467.

38. T. Nohmi and J.B. Fenn, *J. Am. Chem. Soc.*, 1992, **114**, 3241.

39. A.G. Craig and P.J. Derrick, *Aust. J. Chem.*, 1986, **39**, 1421.

40. F.J. Vastola and A.J. Pirone, *Adv. Mass Spectrom.*, 1968, **4**, 107.

41. F.J. Vastola, R.O. Mumma and A.J. Pirone, *Org. Mass Spectrom.*, 1970, **3**, 101.

42. R.J. Conzemius and J.M. Capellen, *Int. J. Mass Spectrom. Ion Proc.*, 1980, **34**, 197.

43. R.J. Cotter, *Anal. Chem.*, 1984, **56**, 485A.

44. A. Vertes, R. Gijbels and R.D. Levine, *Rapid Commun. Mass Spectrom.*, 1990, **4**, 228.

45. R.C. Beavis, J. Lindner, J. Grotemeyer and E.W. Schlag, *Chem. Phys. Lett.*, 1988, **146**, 310.

46. P.K. Hobbs, *Appl. Phys. Lett.*, 1976, **29**, 473.

47. F. Hillenkamp, in Ion Formation from Organic Solids, A. Beaninghoven (ed.), Springer series in Chemical Physics, **25**, Springer-Verlag New York, 1983.

48. O. P. Jonsson, A. B. Hedin, P. L. Hakansson, B. U. R. Sundqvist and B. G. S. Save, *Anal. Chem.*, 1986, **60**, 616.

49. M. Mann, *Org. Mass Spectrom.*, 1990, **25**, 575.

50. R. Stoll and F.W. Rollegen, *Z. Naturforsch*, 1982, **37a**, 9.

51. G.J.Q. van der Peyl, K. Isa, J. Haverkamp and P.G. Kistemaker, *Int. J. Mass Spectrom. Ion Phys.*, 1982, **42**, 125.

52. F. Hillenkamp, D. Holtkamp, M. Karas and P. Klussener, in Ion Formation from Organic Solids (III), A. Beninghoven (ed.), Springer proceeding in Physics, Springer-Verlag New York, 1986, **9**.

53. M. Karas, D. Bachmann and F. Hillenkamp, *Anal. Chem.*, 1985, **57**, 2935.

54. F. Hillenkamp, M. Karas, D. Holtkamp and P. Klüsener, *Int. J. Mass Spectrom. Ion Phys.*, 1986, **69**, 265.

55. M. Karas, D. Bachmann, U. Bahr and F. Hillenkamp, *Int. J. Mass Spectrom. Ion Phys.*, 1987, **87**, 53.

56. R.W. Nelson, M.J. Rainbow, D.E. Lohr and P. Williams, *Science*, 1989, **246**, 1585.

57. R.W. Nelson, R.M. Thomas and P. Williams, *Rapid Commun. Mass Spectrom.*, 1991, **26**, 1052.

58. D.M. Schieltz, C-W. Chou, C-W. Lao, R.M. Thomas and P. Williams, *Rapid. Commun. Mass Spectrom.*, 1992, **6**, 631.

59. G.R. Kinsel, J. Lindner and J. Grotemeyer, *Org. Mass Spectrom.*, 1991, **26**, 1052.

60. Y. Kim, S. Zhao, A.G. Sharkey and D.M. Hercules, Book of Abstracts for the 40th ASMS Conference on Mass Spectrometry and Allied Topics, Washington,1-5 June, 1992, MP120, 40.

61. M. Karas, U. Bahr and F. Hillenkamp, *Int. J. Mass Spectrom. Ion Phys.*, 1989, **92**, 231.

62. R.C. Beavis and B.T. Chait, *Rapid Commun. Mass Spectrom.*, 1989, **3**, 233.

63. F. Hillenkamp, M. Karas, A. Ingendoh and B. Stahl; in A.L. Burlingame and J.A. McCloskey (Eds.), *Biolog. Mass Spectrom.*, Elsevier, Amsterdam, 1990, **49**.

64. R.C. Beavis and B.T. Chait; *Proc. Natl. Acad. Sci. USA*, 1990, **87**, 6873.

65. T-W.D. Chan, A.W. Colburn and P.J. Derrick, *Org. Mass Spectrom.*, 1991, **26**, 342.

66. T-W.D. Chan, A.W. Colburn and P.J. Derrick, *Org. Mass Spectrom.*, 1992, **27**, 188.

67. K. Strupat, M. Karas and F. Hillenkamp, *Int. J. Mass Spectrom. Ion Phys.*, 1991, **111**, 89.

68. P. Juhasz and K. Biemann, Book of Abstracts for the 40th ASMS Conference on Mass Spectrometry and Allied Topics, Washington,1-5 June, 1992, MP147, 53.

69. R.C. Beavis and B.T. Chait, *Rapid Commun. Mass Spectrom.*, 1989, **3**, 432.

70. R.C. Beavis and B.T. Chait, in K.G. Standing and W. Ens (eds.), Methods and Mechanisms for Producing Ions from Large Molecules, NATO ASI series, Series B : Physics **269**, 1990.

71. J.A. Hill, R.S. Annan and K. Biemann, *Rapid Commun. Mass Spectrom.*, 1991, **5**, 395.

72. M. Karas, U. Bahr and U. Giebmanns, *Mass Spectrom. Rev.*, 1991, **10**, 335.

73. M. Karas, A. Ingendoh, U. Bahr and F. Hillenkamp, *Biomed. Environ. Mass Spectrom.*, 1989, **18**, 841.

74. R.C. Beavis, *Org. Mass Spectrom.*, 1992, **27**, 653.

75. H. Ehring, M. Karas and F. Hillenkamp, *Org. Mass Spectrom.*, 1992, **27**, 472.

76. T.Huth-Fehre and C.H. Becker, *Rapid Commun. Mass Spectrom.*, 1991, **5**, 378.

77. S.J. Dolnycz, P.J. Savickas and D.A. Krueger, *Rapid Commun. Mass Spectrom.*, 1991, **5**, 145.

78. R.C. Beavis and B.T. Chait; *Rapid Commun. Mass Spectrom.*, 1989, **3**, 436.

79. R.S. Brown and N.L. Gilfrich, *Anal. Chim. Acta.*, 1991, **248**, 541.

80. W. Ens, Y. Mao, F. Mayer and K.G. Standing, *Rapid Commun. Mass Spectrom.*, 1991, 3, 117.

81. A. Overberg, M. Karas, U. Bahr, R. Kaufmann and F.Hillenkamp, *Rapid Commun. Mass Spectrom.*, 1990, 4, 293.

82. A. Overberg, M. Karas and F.Hillenkamp, *Rapid Commun. Mass Spectrom.*, 1991, 3, 128.

83. P. Demirev, A. Westman, C.T. Reimann, P. Håkansson, D. Barofsky, B.U.R. Sundqvist, Y.D. Cheng, W. Seifert and K. Siegbahn, *Rapid Commun. Mass Spectrom.*, 1992, 6, 187.

84. R.C. Beavis, *Org. Mass Spectrom.*, 1992, 27, 864.

85. A. Vertes and R. Gijbels, *Chem. Phys. Lett.*, 1990, 171, 284.

86. A. Vertes and R. Gijbels, *Scanning Microscopy*, 1991, 5, 317.

87. R.E. Johnson and B.U.R. Sundqvist, *Rapid Commun. Mass Spectrom.*, 1991, 5, 574.

88. B.U.R. Sundqvist, *Anal. Chim. Acta*, 1991, 247, 265.

89. R.E. Johnston and B.U.R. Sundqvist, *Int. J. Mass Spectrom. Ion Phys.*, 1983, 53, 337.

90. P. William and B.U.R. Sundqvist, *Phys. Rev. Lett.*, 1987, 58, 1031.

91. F. Hillenkamp, M. Karas, U. Bahr and A. Ingendoh, in A. Hedin, B.U.R. Sundqvist and A. Benninghoven (eds.), Ion Formation from Organic Solids (IPOS V), John Wiley and Sons, Inc., 1989, 111.

92. B. Spengler and R.J. Cotter, *Anal. Chem.* 1990, 62, 793.

93. Y. Pan and R.J. Cotter, *Org. Mass Spectrom.*, 1992, 27, 3.

94. R.C. Beavis and B.T. Chait, *Chem. Phys. Lett.*, 1991, 181, 479.

95. M.E. Gimon, L.M. Preston, T. Solonki, M.A. White and D.H. Russell, *Org. Mass Spectrom.*, 1992, 27, 827.

96. W.E. Stephens, *Bull. Am. Phys. Soc.*, 1946, 21, 22.

97. A.E. Cameron and D.F. Eggers, Jr., *Rev. Sci. Instrum.*, 1948, 19, 605.

98. V.I. Karataev, B.A. Mamyrin and D.V. Schmikk, *Sov. Phys.-Tech. Phys.*, 1972, 16, 1177.

99. R.Grix, R. Kuncher, G. Li, U. Gruner and H. Wollnik, *Rapid Commun. Mass Spectrom.*, 1988, 2, 83.

100. N.L. Maruhn and G. Sanzone, *Int. J. Mass Spectrom. Ion Phys.*, 1974, 13, 185.

101. J.A. Browder, R.L. Miller, W.A. Thomas and G. Sanzone, *Int. J. Mass Spectrom. Ion Phys.*, 1981, 37, 99.

102. G.R. Kinsel and M.Y. Johnston, *Int. J. Mass Spectrom. Ion Phys.*, 1989, 91, 157.

103. B. Spengler, D. Kirsch, R. Kaufmann, M. Karas, F. Hillenkamp and U. Giessmann, *Rapid Commun. Mass Spectrom.*, 1990, 4, 301.

104. R. Kaufmann, D. Kirsch, H-A Rood and B. Spengler, *Rapid Commun. Mass Spectrom.*, 1992, 6, 00.

105. J. Marteau, W. Ens, K.G. Standing and A. Verentchikov, *Rapid Commun. Mass Spectrom.*, 1992, 6, 147.

106. M.C. Misarow and A.G. Marshall, *Chem. Phys. Lett.*, 1974, 25, 282.

107. A.G. Marshall and P.B. Grosshans, *Anal. Chem.*, 1991, 63, 215A.

108. T.D. Wood, L. Schweikhard and A.G. Marshall, *Anal. Chem.*, 1992, 64, 1461.

109. J.A. Castro, C. Koster and C. Wilkins, *Rapid Commun. Mass Spectrom.*, 1992, 6, 239.

110. R.S. Annan, H.J. Kochling, J.A. Hill and K. Biemann, *Rapid Commun. Mass Spectrom.*, 1992, 6, 298.

111. M. Salehpour, I.K. Perera, J. Kjellberg, A. Hedin, M.A. Islamian, P. Håkansson and B.U.R. Sundqvist, *Rapid Commun. Mass Spectrom.*, 1989, 3, 259.

112. F. Hillenkamp and M. Karas, in J.A. McCloskey (Ed.), Mass Spectrometry, *Method in Enzymology*, 1990, 193, 280.

113. M. Salehpour, I.K. Perera, J. Kjellberg, A. Hedin, M.A. Islamian, P. Håkansson and B.U.R. Sundqvist, in A. Hedin, B.U.R. Sundqvist and A. Beuneaghoven (*eds.*), Ion Formation from Organic Solids (IFOS V), John Wiley and Sons, Inc., 1989, 119.

114. P. Pucci, C. Sepe and G. Marino, *Biol. Mass Spectrom.*, 1992, 21, 22.

115. L. Chan, R.J. Cotter and J.T. Stults, *Anal. Biochem.*, 1989, 183, 190.

116. A. Tsarbopoulos , G.R. Her, Z. Lam, B. Reinhold, V. Reinhold, M. Karas, K. Strupat, F. Hillenkamp and B.N. Pramanik; Proceeding of the 39th ASMS Conference on Mass Spectrometry and Allied Topics, Nashville, TN, 19-24 May, 1991, 488.

117. K.K. Mock, M. Davey and J.S. Cottrell, *Biochem. Biophys. Res. Commun.*, 1991, 177, 644.

118. B. Stahl, M. Steup, M. Karas and F. Hillenkamp, *Anal. Chem.*, 1991, 63, 1463.

119. H. Egge, P-Katulinic, M. Karas and B. Stahl, *Pure and Appl. Chem.*, 1991, 63, 491.

120. P. Juhasz and C.E. Costello, To be published.

121. K. Tang, S.L. Allman and C.H. Chen, *Rapid Commun. Mass Spectrom.*, 1992, 6, 365.

122. T.Huth-Fehre, J.N. Cooline, K.J. Wu and C.H. Becker, *Rapid Commun. Mass Spectrom.*, 1992, 6, 209.

123. R. Parr, M.C. Fitzgerald and L.M. Smith, *Rapid Commun. Mass Spectrom.*, 1992, 6, 369.

124. A. Ingendoh, A. Overberg, M. Karas, P. Cain and F. Hillenkamp, Book of Abstracts for 11th International Mass Spectrometry Society Coference, Amsterdam, 26-30 August, 1991, ThA-834, 295.

125. P.O. Davis, D.E. Kerr, F. Mayer, A. Holle and C.H. Watson, *Org. Mass Spectrom.*, 1992, 27, 843.

126. R.C. Beavis and B.T. Chait, *Anal. Chem.* 1990, 63, 1836.

127. K.O. Borman, M. Schar,E. Gassmann and H.M. Widmer, *Chimia*, 1991, 46, 123.

128. K. Biemann, C.E. Costello, I.A. Papayannopoulos, P. Juhasz, Proceedings of the 39th ASMS Conference on Mass Spectrometry and Allied Topics, Nashville, TN, 19-24 May, 1991, 939.

129. K.O. Borusen, M. Schar and E. Gnaumann, *Biol. Mass Spectrom.*, 1991, 6, 471.

130. K.K. Mock, M.Davey, M.P. Stevenson and J.S. Cottrell, *Biochem. Soc. Trans.*, 1991, 19, 948.

131. B. Spengler, D. Kirsch and R. Kaufmann, *Rapid Commun. Mass Spectrom.*, 1992, 6, 105.

132. R.W. Nelson and T.W. Hutchen, *Rapid Commun. Mass Spectrom.*, 1992, 6, 4.

133. T.W. Hutchen, R.W. Nelson, M.H. Allen, C.M. Li and T-T. Yip, *Biol. Mass Spectrom.*, 1992, 21, 151.

134. T.B. Farmer and R.M. Caprioli, *Biol. Mass Spectrom.*, 1991, 20, 796.

135. D.E. Rogers, Ph. D. thesis, La Trobe University, Victoria, Australia, 1980.

136. G.M. Neumann, Ph. D. thesis, La Trobe University, Victoria, Australia, 1983.

137. M.M. Sheil, Ph. D. thesis, University of New South Wales, Australia, 1988.

138. Alpha-Scientific Corporation, 25393 Huntwood Ave, Hayward, California 94544, U.S.A., Model No. 80A/60V 3038M.

139. A.G. Craig, Ph. D. thesis, University of New South Wales, Australia, 1984.

140. Siemens, Model No. FP110 L60.

141. R. Herzog, *Z. Phys.*, 1935, 97, 596.

142. H. Matsuda, *Int. J. Mass Spectrom. Ion Phys.*, 1976, 22, 259.

143. John Fluke Manufacturing Corporation, P.O. Box 43210, Mountlake Terrace, Washington 98043, U.S.A. Model No. 415B.

144. Granville-Phillips Company, Box 1290, Boulder, Colorado, U.S.A. Model No. 203.

145. ETP Pty Ltd., Ermington, Australia, Model No. AEM 1000.

146. Spellman High Voltage Electronics Corporation, 1930, Adee Ave, New York 10469, U.S.A.,
a) Model No. RHR-100PN 100/220.
b) Model No. RHSR-30P 60/220.

147. Lambda Physik GmbH, Hans-Bockler-Straße 12, D-3400 Gottingen, Germany,
a) Model No. LPX 100i.
b) Model No. FL3002.
c) FL3002 Information pack.

148. Newport Ltd., 4320 First Avenue, Newbury Business Park, London Road, Newbury RG13 2PZ Berks, U.K.,
a) Model No. 20QM20.
b) Model No. 670-TC and 670-BC.
c) Model No. 70 rod.
d) Model No. LP_1.
e) Model No. FL 355-5.

149. see for example : P.W. Milonni and J.H. Eberly, Laser, John Wiley and Sons, Inc., USA, 1988.

150. Eastman Kodak Company, Rochester, N.Y. 14650. U.S.A. Ref. No. 14370.

151. U. Brackmann, Lambdachrome Laser Dyes, Lambda Physik GmbH, D-3400 Gottingen, 1986, III-79.

152. Edwards High Vacuum, Crawley, West Sussex, U.K.,
a) Model No. E2M40, ED330, E200, ES200 or EDM12.
b) Model No. PR10S.
c) Model No. 160/700.
d) Model No. IG5G.

153. S.C. Davis, Ph. D. thesis, University of New South Wales, Australia, 1988.

154. P.W. Gens and R.D. Macfarlane, *Int. J. Mass Spectrom. Ion Phys.*, 1989, 92, 195.

155. LeCroy Corporation, 700 Chestnut Ridge Rd., Chestnut Ridge, N.Y. 10977-6499, U.S.A. Model No. 9400A.

156. Sun Microsystems Europe, Inc., Bagshot Manor, Green Lane, Bagshot, Surrey GU19 5NL, U.K. Model No. Sun-3/80.

157. National Instruments Corporation, 6504 Bridge Point Parkway, Austin, TX 78730-5039, U.S.A. Model No. GPIB-SCSI and NI-488M Driver.

158. The Raman scattering spectroscopy of the solid sample was a collaboration project with Prof. D.J. Gardiner and his group at Newcastle-upon-Tyne polytechnic, U.K. All measurements were made using their Raman Microline Focus spectrometer at Newcastle-upon-Tyne polytechnic.

159. M. Bowden, D.J. Gardiner, G. Rice and D.L. Gerrard, *J. Raman Spectrosc.*, 1990, 21, 41.

160. D.J. Gardiner, M. Bowden and P.R. Graves, *Phil. Trans. Roy. Soc., Lon. Ser. A*, 1986, 320, 295.

161. Polymer Laboratories Ltd., Church Stretton, Shropshire SY6 6AX, U.K. Batch No. 20323-3.

162. Aldrich Chemical Co. Ltd., The Old Brickyard, New Road, Gillingham, Dorset, SP8 4JL, U.K. Catalogue No. 20-233-9.

163. F. Kirchner, *Naturwissenschaften*, 1954, 41, 136.

164. E.W. Muller and K. Bahadur, *Phys. Rev.*, 1956, 102, 624.

165. R.J. Cotter, *Anal. Chem.*, 1980, 52, 1589A.

166. S.S. Wong, U. Giessmann, M. Karas and F.W. Rollgen, *Int. J. Mass Spectrom. Ion Phys.*, 1984, 56, 139.

167. S.C. Davis, V. Natoli, F.M. Neumann and P.J. Derrick, *Int. J. Mass Spectrom. Ion Phys.*, 1987, 78, 17.

168. T-W. D. Chan, A.W. Colburn, D.S. Alderdice and P.J. Derrick, *Int. J. Mass Spectrom. Ion Phys.*, 1991, 107, 491.

169. G M. Neumann, D. E. Rogers, P. J. Derrick and P. J. K. Paterson, *J. Phys. D : Appl. Phys.*, 1980, 13, 485.

170. L.A. Chewter, Shell Thornton Research Centre, U.K., private communication.

171. Trimellitic acid-based polyester samples were synthesised by P.Koenders and co-workers, Koninklijke Shell-Laboratorium, Amsterdam.

172. C.D. Bradley, Ph. D. thesis, University of Warwick, 1992.

173. C.J. McNeal, R.D. Macfarlane and E.L. Thurston, *Anal. Chem.*, 1979, 51, 2036.

174. G. P. Jonsson, A. B. Hedin, P. L. Hakansson, B. U. R. Sundqvist, B.G.S. Save, P.F. Nilsan, P. Roepstorff, K. Johansson, I. Kamensley and M.S.L. Lindberg, *Anal. Chem.*, 1986, **58**, 1091.

175. B.T. Chait, R.C. Beavis and S.B.H. Kent, Book of Abstracts for the 40th ASMS Conference on Mass Spectrometry and Allied Topics, Washington, 1-5 June, 1992, FOB 10:45 , 269.

176. T.Z. Forster, *Electrochem.*, 1950, **54**, 42.

177. R.L. Hettich and M.V. Buchanann, *J. Am. Soc. Mass Spectrom.*, 1991, **2**, 22.

178. S. Zhao, K.V. Somayajula, A.G. Sharkey and D.M. Hercules, *Anal Chem.*, 1991, **63**, 450.

179. Clusters larger than trimers have sometimes been observed for certain matrices, B.T. Chait, private communication, 1991. See also reference 111.

180. M.Karas, U. Bahr, A. Ingendoh, B. Stahl and F. Hillenkamp, in D.H. Russell (ed.), in Mass Spectrom., Plenum, New York, in press.

181. B. Spengler, U. Bahr, M. Karas and F. Hillenkamp, *Anal. Instrum.*, 1988, **17**, 173.

182. P.Y. Yau, T-W.D. Chan, P.G. Cullis, A.W. Colburn and P.J. Derrick, *Chem. Phys. Lett.*, 1992, accepted.

183. J.F. Reading, Effects of High Power Laser Radiation, Academic Press, New York, 1981.

184. B. Spengler, D. Kirsch and R. Kaufmann, *Rapid Commun. Mass Spectrom.*, 1991, **5**, 198.

185. R.C. Beavis, T. Chaudhary and B.T. Chait, *Org. Mass Spectrom.*, 1992, **27**, 156.

186. K. Isa, T. Omote and M. Amaya, *Org. Mass Spectrom.*, 1990, **25**, 620.

187. Sigma Chem Co. Ltd., Fancy Road, Poole, Dorset, BH17 7NH, England.

188. Boehringer Mannheim U.K. (Diagnostics and Biochemicals) Ltd., Bell Lane, Lewes, East Sussex BN7 1NG, England.

189. C.D. Parker and D.M. Hercules, *J. Am. Chem. Soc.*, 1986, **58**, 25.

190. A. Benninghoven, *Int. J. Mass Spectrom. Ion Phys.*, 1983, **53**, 85.

191. E.S. West, W.R. Todd, H.S. Mason, J.T. Mason, Textbook of Biochemistry, 4th ed., Macmillan Co., New York, 1966, 51.

192. J.F. Ireland and P.A.H. Wyatt, *Adv. Phys. Org. Chem.*, 1976, **12**, 131.

193. J.L. Beauchamp and B.S. Prieser, *J. Am. Chem. Soc.*, 1977, **99**, 3214.

194. K. Balasanmugam, S.K. Viswanadham and D.M. Hercules, *J. Am. Chem. Soc.*, 1986, **58**, 1102.

195. S.K. Viswanadham, D.M. Hercules, E.M. Schreiber, R.R. Weller and C.S. Giam, *Anal. Chem.*, 1988, **60**, 2346.

196. Kratos Analytical, Barton Dock Road, Urmston, Manchester, M31 2LD, U.K., Model : Kompact MALDI III, (linear mode).

APPENDIX
TIME-OF-FLIGHT PROGRAMS

This computer software is designed to work under sunview environment and to communicate with Lecroy digital oscilloscope model 9400A. It performs data transfer between the sun-3/80 and the oscillocope and includes routines for graphical output, data processing and spectrum printing. It consists of the following modules:

1. *Makefile* : *A customised program to perform checking file changes and also auto-complilation.*
2. *main.c* : *Main program.*
3. *win.c* : *This module generates windows, pop-up windows and various functional icons.*
4. *sub.c* : *This module performs functions such as file loading, spectrum display and baseline substraction.*
5. *cali.c* : *This module performs time-to-mass calibration.*
6. *dso1.c* : *This module performs data transfer to and from the LeCroy 9400A digital ocilloscope and the Sun 3/80 workstation (GPIB parallel transfer using ASCII data format).*
7. *dso2.c* : *This module performs data transfer to and from the LeCroy 9400A digital ocilloscope and the Sun 3/80 workstation (RS232-C serial transfer using Hexadecimal data format).*
8. *prt.c* : *This module produces bit mapping file for the time-of-flight spectrum.*

N.B. : The subunit "dso1.c" was written by Desmond Yau and will not be displayed in this appendix.

Makefile : A customised program to perform checking file changes and also auto-compilation.

```
DESTDIR=
CFILES= main.c win.c sub1.c dao1.c dao2.c prt.c call.c cib.c

OBJS= $(CFILES:%.c=%.o)
BINS=  tof
CC= cc
#
# If you want to compile for debugging, change "-O" to "-g"
#
CFLAGS= -g
#
# if you want special to pass special loader options to ld, set
# LDFLAGS=
#
LIBS = -lm -lauxtool -lauxwindow -lpixrect -lg

all: ${BINS}

tof: main.o win.o sub1.o dao1.o dao2.o prt.o call.o cib.o
        ${CC} ${CFLAGS} ${LDFLAGS} -o tof main.o win.o sub1.o dao1.o dao2.o prt.o call.o cib.o
${LIBS}

clean:
        rm -f ${OBJS} ${BINS}
```

main.c : Main program.

```
#include <stdio.h>
#include <math.h>

#define  MAXNUM  26000
float    ydig[MAXNUM], xdig[MAXNUM], yclip[MAXNUM], xclip[MAXNUM],
         xs[MAXNUM], ys[MAXNUM];
int      datstring[10];
int      fd, fd1;

main()
{
void Screen_main();
         Screen_main();
}
```

win.c : This module generates windows, pop-up windows and various functional icons.

```
#include <stdio.h>
#include <stdlib.h>
#include <string.h>
#include <ctype.h>
#include <math.h>
#include <floatingpoint.h>
#include <fcntl.h>
#include <suntool/sunview.h>
#include <suntool/textsw.h>
#include <suntool/panel.h>
#include <suntool/canvas.h>
#include <suntool/tty.h>
#include <suntool/icon.h>
#include <suntool/alert.h>
#include <pixrect/pixrect_hs.h>
#include <sys/stat.h>
#define MAX_PATH_LEN        1024
#define MAXIMUM             26000
int     dig_max,Y_max,no_of_smooth=0,calibrated=0,backgd_on =0,marking_on=0;
int     xmin,xmax,ymin,ymax, multi_factor, n_ave, tot_dat, cent_on=0;
int     plot_1 = 1, plot_2 = 1, sam_int, cent_count = 0, hf_cent_chan, shown_1;
int     ix, ix1, ix2, spectrum_load=0, m_space1=0, m_length=0, s1=0,s2=0;
int     peak_range, dis_pix, dis_count;
float   s_leftx, s_lefty, s_rightx, s_righty;
char    pstring[256], data_len[10], start_data[10], show_xy='n',dom;
float   y_calibration, x_calibration, x_scale, y_scale,cal_coeff[3], cal_int,
        time_pix, volt_pix, backgd_level, time_center,x_center,y_center;
double  time_tip[10],mass_tip[10];

Frame           Base_frame,Filer_frame, Edit_frame,DSO_to_Sun_frame,
                Sun_to_DSO_frame, Cent_frame, Mark_frame, Peak_frame;
Textsw                  Editsw;
Panel           Filer_panel, Parameter_panel, File_panel,Dir_panel,
                Source_panel, le_flags_panel, le_done_panel,
                L_S_panel, Verw_panel, Location_panel,
                Transfer_panel, Function_panel, Calibration_panel,
                Header_panel, Edit_panel, Cent_panel, Quit_panel,
                DSO_to_Sun_panel, Sun_to_DSO_panel, Mark_panel,
                Show_panel, Data_panel;
Canvas          canvas, canvas1;
Tty             File_tty;
Icon            icon_OS;
Cursor          cursor;
Panel_item      dir_item, source_item, target_item, input_done_item,
                copy_item, done_item, load_file_item, save_file_item,
                data_base_item, spectrum_mode_item, datamo_item,
                xlower_range_item, xupper_range_item,
                ylower_range_item, yupper_range_item, backgd_item,
                transfer_mode_item, connection_item,
                x_location_item, y_location_item,
                channel_item, identifier_item, ldata_file_item,
                sdata_file_item, ex_cal_item, in_cal_item, mass_item,
                header1_item, header2_item, chan_cent_item, chan_smooth_item,
                save_cali_item, charge_item, cluster_item, symbol_item,
                mass_apply_item, dac_apply_item, polarity_item,
                border_item, tlop_item, tmin_item, tmax_item, vmag_item,
                wsweep_item, rsweep_item, smooth_item, integral_item;
Pixwin          *pw, *pw1;
char            *getwd();
```

```
static short os_array[] =
{
#include "osicon"
};
mpr_static(os,64,64,1,os_array);

extern float x_calibration, y_calibration;
Screen_main(argc,argv)

int argc;
char **argv;

{
        x_calibration = 0.0;
        y_calibration = 0.0;
        icon_OS = icon_create(ICON_IMAGE, &os,0);
        Base_frame=window_create(NULL, FRAME,
                FRAME_ARGS,                     argc, argv,
                FRAME_LABEL,                    "Main manual",
                FRAME_ICON,                     icon_OS,
                WIN_X,                          200,
                WIN_Y,                          60,
                0);
        Create_panel_sw();
        Create_canvas_sw();
        Create_subcanvas_sw();
        Create_cent_popup();
        Create_marking_popup();
        Create_DSO_to_Sun_popup();
        Create_Sun_to_DSO_popup();
        window_fit(Base_frame);
        window_main_loop(Base_frame);
        exit(0);
}

Create_panel_sw()
{
void    File_proc(), Edit_file_proc(), Load_data_proc(),
        Save_data_proc(), Search_peak_proc(), Base_transfer_proc(),
        Quit_proc(),Redisplay_proc(),Whole_spectrum_proc(),
        Background_proc(), Centriod_proc(), Smooth_proc(),
        Ex_Cali_proc(), In_Cali_proc(),Prt_graph_proc(),
        Calibration_proc(), Marking_proc(),Prt_header_proc(),
        save_cali_proc(), S_data_proc();

        Filer_panel = window_create(Base_frame, PANEL,0);

        panel_create_item(Filer_panel, PANEL_BUTTON,
                PANEL_LABEL_IMAGE,
                panel_button_image(Filer_panel,"Filer",5,0),
                0);

        window_fit(Filer_panel);

        Transfer_panel = window_create(Base_frame, PANEL,
                WIN_RIGHT_OF,           Filer_panel,
                0);

        transfer_mode_item = panel_create_item(Transfer_panel, PANEL_CYCLE,
                PANEL_LABEL_STRING,             "Transfer mode : ",
                PANEL_CHOICE_STRINGS,           "Oscilloscope to SUN",
                                                "SUN to Oscilloscope",0,
                PANEL_ITEM_X,                   15,
```

```
        0);

connection_item = panel_create_item(Transfer_panel, PANEL_CYCLE,
        PANEL_LABEL_STRING,     "I/F:",
        PANEL_CHOICE_STRINGS,   "GPIB",
                                "RS232",0,
        0);

panel_create_item(Transfer_panel, PANEL_BUTTON,
        PANEL_LABEL_IMAGE,
        panel_button_image(Transfer_panel,"TRANSFER",5,0),
        PANEL_ITEM_X,           ATTR_COL(55),
        PANEL_NOTIFY_PROC,      Base_transfer_proc,
        0);

window_fit(Transfer_panel);

Quit_panel = window_create(Base_frame, PANEL,
        WIN_RIGHT_OF,           Transfer_panel,
        0);

panel_create_item(Quit_panel, PANEL_BUTTON,
        PANEL_LABEL_IMAGE,
        panel_button_image(Quit_panel,  "Quit",5,0),
        PANEL_ITEM_X,           10,
        PANEL_NOTIFY_PROC,      Quit_proc,
        0);

window_fit_height(Quit_panel);

L_S_panel = window_create(Base_frame, PANEL,
        0);

panel_create_item(L_S_panel, PANEL_BUTTON,
        PANEL_LABEL_IMAGE,
        panel_button_image(Filer_panel, "Write database",5,0),
        PANEL_NOTIFY_PROC,      Edit_file_proc,
        0);

data_base_item = panel_create_item(L_S_panel, PANEL_TEXT,
        PANEL_LABEL_STRING,     ":",
        PANEL_VALUE_DISPLAY_LENGTH,  20,
        PANEL_VALUE,            "database",
        PANEL_ITEM_X,           ATTR_COL(15),
        PANEL_ITEM_Y,           ATTR_ROW(0),
        0);

panel_create_item(L_S_panel, PANEL_BUTTON,
        PANEL_LABEL_IMAGE,
        panel_button_image(L_S_panel,"Load Data",5,0),
        PANEL_ITEM_X,           ATTR_COL(0),
        PANEL_ITEM_Y,           ATTR_ROW(1),
        PANEL_NOTIFY_PROC, Load_data_proc,
        0);

load_file_item = panel_create_item(L_S_panel, PANEL_TEXT,
        PANEL_LABEL_STRING,     ":",
        PANEL_VALUE_DISPLAY_LENGTH,  20,
        PANEL_ITEM_X,           ATTR_COL(11),
        PANEL_ITEM_Y,           ATTR_ROW(1),
        0);

panel_create_item(L_S_panel, PANEL_BUTTON,
```

```
        PANEL_LABEL_IMAGE,
        panel_button_image(L_S_panel,"Save as",5,0),
        PANEL_ITEM_X,                   ATTR_COL(0),
        PANEL_ITEM_Y,                   ATTR_ROW(2),
        PANEL_NOTIFY_PROC, Save_data_proc,
        0);

save_file_item = panel_create_item(L_S_panel, PANEL_TEXT,
        PANEL_LABEL_STRING,             ": ",
        PANEL_VALUE_DISPLAY_LENGTH,  20,
        PANEL_ITEM_X,                   ATTR_COL(11),
        PANEL_ITEM_Y,                   ATTR_ROW(2),
        0);

window_fit(L_S_panel);

Veiw_panel = window_create(Base_frame, PANEL,
        WIN_RIGHT_OF,                   L_S_panel,
        0);

spectrum_mode_item = panel_create_item(Veiw_panel, PANEL_MESSAGE,
        PANEL_LABEL_STRING,"Spectrum mode : Time-of-flight spectrum",
        PANEL_LABEL_BOLD,               TRUE,
        0);

panel_create_item(Veiw_panel, PANEL_BUTTON,
        PANEL_LABEL_IMAGE,
        panel_button_image(Veiw_panel,"Whole spectrum",5,0),
        PANEL_ITEM_Y,                   ATTR_ROW(0),
        PANEL_ITEM_X,                   ATTR_COL(45),
        PANEL_NOTIFY_PROC, Whole_spectrum_proc,
        0);

xlower_range_item = panel_create_item(Veiw_panel, PANEL_TEXT,
        PANEL_LABEL_STRING,             "X - display range: ",
        PANEL_VALUE_DISPLAY_LENGTH,  10,
        PANEL_VALUE,                    "0",
        PANEL_ITEM_Y,                   ATTR_ROW(1),
        PANEL_ITEM_X,                   ATTR_COL(0),
        0);

xupper_range_item = panel_create_item(Veiw_panel, PANEL_TEXT,
        PANEL_LABEL_STRING,             " to ",
        PANEL_VALUE_DISPLAY_LENGTH,  10,
        PANEL_VALUE,                    "0",
        0);

ylower_range_item = panel_create_item(Veiw_panel, PANEL_TEXT,
        PANEL_LABEL_STRING,             "Y - display range: ",
        PANEL_VALUE_DISPLAY_LENGTH,  10,
        PANEL_VALUE,                    "0",
        PANEL_ITEM_Y,                   ATTR_ROW(2),
        PANEL_ITEM_X,                   ATTR_COL(0),
        0);

yupper_range_item = panel_create_item(Veiw_panel, PANEL_TEXT,
        PANEL_LABEL_STRING,             " to ",
        PANEL_VALUE_DISPLAY_LENGTH,  10,
        PANEL_VALUE,                    "0",
        0);

panel_create_item(Veiw_panel, PANEL_BUTTON,
        PANEL_LABEL_IMAGE,
```

```
        panel_button_image(Veiw_panel,"Redisplay",5,0),
        PANEL_ITEM_Y,                   ATTR_ROW(2),
        PANEL_ITEM_X,                   ATTR_COL(50),
        PANEL_NOTIFY_PROC, Redisplay_proc,
        0);

window_fit_height(Veiw_panel);

Location_panel = window_create(Base_frame, PANEL,0);

x_location_item = panel_create_item(Location_panel, PANEL_TEXT,
        PANEL_LABEL_STRING,         "X : ",
        PANEL_VALUE_DISPLAY_LENGTH,   10,
        0);

y_location_item = panel_create_item(Location_panel, PANEL_TEXT,
        PANEL_LABEL_STRING,         "Y : ",
        PANEL_VALUE_DISPLAY_LENGTH,   10,
        0);

panel_create_item(Location_panel, PANEL_BUTTON,
        PANEL_LABEL_IMAGE,
        panel_button_image(Location_panel,"Peak-analysis",5,0),
        PANEL_NOTIFY_PROC, S_data_proc,
        PANEL_ITEM_X,                   ATTR_COL(50),
        0);

chan_cent_item = panel_create_item(Location_panel, PANEL_TEXT,
        PANEL_LABEL_BOLD,           TRUE,
        PANEL_LABEL_STRING,         "Centroiding width : ",
        PANEL_VALUE_DISPLAY_LENGTH,   10,
        PANEL_ITEM_X,                   ATTR_COL(70),
        0);

window_fit_height(Location_panel);

Function_panel = window_create(Base_frame, PANEL,0);

panel_create_item(Function_panel, PANEL_BUTTON,
        PANEL_LABEL_IMAGE,
        panel_button_image(Function_panel,"Print Graph",5,0),
        PANEL_NOTIFY_PROC, Prt_graph_proc,
        0);

panel_create_item(Function_panel, PANEL_BUTTON,
        PANEL_LABEL_IMAGE,
        panel_button_image(Function_panel,"Time/Mass mark",5,0),
        PANEL_NOTIFY_PROC, Marking_proc,
        0);

backgd_item = panel_create_item(Function_panel, PANEL_BUTTON,
        PANEL_LABEL_IMAGE,
        panel_button_image(Function_panel,"Baseline subtraction",5,0),
        PANEL_NOTIFY_PROC, Background_proc,
        0);

panel_create_item(Function_panel, PANEL_BUTTON,
        PANEL_LABEL_IMAGE,
        panel_button_image(Function_panel,"Smoothing",5,0),
        PANEL_NOTIFY_PROC, Smooth_proc,
        0);

smooth_item = panel_create_item(Function_panel, PANEL_CYCLE,
```

```
        PANEL_LABEL_STRING,         "channels: ",
        PANEL_CHOICE_STRINGS,       "0","2","4","8","16","32","64","128",
                                    0,
        PANEL_ITEM_Y,               ATTR_COL(0),
        0);

window_fit_height(Function_panel);

Calibration_panel = window_create(Base_frame, PANEL,0);

panel_create_item(Calibration_panel, PANEL_BUTTON,
        PANEL_LABEL_IMAGE,
        panel_button_image(Calibration_panel,
                           "Do Internal Calibration",5,0),
        PANEL_NOTIFY_PROC,          In_Cali_proc,
        0);

panel_create_item(Calibration_panel, PANEL_BUTTON,
        PANEL_LABEL_IMAGE,
        panel_button_image(Function_panel,"Enter Calibration point",5,0),
        PANEL_NOTIFY_PROC, Calibration_proc,
        PANEL_ITEM_Y,               ATTR_ROW(0),
        0);

panel_create_item(Calibration_panel, PANEL_BUTTON,
        PANEL_LABEL_IMAGE,
        panel_button_image(Calibration_panel,
                           "Save Calibration",5,0),
        PANEL_NOTIFY_PROC.          save_cali_proc,
        0);

save_cali_item = panel_create_item(Calibration_panel, PANEL_TEXT,
        PANEL_LABEL_STRING,         ":",
        PANEL_VALUE_DISPLAY_LENGTH,  15,
        PANEL_VALUE,                "cf/default",
        PANEL_ITEM_Y.               ATTR_ROW(0),
        0);

panel_create_item(Calibration_panel, PANEL_BUTTON,
        PANEL_LABEL_IMAGE,
        panel_button_image(Calibration_panel,
                           "Do External Calibration",5,0),
        PANEL_ITEM_Y,               ATTR_ROW(1),
        PANEL_ITEM_X,               ATTR_COL(0),
        PANEL_NOTIFY_PROC, Ex_Cali_proc,
        0);

ex_cal_item = panel_create_item(Calibration_panel, PANEL_TEXT,
        PANEL_LABEL_STRING,         ":",
        PANEL_VALUE_DISPLAY_LENGTH,  30,
        PANEL_VALUE,                "cf/off_axis_nlb",
        PANEL_ITEM_Y.               ATTR_ROW(1),
        0);

window_fit_height(Calibration_panel);

Header_panel = window_create(Base_frame, PANEL,0);

panel_create_item(Header_panel, PANEL_BUTTON,
        PANEL_LABEL_IMAGE,
        panel_button_image(Header_panel,"Header",5,0),
        PANEL_NOTIFY_PROC, Pri_header_proc,
        0);
```

```
        header1_item = panel_create_item(Header_panel, PANEL_TEXT,
                PANEL_LABEL_STRING,             " : ",
                PANEL_VALUE_DISPLAY_LENGTH,     80,
                PANEL_VALUE,                    "MALD ",
                PANEL_ITEM_X,                   ATTR_COL(20),
                PANEL_ITEM_Y,                   ATTR_ROW(0),
                0);

        header2_item = panel_create_item(Header_panel, PANEL_TEXT,
                PANEL_LABEL_STRING,             " : ",
                PANEL_VALUE_DISPLAY_LENGTH,     80,
                PANEL_VALUE,                    "",
                PANEL_ITEM_X,                   ATTR_COL(20),
                PANEL_ITEM_Y,                   ATTR_ROW(1),
                0);

        window_fit_height(Header_panel);
}

Create_canvas_sw()
{
        void handle_event();
        canvas = window_create(Base_frame,CANVAS,
                WIN_CONSUME_PICK_EVENT, LOC_DRAG,
                WIN_EVENT_PROC, handle_event,
                WIN_CURSOR,
                cursor_create(CURSOR_SHOW_CROSSHAIRS,FALSE,
                                0),
                CANVAS_FAST_MONO,       TRUE,
                0);

        window_set(canvas,
                WIN_ROWS,30,
                WIN_COLUMNS,100,
                0);

        window_set(canvas,
                CANVAS_AUTO_EXPAND, FALSE,
                CANVAS_AUTO_SHRINK, FALSE,
                0);

        pw = canvas_pixwin(canvas);
}

Create_subcanvas_sw()
{
        void handle_event();
        void S_smooth_proc();
        void S_done_proc();
        void S_restart_proc();

        Peak_frame = window_create(Base_frame, FRAME,
                FRAME_LABEL,            "Peak analysing",
                FRAME_SHOW_LABEL,       TRUE,
                WIN_X,                  200,
                WIN_Y,                  60,
                0);

        Data_panel = window_create(Peak_frame, PANEL,0);


        sorder_item = panel_create_item(Data_panel, PANEL_CYCLE,
```

```
        PANEL_LABEL_STRING,         "Smoothing channels : ",
        PANEL_CHOICE_STRINGS,       "0","2","4","8","16","32","64","128",
                                    0,
        PANEL_ITEM_X,               ATTR_COL(0),
        0);

ttop_item = panel_create_item(Data_panel, PANEL_TEXT,
        PANEL_LABEL_STRING,         "Peak center : ",
        PANEL_VALUE_DISPLAY_LENGTH, 10,
        PANEL_ITEM_X,               ATTR_COL(0),
        PANEL_ITEM_Y,               ATTR_ROW(1),

        0);

vmag_item = panel_create_item(Data_panel, PANEL_TEXT,
        PANEL_LABEL_STRING,         "Peak height : ",
        PANEL_VALUE_DISPLAY_LENGTH, 10,
        PANEL_ITEM_X,               ATTR_COL(0),
        PANEL_ITEM_Y,               ATTR_COL(2),
        0);

tmin_item = panel_create_item(Data_panel, PANEL_TEXT,
        PANEL_LABEL_STRING,         "Low-time HHFW : ",
        PANEL_VALUE_DISPLAY_LENGTH, 10,
        PANEL_ITEM_X,               ATTR_COL(0),
        PANEL_ITEM_Y,               ATTR_COL(3),
        0);

tmax_item = panel_create_item(Data_panel, PANEL_TEXT,
        PANEL_LABEL_STRING,         "High-time HHFW : ",
        PANEL_VALUE_DISPLAY_LENGTH, 10,
        PANEL_ITEM_X,               ATTR_COL(0),
        PANEL_ITEM_Y,               ATTR_COL(4),
        0);

integral_item = panel_create_item(Data_panel, PANEL_TEXT,
        PANEL_LABEL_STRING,         "Integral : ",
        PANEL_VALUE_DISPLAY_LENGTH, 10,
        PANEL_ITEM_X,               ATTR_COL(0),
        PANEL_ITEM_Y,               ATTR_COL(5),
        0);

window_fit_height(Data_panel);

Show_panel = window_create(Peak_frame, PANEL,0);

panel_create_item(Data_panel, PANEL_BUTTON,
        PANEL_LABEL_IMAGE,
        panel_button_image(Show_panel,"Restart",5,0),
        PANEL_NOTIFY_PROC, S_restart_proc,
        0);

panel_create_item(Show_panel, PANEL_BUTTON,
        PANEL_LABEL_IMAGE,
        panel_button_image(Show_panel,"Smooth",5,0),
        PANEL_NOTIFY_PROC, S_smooth_proc,
        0);

panel_create_item(Show_panel, PANEL_BUTTON,
        PANEL_LABEL_IMAGE,
        panel_button_image(Show_panel,"Done",5,0),
        PANEL_NOTIFY_PROC, S_done_proc,
        0);
```

```
        window_fit_height(Show_panel);

        canvas1 = window_create(Peak_frame,CANVAS,
                WIN_CONSUME_PICK_EVENT, LOC_DRAG,
                WIN_EVENT_PROC, handle_event,
                CANVAS_FAST_MONO,       TRUE,
                0);

        window_set(canvas1,
                WIN_ROWS,20,
                WIN_COLUMNS,50,
                0);

        window_set(canvas1,
                CANVAS_AUTO_EXPAND, FALSE,
                CANVAS_AUTO_SHRINK, FALSE,
                0);

        pw1 = canvas_pixwin(canvas1);
        window_fit(Peak_frame);
}

/* ARGSUSED */
extern char     plotting[], show_xy;
extern int      xmin,xmax,ymin,ymax, multi_factor, backgd_on, marking_on, a1, a2;
extern float    a_leftx, a_lefty, a_rightx, a_righty;
extern float    y_calibration, x_calibration, backgd_level, time_center,
                x_center, y_center;

static void
handle_event(canvas, event, arg)
Canvas  canvas;
Event   *event;
caddr_t arg;
{
        void fhon();
        void substract();
        void cent_mass_proc();
        void mark_acquire_proc();
        void Clip_proc();
        int power();

        Pixwin *pw      = canvas_pixwin(canvas);
        short   draw    = FALSE;
        short   erase   = FALSE;
        int     ptx, pty, lx, ly, decx, decy;
        float   x, y;

        if(show_xy == 'n') return;
        ptx = event_x(event);
        pty = event_y(event);
        if(pty < 50 || pty > 400 || ptx < 100 || ptx > 700)
        {
        cursor = window_get(canvas,WIN_CURSOR);
        cursor_set(cursor, CURSOR_SHOW_CROSSHAIRS, FALSE,
                        0);
        window_set(canvas, WIN_CURSOR, cursor, 0);
        panel_set(x_location_item,
                PANEL_VALUE, "", 0);
        panel_set(y_location_item,
                PANEL_VALUE, "", 0);
        return;
```

```
    }

    cursor = window_get(canvas,WIN_CURSOR);
    cursor_set(cursor, CURSOR_SHOW_CROSSHAIRS, TRUE,
                0);
    window_set(canvas, WIN_CURSOR, cursor, 0);

    x = (ptx-100)/(x_calibration);
    ix = (int)x;
    decx = (int)((x-ix)*1000);

    y = (400 - pty)/(y_calibration);
    iy = (int)y;
    decy = (int)((y-iy)*1000);

    ftoa(ix+xmin, decx,3);
    panel_set(x_location_item,
            PANEL_VALUE, ptstring, 0);
    ftoa(iy+ymin, decy,3);
    panel_set(y_location_item,
            PANEL_VALUE, ptstring, 0);

    if(levent_is_up(event) && event_action(event) == MS_RIGHT && backgd_on)
                {
                backgd_on = 0;
                backgd_level = iy  + ((decy*1.0)/1000);
                subtract();
                }

    else if(levent_is_up(event) && event_action(event) == MS_RIGHT && cent_on)
                {
                cent_on = 0;
                time_center = x + xmin;
                cent_mass_proc();
                }

    else if(levent_is_up(event) && event_action(event) == MS_RIGHT && marking_on)
                {
                marking_on = 0;
                x_center = x + xmin;
                time_center = x + xmin;
                y_center = y + ymin;
                mark_acquire_proc();
                }

    else if(levent_is_up(event) && event_action(event) == MS_RIGHT && s1 && !s2)
                {
                s_leftx = x + xmin;
                s_lefty = y + ymin;
                s2 = 1;
                msg("Locate the crosshair to enter right boundary",1);
                }

    else if(levent_is_up(event) && event_action(event) == MS_RIGHT && s1 && s2)
                {
                s_rightx = x + xmin;
                s_righty = y + ymin;
                s1=s2=0;
                Clip_proc();
                }
    return;

}
```

```
Create_Sun_to_DSO_popup()
{
        void sun_to_dso_proc() ;

        Sun_to_DSO_frame = window_create(Base_frame, FRAME,
                        FRAME_SHOW_LABEL,       TRUE,
                        FRAME_LABEL,            "Data transfer parameters",
                        WIN_X,                  200,
                        WIN_Y,                  250,
                        0);

        Sun_to_DSO_panel = window_create(Sun_to_DSO_frame, PANEL,0);

        channel_item = panel_create_item(Sun_to_DSO_panel, PANEL_CYCLE,
                PANEL_LABEL_STRING,     "Channel Identifer : ",
                PANEL_CHOICE_STRINGS,   "Memory C",
                                        "Memory D",0,
                0);

        wsweep_item = panel_create_item(Sun_to_DSO_panel, PANEL_CYCLE,
                PANEL_LABEL_STRING,     "Sweep number    : ",
                PANEL_CHOICE_STRINGS,   "1", "2", "3", "4", "5",
                                        "6", "7", "8",0,
                PANEL_ITEM_X,           ATTR_ROW(0),
                PANEL_ITEM_Y,           ATTR_COL(1),
                        0);

        sdata_file_item = panel_create_item(Sun_to_DSO_panel, PANEL_TEXT,
                PANEL_LABEL_STRING,     "Enter filename    : ",
                PANEL_VALUE_DISPLAY_LENGTH,  20,
                PANEL_ITEM_X,           ATTR_ROW(0),
                PANEL_ITEM_Y,           ATTR_COL(2),
                0);

        panel_create_item(Sun_to_DSO_panel, PANEL_BUTTON,
                PANEL_LABEL_IMAGE,
                panel_button_image(Sun_to_DSO_panel,"OK",5,0),
                PANEL_ITEM_X,           ATTR_COL(0),
                PANEL_ITEM_Y,           ATTR_ROW(3),
                PANEL_NOTIFY_PROC,      sun_to_dso_proc,
                0);

        window_fit(Sun_to_DSO_panel);
        window_fit(Sun_to_DSO_frame);
}

Create_DSO_to_Sun_popup()
{
        void dso_to_sun_proc();

        DSO_to_Sun_frame = window_create(Base_frame, FRAME,
                        FRAME_SHOW_LABEL, TRUE,
                        FRAME_LABEL,            "Data transfer parameters",
                        WIN_X,                  200,
                        WIN_Y,                  250,
                        0);

        DSO_to_Sun_panel = window_create(DSO_to_Sun_frame, PANEL,0);

        identifier_item = panel_create_item(DSO_to_Sun_panel, PANEL_CYCLE,
                PANEL_LABEL_STRING,     "Channel identifer    :",
                PANEL_CHOICE_STRINGS,   "Channel 1",
```

```
                                        "Channel 2",
                                        "Memory C",
                                        "Memory D",
                                        "Function E",
                                        "Function F",0,
                0);

        nsweep_item = panel_create_item(DSO_to_Sun_panel, PANEL_CYCLE,
                PANEL_LABEL_STRING,     "Sweep number    :",
                PANEL_CHOICE_STRINGS,   "1", "2", "3", "4", "5",
                                        "6", "7", "8",0,
                PANEL_ITEM_X,           ATTR_COL(0),
                PANEL_ITEM_Y,           ATTR_ROW(1)
                        0);

        idata_file_item = panel_create_item(DSO_to_Sun_panel, PANEL_TEXT,
                PANEL_LABEL_STRING,     "Enter filename  :",
                PANEL_VALUE_DISPLAY_LENGTH,  20,
                PANEL_ITEM_X,           ATTR_COL(0),
                PANEL_ITEM_Y,           ATTR_ROW(2),
                0);

        panel_create_item(DSO_to_Sun_panel, PANEL_BUTTON,
                PANEL_LABEL_IMAGE,
                panel_button_image(DSO_to_Sun_panel,
                                        "Transfer",5,0),
                PANEL_NOTIFY_PROC,      dso_to_sun_proc,
                PANEL_ITEM_X,           ATTR_COL(0),
                PANEL_ITEM_Y,           ATTR_ROW(3),
                0);

        window_fit(DSO_to_Sun_panel);
        window_fit(DSO_to_Sun_frame);

}

Create_cent_popup()
{
        void mass_acquire_proc();
        void mass_reset_proc();
        void display_cancel_proc();

        Cent_frame = window_create(Base_frame, FRAME,
                        FRAME_SHOW_LABEL,       TRUE,
                        FRAME_LABEL,            "Centroiding",
                        WIN_X,                  200,
                        WIN_Y,                  250,
                        0);

        Cent_panel = window_create(Cent_frame, PANEL,0);

        datamo_item = panel_create_item(Cent_panel, PANEL_TEXT,
                PANEL_LABEL_STRING,     "Calibration data :",
                PANEL_LABEL_BOLD,       TRUE,
                PANEL_VALUE_DISPLAY_LENGTH,  10,
                0);

        mass_item = panel_create_item(Cent_panel, PANEL_TEXT,
                PANEL_LABEL_STRING,
                "Enter the corresponding M/z : ",
                PANEL_VALUE_DISPLAY_LENGTH,  20,
                PANEL_ITEM_Y,           ATTR_ROW(1),
                PANEL_ITEM_X,           ATTR_COL(0),
```

```
                0);

        panel_create_item(Cent_panel, PANEL_BUTTON,
                PANEL_LABEL_IMAGE,
                panel_button_image(Cent_panel,"Enter",5,0),
                PANEL_ITEM_X,                   ATTR_COL(20),
                PANEL_ITEM_Y,                   ATTR_ROW(2),
                PANEL_NOTIFY_PROC,              mass_acquire_proc,
                0);

        panel_create_item(Cent_panel, PANEL_BUTTON,
                PANEL_LABEL_IMAGE,
                panel_button_image(Cent_panel,"Cancel",5,0),
                PANEL_ITEM_X,                   ATTR_COL(30),
                PANEL_ITEM_Y,                   ATTR_ROW(2),
                PANEL_NOTIFY_PROC,              display_cancel_proc,
                0);

        panel_create_item(Cent_panel, PANEL_BUTTON,
                PANEL_LABEL_IMAGE,
                panel_button_image(Cent_panel,"Reset",5,0),
                PANEL_ITEM_X,                   ATTR_COL(40),
                PANEL_ITEM_Y,                   ATTR_ROW(2),
                PANEL_NOTIFY_PROC,              mass_reset_proc,
                0);

        window_fit(Cent_panel);
        window_fit(Cent_frame);
}

Create_marking_popup()
{
        void put_mark_proc();
        void remove_mark_proc();
        void mark_done_proc();

        Mark_frame = window_create(Base_frame, FRAME,
                        FRAME_SHOW_LABEL, TRUE,
                        FRAME_LABEL,            "Mass/Time marking",
                        WIN_X,                  200,
                        WIN_Y,                  250,
                        0);

        Mark_panel = window_create(Mark_frame, PANEL,0);

        polarity_item = panel_create_item(Mark_panel, PANEL_TEXT,
                PANEL_LABEL_STRING,             "Polarity (+/-)",
                PANEL_VALUE_DISPLAY_LENGTH,  3,
                PANEL_VALUE,                    "+",
                0);

        charge_item = panel_create_item(Mark_panel, PANEL_TEXT,
                PANEL_LABEL_STRING,             "Number of charge(s) :",
                PANEL_ITEM_Y,                   ATTR_ROW(1),
                PANEL_ITEM_X,                   ATTR_COL(0),
                PANEL_VALUE_DISPLAY_LENGTH,  3,
                PANEL_VALUE,                    "1",
                0);

        cluster_item = panel_create_item(Mark_panel, PANEL_TEXT,
                PANEL_LABEL_STRING,             "Number of cluster :",
                PANEL_VALUE_DISPLAY_LENGTH,  3,
                PANEL_ITEM_Y,                   ATTR_ROW(2),
```

```
                PANEL_ITEM_X,                   ATTR_COL(0),
                PANEL_VALUE,                    "1",
                0);

        symbol_item = panel_create_item(Mark_panel, PANEL_TEXT,
                PANEL_LABEL_STRING,             "Enter the symbol used :",
                PANEL_VALUE_DISPLAY_LENGTH,     10,
                PANEL_ITEM_Y,                   ATTR_ROW(3),
                PANEL_ITEM_X,                   ATTR_COL(0),
                PANEL_VALUE,                    "M",
                0);

        mass_apply_item = panel_create_item(Mark_panel, PANEL_CYCLE,
                PANEL_LABEL_STRING,             "Display mass /time ?",
                PANEL_CHOICE_STRINGS,           "Y",
                                                "N",0,
                PANEL_ITEM_Y,                   ATTR_ROW(4),
                PANEL_ITEM_X,                   ATTR_COL(0),
                0);

        dec_apply_item = panel_create_item(Mark_panel, PANEL_CYCLE,
                PANEL_LABEL_STRING,             "Enter no. of decimal point :",
                PANEL_CHOICE_STRINGS,           "0",
                                                "1",
                                                "2",
                                                "3",
                                                "4",
                                                "5",0,
                PANEL_ITEM_Y,                   ATTR_ROW(5),
                PANEL_ITEM_X,                   ATTR_COL(0),
                0);

        panel_create_item(Mark_panel, PANEL_BUTTON,
                PANEL_LABEL_IMAGE,
                panel_button_image(Mark_panel,"Apply",5,0),
                PANEL_ITEM_X,                   ATTR_COL(10),
                PANEL_ITEM_Y,                   ATTR_ROW(7),
                PANEL_NOTIFY_PROC,              put_mark_proc,
                0);

        panel_create_item(Mark_panel, PANEL_BUTTON,
                PANEL_LABEL_IMAGE,
                panel_button_image(Mark_panel,"Remove",5,0),
                PANEL_ITEM_Y,                   ATTR_ROW(7),
                PANEL_NOTIFY_PROC,              remove_mark_proc,
                0);

        panel_create_item(Mark_panel, PANEL_BUTTON,
                PANEL_LABEL_IMAGE,
                panel_button_image(Mark_panel,"Done",5,0),
                PANEL_ITEM_Y,                   ATTR_ROW(7),
                PANEL_NOTIFY_PROC,              mark_done_proc,
                0);

        window_fit(Mark_panel);
        window_fit(Mark_frame);
}

msg(msg, beep)
        char *msg;
        int  beep;
{
char    buf[300];
```

```
int     result;
Event   event;   /* unused */
char    *continue_msg = "Press \"Continue\" to proceed.";

        result = alert_prompt(Base_frame, &event,
        ALERT_MESSAGE_STRINGS,
        msg,
        continue_msg,
        0,
        ALERT_NO_BEEPING, (beep) ? 0:1,
        ALERT_BUTTON_YES, "Continue",
        ALERT_TRIGGER,          ACTION_STOP, /* allow either YES or NO answer */
        0);
        switch (result) {
                case ALERT_YES:
                case ALERT_TRIGGERED: /* result of ACTION_STOP trigger */
                        break;
                case ALERT_FAILED: /* not likely to happen unless out of memory
                        sprintf(buf, "%s  Press \"Continue\" to proceed.", msg);
                        result = confirm_ok(buf); */
                        break;
                }
}
```

sub.c : This module performs functions such as file loading, spectrum display and baseline substraction.

```
#include <stdio.h>
#include <string.h>
#include <ctype.h>
#include <floatingpoint.h>
#include <stdlib.h>
#include <fcntl.h>
#include <suntool/sunview.h>
#include <suntool/textsw.h>
#include <suntool/panel.h>
#include <suntool/canvas.h>
#include <suntool/tty.h>
#include <suntool/alert.h>
#include <pixrect/pixrect_hs.h>
#include <sys/stat.h>

#define MAX_FILENAME_LEN        256
#define MAX_PATH_LEN            1024
#define X_BASE                  100
#define Y_BASE                  400
#define X_AXIS_WIDTH            600
#define Y_AXIS_HEIGHT           300
#define Pos_1           0.0625
#define Pos_4           0.25
#define Pos_6           0.375

Frame           Base_frame,Filer_frame,DSO_to_Sun_frame,
                Sun_to_DSO_frame, Edit_frame, Peak_frame;
Textsw                  Editsw, textsw;
Panel           Filer_panel, File_panel,Dir_panel,
                Source_panel, ls_flags_panel, ls_done_panel,
                L_S_panel, Veiw_panel, Location_panel,
                Transfer_panel, Function_panel, Calibration_panel,
                Header_panel, Edit_panel,Quit_panel,
                DSO_to_Sun_panel, Sun_to_DSO_panel;
Canvas          canvas, canvas1;
Tty             File_tty;
Icon            icon_OS;
Cursor          cursor;
Panel_item      dir_item, source_item, target_item, input_done_item,
                copy_item, done_item, load_file_item, save_file_item,
                data_base_item, spectrum_mode_item,
                xlower_range_item, xupper_range_item,
                ylower_range_item, yupper_range_item, backgd_item,
                transfer_mode_item, connection_item, geometry_item,
                acceleration_item, y_focus_item, z_focus_item,
                cinzel_lens_item, pad_item, em_item, x_location_item,
                y_location_item, chan_cent_item,chan_smooth_item,
                channel_item, identifier_item, time_scale_item,
                data_file_item, voltage_item, average_item,smooth_item,
                in_col_item, ex_col_item, header1_item, header2_item,
                sender_item, stop_item, tmin_item, tmax_item, vmag_item,
                integral_item;

Pixwin *pw, *pw1;
Pixfont *dis_font;

/********** File_proc : File manipulate pop-up window *****/
void File_proc()
{
        window_set(Filer_frame, WIN_SHOW, TRUE,0);
```

```
}

extern char ptstring[];

void Edit_file_proc()
{
        char cmdstring[20], *filename;

        if(!strlen(filename = (char*)panel_get_value(data_base_item)))
        {
        msg("Enter the filename",1);
        return;
        }

        if (!stat_file(filename))
        {
                sprintf(cmdstring, "%s is not found.", ptstring);
                msg(cmdstring, 1);
                return;
        }

        window_set(Editsw, TEXTSW_FILE, filename,0);
        window_set(Edit_frame,FRAME_LABEL, filename,
                WIN_SHOW, TRUE,
                0);
}

/******** DSO_Remote_proc: Remote control of the DSO *******/
void Base_transfer_proc()
{
void Edit_file_proc();
        int transfer_mode;

        transfer_mode = (int)panel_get_value(transfer_mode_item);
        if(transfer_mode)
                window_set(Sun_to_DSO_frame, WIN_SHOW, TRUE,0);
        else
                window_set(DSO_to_Sun_frame, WIN_SHOW, TRUE,0);
                return;
}

void sun_to_dso_proc()
{
void StoD_GPIB_proc(), StoD_RS232_proc();
        int connection;

        connection = (int)panel_get_value(connection_item);
        if(connection)
                StoD_RS232_proc();
        else
                StoD_GPIB_proc();
                return;
}

void dso_to_sun_proc()
{
void DtoS_GPIB_proc(), DtoS_RS232_proc();
        int connection;

        connection = (int)panel_get_value(connection_item);
        if(connection)
                DtoS_RS232_proc();
        else
```

```
                DtoS_GPIB_proc();
                return;
}

/****************** End of DSO_Remote_proc ********************/

/****** Load_data_proc : Loading of signal data (hex) *******/

extern int dig_max, Y_max, xmin,xmax,ymin,ymax,sam_int, cent_count;
extern int backgd_on, int_dat, plot_1, plot_2, calibrated;
extern int spectrum_load, dis_pix, dis_count;
extern float ydig[], xdig[], x_scale, y_scale, time_pix, volt_pix;
extern char show_xy, pstring[];

void Load_data_proc()
{
int     stat_file();
void    Graph_proc();
void    Clear_canvas();
void    float();
int     power();

        int count, i, j, buf[BUFSIZ], fd1, ver_axis;
        char cmdstring[256], *filename, *c_count, c;
        int c1, c2, index, tim_div, fix_ver_gain;
        float x_s_digmax;
        FILE *fp;

        calibrated =0;
        backgd_on = 0;
        xdig[0]=0;
        ydig[0]=0;

        if(!strlen(filename = (char*)panel_get_value(load_file_item)))
        {
        msg("Enter the data file",1);
        return;
        }
        show_xy = 'y';

        i=0;
        sprintf(cmdstring,"%s%s", panel_get_value(load_file_item),".dat");

        fd1 = open(cmdstring,O_RDWR,0);
        if(fd1 < 0)
                {
                printf("%d\n",errno);
                return;
                }
        read(fd1,buf,1);
        read(fd1,&c,1);
        if(c == 'A')
        {
        read(fd1,buf,2);

        read(fd1,&c,1);
        index = c;
        if(index < 0) index = 256 + index;
        index = index - 21;
        if (!((index-1)%3))
                fix_ver_gain = 5*power(10,(int)((index-1)/3));
        else if (!((index-2)%3))
                fix_ver_gain = 10*power(10,(int)((index-2)/3));
```

```
else
        flx_ver_gain = 20*power(10,(int)((index-3)/3));
y_scale = (float)(8*flx_ver_gain);

read(fd1,buf,8);
read(fd1,&c,1);
index = c;
if(index < 0) index = 256 + index;
index = index - 4;
if (!((index-1)%3))
        tim_div = 5*power(10,(int)((index-1)/3));
else if (!((index-2)%3))
        tim_div = 10*power(10,(index-2)/3);
        else
        tim_div = 20*power(10,(int)((index-3)/3));

x_scale =(float)(tim_div*10/1000);

read(fd1,&c,1);
index = c;
if(index < 0) index = 256 + index;
index = index - 16;
if(!(index))
        sam_int = 10;
else if (!((index-1)%3))
        sam_int = 20*power(10,(int)((index-1)/3));
else if (!((index-2)%3))
        sam_int = 40*power(10,(index-2)/3);
        else
        sam_int = 80*power(10,(int)((index-3)/3));
dig_max = (int)(x_scale*1000/sam_int);
close(fd1);

time_pix = x_scale/dig_max;
volt_pix = y_scale/255;

sprintf(filename,"%s%s", panel_get_value(load_file_item),".dat");
fp=fopen(filename,"r");
read(fd1,buf,2);

tot_dat = 0;
for(i=0; i < 2; i++)
{
c = getc(fp);
index = c;
if(index < 0) index = 256 + index;
tot_dat = tot_dat + index*(power(256,1-i));
        }

x_s_digmax = x_scale/dig_max;

for(i=1; i <= dig_max+1 ; ++i)
        {
        ydig[i] = 0;
        c = getc(fp);
        if(c < 0)
                ydig[i] = (256+c)*256;
        else
                ydig[i] = c*256;
        c = getc(fp);
        if(c < 0)
                ydig[i] = (ydig[i]+(256+c))/256;
        else
```

```
                ydig[i] = (ydig[i]+c)/256;
        xdig[i] = i*x_s_digmax;
        }
}

if(c == 'L')
{
read(fd1,buf,4);
index = 0;
for(i=0; i < 2 ; i++)
        {
        read(fd1,&c,1);
        if(c < '0' || c > '9')
                c = c - 'A' +10;
        else
                c = c - '0';
        index = index + c*(power(16,1-i));
        }
index = index - 21;
if (!((index-1)%3))
        fix_ver_gain = 5*power(10,(int)((index-1)/3));
else if (!((index-2)%3))
        fix_ver_gain = 10*power(10,(int)((index-2)/3));
else
        fix_ver_gain = 20*power(10,(int)((index-3)/3));
y_scale = (float)(8*fix_ver_gain);

read(fd1,buf,16);
index = 0;
for(i=0; i < 2 ; i++)
        {
        read(fd1,&c,1);
        if(c < '0' || c > '9')
                c = c - 'A' + 10;
        else
                c = c - '0';

        index = index + c*(power(16,1-i));
        }

index = index - 4;
if (!((index-1)%3))
        tim_div = 5*power(10,(int)((index-1)/3));
else if (!((index-2)%3))
        tim_div = 10*power(10,(index-2)/3);
        else
        tim_div = 20*power(10,(int)((index-3)/3));

x_scale =(float)(tim_div*10/1000);

index = 0;
for(i=0; i < 2 ; i++)
        {
        read(fd1,&c,1);
        if(c < '0' || c > '9')
                c = c - 'A' + 10;
        else
                c = c - '0';
        index = index + c*(power(16,1-i));
        }
index = index - 16;
if(!(index))
        sam_int = 10;
```

```
else if (!((index-1)%3))
        sam_int = 20*power(10,(int)((index-1)/3));
else if (!((index-2)%3))
        sam_int = 40*power(10,(index-2)/3);
        else
        sam_int = 80*power(10,(int)((index-3)/3));
dig_max = (int)(x_scale*1000/sam_int);

close(fd1);

time_pix = x_scale/dig_max;
volt_pix = y_scale/255;

sprintf(filename,"%s%s", panel_get_value(load_file_item),".dat");
fp=fopen(filename,"r");

do
        {
        c = getc(fp);
        } while(c != 'L');
tot_dat = 0;
for(i=0; i < 4 ; i++)
        {
        c = getc(fp);
        if(c < '0' || c > '9')
                c = c - 'A' + 10;
        else
                c = c - '0';
        tot_dat = tot_dat + c*(power(16,3-i));
        }

x_s_digmax = x_scale/dig_max;
for(i=1; i <= dig_max+1 ; ++i)
        {
        ydig[i] = 0;
        for(j=0; j < 2; j++)
                {
                c = getc(fp);
                if(c < '0' || c > '9')
                        c = c - 'A' + 10;
                else
                        c = c - '0';
                ydig[i] = ydig[i] + c*(power(16,1-j));
                }
        xdig[i] = i*x_s_digmax;
        }
}
fclose(fp);

Clear_canvas();
msg("Data loaded",1);

panel_set(ylower_range_item,
        PANEL_VALUE,        "0",
        0);

fnos((int)x_scale,0,0);
panel_set(xupper_range_item,
        PANEL_VALUE, pixstring,0);

panel_set(ylower_range_item,
        PANEL_VALUE,        "0",
        0);
```

```
        ftoa((int)y_scale,0,0);
        panel_set(yupper_range_item,
                PANEL_VALUE, ptstring,0);

        xmin =0;
        xmax = (int)(x_scale);
        ymin = 0;
        ymax = (int)(y_scale);

        panel_set(backgd_item,
                PANEL_SHOW_ITEM,  TRUE,0);
        panel_set(spectrum_mode_item,
                PANEL_LABEL_STRING,"Spectrum mode : Time-of-flight spectrum",
                PANEL_LABEL_BOLD,          TRUE,
                0);

        ftoa((int)(dig_max/100),0,0);
        panel_set(chan_cent_item,
                PANEL_VALUE,ptstring,0);

        plot_1 = 0;
        plot_2 = dig_max;
        cent_count = 0;
        Graph_proc();
        spectrum_load = 1;
}

extern int xmin,xmax,ymin,ymax,dig_max, plot_1, plot_2, spectrum_load;
extern char ptstring[];
void Whole_spectrum_proc()
{
void    Graph_proc();
void    Clear_canvas();

        if(!spectrum_load)
        {
        msg("No spectrum is loaded!!",1);
        return;
        }

        xmin = 0;
        xmax = (int)x_scale;

        panel_set(xlower_range_item,
                PANEL_VALUE,        "0",
                0);
        ftoa((int)(x_scale),0,0);

        panel_set(xupper_range_item,
                PANEL_VALUE, ptstring,0);

        ymin = 0;
        ymax = (int)y_scale;

        panel_set(ylower_range_item,
                PANEL_VALUE,        "0",
                0);
        ftoa((int)(y_scale),0,0);

        panel_set(yupper_range_item,
                PANEL_VALUE, ptstring,0);
```

```
        plot_1 = 0;
        plot_2 = dig_max;

        Clear_canvas();
        Graph_proc();
        return;
}

void Prt_header_proc()
{
        int height = (int)window_get(canvas, CANVAS_HEIGHT);
        char    *head1string, *head2string;

        dis_font = pf_open("/usr/lib/fonts/fixedwidthfonts/cour.b.18");

        if(!strlen(head2string = (char*)panel_get_value(header2_item)))
                {
                head1string = (char*)panel_get_value(header1_item);
                pw_text(pw, 100, height-405, PIX_SRC, dis_font,head1string);
                }
        else
                {
                pw_text(pw, 100, height-405, PIX_SRC, dis_font,head2string);
                head1string = (char*)panel_get_value(header1_item);
                pw_text(pw, 100, height-425, PIX_SRC, dis_font,head1string);
                }
        pf_close(dis_font);


return;
}

extern int s1, s2, spectrum_load;
void S_data_proc()
{
        if(!spectrum_load)
        {
        msg("No spectrum is loaded!!",1);
        return;
        }
        if(!s1)
        {
        msg("Locate the crosshair to enter left boundary",1);
        s1=1;
        }
}

void S_restart_proc()
{
        void Clip_proc();

        panel_set(sorder_item,
                        PANEL_VALUE, 0, 0);
        Clip_proc();
        return;
}

extern float s_leftx, s_lefty, s_rightx, s_righty;
extern float yclip[], xclip[], xs[], ys[];
extern int dig_max, peak_range, showx_1;
void Clip_proc()
{
        void S_smooth_proc();
```

```
        float peak_slope, sub1, sub2, s_baseline;
        int   i, shown_2;

        window_set(Peak_frame, WIN_SHOW, TRUE,0);

        for(i=0; i<= dig_max; i++)
        {
                sub1 = (xdig[i] - s_leftx);
                if(sub1 <= 0)       shown_1 = i;

                sub2 = (xdig[i] - s_rightx);
                if(sub2 <= 0)       shown_2 = i;
        }
        shown_2 = shown_2 - 1;

        peak_range = shown_2-shown_1;

        if(ydig[shown_2] > ydig[shown_1])
        {
        s_baseline =  ydig[shown_1];
        peak_slope = (ydig[shown_2] - ydig[shown_1])/(shown_2 - shown_1);
        for(i=0; i <= peak_range; i++)
                {
                yclip[i] = ydig[i+shown_1] - (s_baseline + i*peak_slope);
                ys[i] = yclip[i];
                xclip[i] = xdig[i+shown_1];
                xs[i] = xclip[i];
                }
        }
        else
        {
        s_baseline =  ydig[shown_2];
        peak_slope = (ydig[shown_1] - ydig[shown_2])/(shown_2 - shown_1);
        for(i=peak_range; i > 0; i--)
                {
                yclip[i] = ydig[i+shown_1] - s_baseline;
                ys[i] = yclip[i];
                xclip[i] = xdig[i+shown_1];
                xs[i] = xclip[i];
                }
        }
        S_smooth_proc();
        return;
}

extern float ys[], yclip[], y_scale;
extern int peak_range, shown_1;
extern char ptstring[];
void S_smooth_proc()
{
        void Show_clip_proc();
        void float();
        int power();
        float area_b4=0, area_a5=0, red_factor=0, vmag, tiop;
        float integral, tmin, tmax, hvmag;
        int i, ivmag, itiop, itmin, itmax, decvmag, decliop, decimin, decimax;
        int iintegral, decintegral, pt_temp, sf=0;

        for(i=0; i<= peak_range; i++)
                area_b4 = area_b4 + yclip[i];

        integral = area_b4;
```

```
if(!(int)panel_get_value(sorder_item))
        nf = 0;
else
        nf = 2*power(2,(int)panel_get_value(sorder_item)-1);

for(i=nf; i <= peak_range-nf; i++)
        ys[i] = (ys[i-nf]+ys[i+nf])*Pas_1 +
                        (ys[i-nf/2]+ys[i+nf/2])*Pas_4 +
                        ys[i]*Pas_6;

for(i= peak_range-nf; i >= nf; i--)
        ys[i] = (ys[i-nf]+ys[i+nf])*Pas_1 +
                        (ys[i-nf/2]+ys[i+nf/2])*Pas_4 +
                        ys[i]*Pas_6;

for(i=0; i<= peak_range; i++)
        area_a5 = area_a5 + ys[i];

red_factor = area_a5/area_b4;

for(i=0; i<= peak_range; i++)
        ys[i] = ys[i]/red_factor;

vmag = 0;
for(i=0; i<= peak_range; i++)
if(ys[i] > vmag)
        {
        vmag = ys[i];
        itop = i;
        }
hvmag = vmag/2;
for(i=itop; i <= peak_range; i++)
        if(ys[i] >= hvmag) tmax = i;
for(i=itop; i >=0; i--)
        if(ys[i] >= hvmag) tmin = i;

itop = xdig[(int)itop + shown_1];
tmax = xdig[(int)tmax + shown_1];
tmin = xdig[(int)tmin + shown_1];

vmag = (vmag/256.0)*y_scale;

ivmag = (int)vmag;
decvmag = (int)((vmag-ivmag)*1000);

itop = (int)itop;
dectop = (int)((itop-itop)*1000);

itmin = (int)tmin;
dectmin = (int)((tmin-itmin)*1000);

itmax = (int)tmax;
dectmax = (int)((tmax-itmax)*1000);

iintegral = (int)integral;
deciintegral = (int)((integral-iintegral)*1000);

ftoa(ivmag, decvmag,3);
panel_set(vmag_item,
        PANEL_VALUE, ptstring, 0);

ftoa(itop, dectop,3);
panel_set(itop_item,
```

```
                PANEL_VALUE, ptstring, 0);

        ftoa(itmin, dectmin,3);
        panel_set(tmin_item,
                PANEL_VALUE, ptstring, 0);

        ftoa(itmax, dectmax,3);
        panel_set(tmax_item,
                PANEL_VALUE, ptstring, 0);

        ftoa(iintegral, decintegral,3);
        panel_set(integral_item,
                PANEL_VALUE, ptstring, 0);

        Show_clip_proc();

        return;
}

extern int peak_range;
extern float yclip[], xclip[], ys[];
void Show_clip_proc()
{
        void Clear_canvas1();

        int c_width = (int)window_get(canvas1,CANVAS_WIDTH);
        int c_height = (int)window_get(canvas1, CANVAS_HEIGHT);
        float gr_max=0, c_xscale, c_yscale;
        int i, ix1, ix2, iy1, iy2;

        Clear_canvas1();
        for(i=0; i <= peak_range; i++)
        {
        if(yclip[i] > gr_max) gr_max = yclip[i];
        }
        c_xscale = c_width/(peak_range*1.0);
        c_yscale = c_height/(gr_max);

        ix1 = (int)(1*c_xscale);
        iy1 = (int)(c_height -(yclip[1]*c_yscale));
        pw_vector(pw1,ix1,iy1,ix1,iy1,PIX_SRC,1);

        for(i= 1; i <= peak_range; i++)
        {
        ix2 = (int)(i*c_xscale);
        iy2 = (int)(c_height - (yclip[i]*c_yscale));
        pw_vector(pw1,ix1,iy1,ix2,iy2,PIX_SRC,1);
        ix1 = ix2;
        iy1 = iy2;
        }

        ix1 = (int)(1*c_xscale);
        iy1 = (int)(c_height -(ys[1]*c_yscale));
        pw_vector(pw1,ix1,iy1,ix1,iy1,PIX_SRC,1);

        for(i= 1; i <= peak_range; i++)
        {
        ix2 = (int)(i*c_xscale);
        iy2 = (int)(c_height - (ys[i]*c_yscale));
        pw_vector(pw1,ix1,iy1,ix2,iy2,PIX_SRC,1);
        ix1 = ix2;
        iy1 = iy2;
        }
```

```
        return;
}

void S_done_proc()
{
        window_set(Peak_frame, WIN_SHOW, FALSE,0);
        return;
}

extern int dig_max, no_of_smooth, spectrum_load;
extern float ydig[];
void Smooth_proc()
{
        void Redisplay_proc();
        int i,j, n, temp, sf;
        float area_b4=0, area_a5=0, red_factor;

        if(!spectrum_load)
        {
        msg("No spectrum is loaded!!",1);
        return;
        }

        for(i=0; i<= dig_max; i++)
                area_b4 = area_b4 + ydig[i];

        if(!(int)panel_get_value(smooth_item))
                sf = 0;
        else
                sf = 2*power(2,(int)panel_get_value(smooth_item)-1);

        for(i=sf; i <= dig_max-sf; i++)
                ydig[i] = (ydig[i-sf]+ydig[i+sf])*Pas_1 +
                                (ydig[i-sf/2]+ydig[i+sf/2])*Pas_4 +
                                ydig[i]*Pas_6;

        for(i= dig_max-sf; i >= sf; i--)
                ydig[i] = (ydig[i-sf]+ydig[i+sf])*Pas_1 +
                                (ydig[i-sf/2]+ydig[i+sf/2])*Pas_4 +
                                ydig[i]*Pas_6;

        for(i=0; i<= dig_max; i++)
                area_a5 = area_a5 + ydig[i];

        red_factor = area_a5/area_b4;

        for(i=0; i<= dig_max; i++)
                ydig[i] = ydig[i]/red_factor;

        Redisplay_proc();
        return;
}

extern int backgd_on, spectrum_load;

void Background_proc()
{
        if(!spectrum_load)
        {
        msg("No spectrum is loaded!!",1);
        return;
        }
```

```
        backgd_on = 1;
        panel_set(backgd_item,
                PANEL_SHOW_ITEM,  FALSE,0);
        msg("Locate the cross-hair onto the baseline and kick on the right mouse button",1);
        return;
}

extern int dig_max, ymax, spectrum_load, backgd_on;
extern float ydig[], backgd_level, y_scale;
void subtract()
{
        int i;
        float j;

        if(!spectrum_load)
        {
        msg("No spectrum is loaded!!",1);
        return;
        }

        j = (backgd_level/ymax)*(255*(ymax/y_scale));
        for(i=0; i <= dig_max; i++)
                {
                        ydig[i] = ydig[i]-j;
                        if(ydig[i] < 0.001) ydig[i] = 0;
                }
        backgd_on = 0;
        Redisplay_proc();
        return;
}

extern int xmin,xmax,ymin,ymax, plot_1, plot_2, sum_int, calibrated;
extern int spectrum_load;
extern float xdig[];
void Redisplay_proc()
{
void    Graph_proc();
void    Clear_canvas();

        char    cmdstring[10];
        int     i;
        float   sub1, sub2;

        if(!spectrum_load)
        {
        msg("No spectrum is loaded!!",1);
        return;
        }

        sprintf(cmdstring,panel_get_value(xlower_range_item));
        xmin = atoi(cmdstring);
        sprintf(cmdstring,panel_get_value(xupper_range_item));
        xmax= atoi(cmdstring);

        for(i=0; i<= dig_max; i++)
        {
                sub1 = (xdig[i] - xmin);
                if(sub1 <= 0)       plot_1 = i;

                sub2 = (xdig[i] - xmax);
                if(sub2 <= 0)       plot_2 = i;
        }
```

```
        plot_2 = plot_2 - 1;

        sprintf(cmdstring,panel_get_value(ylower_range_item));
        ymin = atoi(cmdstring);
        sprintf(cmdstring,panel_get_value(yupper_range_item));
        ymax = atoi(cmdstring);

        Clear_canvas();
        Graph_proc();
        return;
}

extern  int dig_max, tot_dat;
extern float ydig[], x_scale, y_scale;
void Save_data_proc()
{
        int i, n, j;
        char cmdstring[256], *filename;
        FILE *fp;

        if(!strlen(filename = (char*)panel_get_value(save_file_item)))
        {
        msg("Enter the target filename",1);
        return;
        }
        sprintf(cmdstring,"%s%s", panel_get_value(save_file_item),".den");

        if (stat_file(cmdstring))
        {
                sprintf(cmdstring, "%s is already exist.", ptstring);
                msg(cmdstring, 1);
                return;
        }

        i=0;
        fp=fopen(cmdstring,"w");
        fprintf(fp,"%d %f %f %d",dig_max, x_scale/10, y_scale/8000);
        fclose(fp);

        sprintf(filename,"%s%s", panel_get_value(save_file_item),".dat");
        fp=fopen(filename,"w");
        fprintf(fp,"#L");
        for(i=0; i < 4 ; i++)
                {
                n = tot_dat / power(16,3-i);
                if(n < 10)
                        putc(n + '0',fp);
                else
                        putc('@' + (n-10), fp);
                tot_dat = tot_dat - n*power(16,3-i);
                }
        for(i=0; i<= dig_max; i++)
                {
                n = (int)(ydig[i+1]/16);
                for(j=0; j < 2; j++)
                        {
                        if(n < 10)
                                putc(n + '0',fp);
                        else
                                putc('@' + (n-10), fp);

                        n = (int)(ydig[i+1]) % 16;
                        }
```

```
                }
        fprintf(fp,"^M^M#I^M^M");
        fclose(fp);
        msg("Data stored",1);
        return;
}

/* ARGSUSED */
static void
Clear_canvas()
{
Pixwin *pw      = canvas_pixwin(canvas);
(void)pw_writebackground(pw,0,0,(int)(LINT_CAST(window_get(canvas, CANVAS_WIDTH))),
        (int)(LINT_CAST(window_get(canvas, CANVAS_HEIGHT))), PIX_CLR);
}

static void
Clear_canvas1()
{
Pixwin *pw1     = canvas_pixwin(canvas1);
(void)pw_writebackground(pw1,0,0,(int)(LINT_CAST(window_get(canvas1, CANVAS_WIDTH))),
        (int)(LINT_CAST(window_get(canvas1, CANVAS_HEIGHT))), PIX_CLR);
}

/******************** End of Load_data-proc ********************/

/********** Graph_proc : Spectrum draw panel ***************/
extern float y_calibration, x_calibration, x_scale, y_scale;
extern float  ydig[], time_pix, volt_pix;
extern int  dig_max, xmin,xmax,ymin,ymax, calibrated, dis_pix, dis_count;
extern int plot_1, plot_2;
extern char ptstring[];

void Graph_proc()
{
        int Draw_scale();

        int width = (int)window_get(canvas,CANVAS_WIDTH);
        int height = (int)window_get(canvas, CANVAS_HEIGHT);
        int i, j, Y_max,ix,iy,ix1,ix2,iy1,iy2,p_err, yup, ylo;
        int x_scale_space, y_scale_space, extra_y,draw_y_max, draw_x_max;
        float  x1,x2,y1,y2;

/*      REM : draw top, right, bottom, left, borders of box
        REM : pw_vector(pw, x1, y1, x2, y2, PIX_SRC,1)
        REM : the area for spectrum output is defined by the rectangle
        REM : (x1=100; y1=100; x2=700; y2=400)
        REM : height = 480; width = 800;
*/

        pw_vector(pw, width-100, height-80, 100, height-80, PIX_SRC,1);
        pw_vector(pw, 100, height-80, 100, 100, PIX_SRC,1);

        dis_font = pf_open("/usr/lib/fonts/fixedwidthfonts/gallant.r.19");

        if(!(calibrated))
                pw_text(pw, 350, height-25, PIX_SRC, dis_font,"Time / \265s");
        else
                pw_text(pw, 380, height-25, PIX_SRC, dis_font,"m/z");

        pw_text(pw, 30, 125, PIX_SRC, dis_font,"I");
        pw_text(pw, 30, 145, PIX_SRC, dis_font,"o");
        pw_text(pw, 30, 165, PIX_SRC, dis_font,"n");
```

```
        pw_text(pw, 30, 185, PIX_SRC, dis_font,"e");
        pw_text(pw, 30, 205, PIX_SRC, dis_font,"a");
        pw_text(pw, 30, 225, PIX_SRC, dis_font,"t");
        pw_text(pw, 30, 245, PIX_SRC, dis_font,"i");
        pw_text(pw, 30, 265, PIX_SRC, dis_font,"s");
        pw_text(pw, 30, 285, PIX_SRC, dis_font,"l");
        pw_text(pw, 30, 315, PIX_SRC, dis_font,"/");
        pw_text(pw, 30, 345, PIX_SRC, dis_font,"m");
        pw_text(pw, 30, 365, PIX_SRC, dis_font,"V");

        pf_close(dis_font);

        dis_font = pf_open("/usr/lib/fonts/fixedwidthfonts/cour.b.16");

        draw_x_max = Draw_scale(1,xmin,xmax);
        x_calibration = (float)(X_AXIS_WIDTH*1.0)/(draw_x_max);
        draw_y_max = Draw_scale(2,ymin,ymax);
        y_calibration = (float)(Y_AXIS_HEIGHT*1.0)/(draw_y_max);

        p_arr = -10;
        i = plot_1;
        ix1 = (int)((X_BASE )+ (xdig[i]-xmin)*x_calibration);
        iy1 = (int)((Y_BASE) - (ydig[i]*volt_pix-ymin)*y_calibration);
        if(iy1 < 100) iy1 = 100;

        pw_vector(pw,ix1,iy1,ix1,iy1,PIX_SRC,1);

        for(i= plot_1; i <= plot_2; ++i)

        {
        ix2 = (int)((X_BASE )+ (xdig[i]-xmin)*x_calibration);
        iy2 = (int)((Y_BASE) - (ydig[i]*volt_pix-ymin)*y_calibration);

        if(iy2 < 100)
                {
                if((ix1-p_arr) > 10)
                        {
                        pw_text(pw, ix1-5, 95, PIX_SRC, dis_font,"\177");
                        p_arr = ix1;
                        }
                iy2 = 100;
                }
        pw_vector(pw,ix1,iy1,ix2,iy2,PIX_SRC,1);
        ix1 = ix2;
        iy1 = iy2;
        }

        pf_close(dis_font);

}
/*****************  End of Graph_proc **********************/

/*      REM : Draw_scale will return the gap between stroke
        REM : axis_type             => 1 = x_axis; 2 = y-axis
        REM : axis_min & axis_max => minimum & maximum range
*/

#define long_scale_bar 10
#define short_scale_bar 5
#define scale_xpx 30
#define scale_ypy 35

int Draw_scale(axis_type, axis_min, axis_max)
```

```
int axis_type, axis_min, axis_max;

{

void  floa();
int       i, j, ix, iy, range1, factor, num_sp, start_scale;
int       range, total_stroke, first_stroke_pos,unit_before_first_stroke,
          no_min_before_maj, unit_first_stroke;
int       minor_scale, major_scale;
float     sp_per_unit, sp_before_first_stroke, sp_per_step,
          local_X_BASE, local_Y_BASE, fix, fiy, decx, decy;

major_scale = 1;
factor = 1;
range = axis_max - axis_min;
while(range < 10)
          {
          range = range*10;
          factor = factor * 10;
          }
range1 = range;
while((range / 10) > 0)
          {
          range = range /10;
          major_scale= major_scale*10;
          }
minor_scale = major_scale / 10;
if(axis_type == 1)
          sp_per_unit = (X_AXIS_WIDTH*1.0)/range1;
else
          sp_per_unit = (Y_AXIS_HEIGHT*1.0)/range1;

total_stroke = range1 / minor_scale;
first_stroke_pos = 0;
while(first_stroke_pos < axis_min)
          first_stroke_pos = first_stroke_pos + minor_scale;
unit_before_first_stroke = (first_stroke_pos - axis_min);
sp_before_first_stroke = unit_before_first_stroke*sp_per_unit;
if(axis_type == 1)
          local_X_BASE = (X_BASE + sp_before_first_stroke);
else
          local_Y_BASE = (Y_BASE - sp_before_first_stroke);

no_min_before_maj = 0;
unit_first_stroke = axis_min + unit_before_first_stroke;
while((unit_first_stroke*factor) % major_scale != 0)
          {
          ++no_min_before_maj;
          unit_first_stroke = unit_first_stroke + minor_scale;
          }
sp_per_step = minor_scale*sp_per_unit;
start_scale = 0;
while(start_scale < axis_min) start_scale = start_scale+(major_scale/factor);
j=0;
if(axis_type == 1)
{
for(i = 0;  i <= (total_stroke); i++)
          {
          fix = (local_X_BASE + i*sp_per_step);
          decx = (fix*10) - (int)(fix)*10;
          if( decx > 4)
                    ix = (int)(fix)+1;
          else
                    ix = (int)fix;
          if((i-no_min_before_maj) % 10 == 0)
```

```
                {
                        pw_vector(pw,ix,Y_BASE,ix,Y_BASE+long_scale_bar,PIX_SRC,1);
                        floa(start_scale+(j*major_scale/factor),0,0);
                        num_sp = (int)(8*(strlen(ptstring)*1.0/2));
                        pw_text(pw, ix-num_sp, Y_BASE+scale_spx, PIX_SRC,
                                dia_font,ptstring);
                        j++;
                }
                else
                        pw_vector(pw,ix,Y_BASE,ix,Y_BASE+short_scale_bar,PIX_SRC,1);
                }
        }
        else
        {
        for(i = 0;  i <= (total_stroke); i++)
                {
                fly = (local_Y_BASE - i*sp_per_step);
                decy = (fly*10) - (int)(fly)*10;
                if( decy > 4)
                        iy = (int)(fly)+1;
                else
                        iy = (int)fly;
                if((i-no_min_before_ma)) % 10 ==0)
                        {
                        pw_vector(pw,X_BASE,iy,X_BASE-long_scale_bar,iy,PIX_SRC,1);
                        floa(start_scale+(j*major_scale/factor),0,0);
                        num_sp = (int)(4*(strlen(ptstring)));
                        pw_text(pw, X_BASE-scale_spy-num_sp, iy+4, PIX_SRC,
                                dia_font,ptstring);
                        j++;
                        }
                else
                        pw_vector(pw,X_BASE,iy,X_BASE-short_scale_bar,iy,PIX_SRC,1);
                }
        }
        return (range1/factor);
}

/* return 1 if file exists, else print error message and return 0 */
stat_file(filename)
char *filename;
{
static char previous_dir[MAX_PATH_LEN];
char *current_dir;
char  this_file[MAX_PATH_LEN];
struct stat statbuf;
current_dir = (char *)panel_get_value(dir_item);
if (strcmp(current_dir, previous_dir)) {
        chdir((char *)panel_get_value(dir_item));
        strcpy(previous_dir, current_dir);
}
sprintf(ptstring, "%s/%s", current_dir, filename);
if (stat(ptstring, &statbuf) < 0)
        return 0;
else
        return 1;
}

/******* Done_proc : Close the file-transfer pop-up window *****/

void Done_proc()
{
```

```
        window_set(Filer_frame,WIN_SHOW,FALSE,0);
}
/**************** End of Done_proc ************************/
*
/****** Quit_proc : Exit from the TOF operating sysytem *******/
void Quit_proc()
{
        window_destroy(Base_frame);
}
/**************** End of Quit_proc ************************/
*
/******* ls_proc : Listing of files ***************************/
void ls_proc()
{
        static char previous_dir[MAX_PATH_LEN];
        char *current_dir;
        char cmdstring[100];

        current_dir = (char*)panel_get_value(dir_item);
        if(strcmp(current_dir,previous_dir))
        {
        chdir((char*)panel_get_value(dir_item));
        strcpy(previous_dir, current_dir);
        }
        sprintf(cmdstring, "ls  %s %s %s \n",
                current_dir,
                panel_get_value(source_item));
        ttysw_input(File_tty,cmdstring, strlen(cmdstring));
}
/**************** End of ls_proc ***************************/

/******* Search_peak : Search for signal peak ******************/

#define MAXPEAK 1000
extern float ydig[];
int  tty_rw;

void Search_peak_proc()
{
int count,i,k,numdig,starti, Search_Max();
int peak[MAXPEAK];
char cont, *c_theshold, cmdstring[256],*message;
int  theshold;
        i = k = 1;
        starti=1;
        cont = 'y';
        numdig=0;
        ttysw_output(File_tty,"Enter the theshold value =  ", 40);

/*      ttysw_output(idtty,c_theshold,20);
        theshold = atoi(c_theshold);*/
        theshold = 50;
for(k=1; cont=='y'; ++k){
                peak[k] = Search_Max(count,starti,theshold);
        if(peak[k] != -1) {
                sprintf(cmdstring, "Peak %d is number %d and has an intensity of %f\n",
                                k,peak[k],ydig[peak[k]]);
                ttysw_input(File_tty,cmdstring, strlen(cmdstring));
                starti=peak[k]+1;
                }
        else{
                ttysw_output(File_tty,"End of searching!\n",50);
                cont = 'n';
```

```
                }

                        }
}
/*************** End of Search_peak ***************************/

/****** Search_Max : Search for peak maximum ******************/
extern float ydig[];
Search_Max(ul, sl, th)

{
        int i, slope =- 1, localmax = th;
        for(i = sl; i <= ul; ++i){
        if(ydig[i] > ydig[i-1]) {
        if(ydig[i] > th && ydig[i] > localmax) {
        localmax = ydig[i];
        slope = 1;}}
        if(ydig[i] < localmax && slope > 0) return i-1;
        }
        return -1;
}

/********************** End of Search_Max **********************/

/******** Copy_proc: Copy file procedure ********/

void Copy_set_proc()
{
        panel_set(target_item,
                PANEL_SHOW_ITEM,  TRUE,0);
        panel_set(source_item,
                PANEL_LABEL_STRING,        "Source File: ",
                PANEL_VALUE,               "",
                PANEL_SHOW_ITEM,  TRUE,0);

        panel_set(input_done_item,
                PANEL_SHOW_ITEM,  TRUE,0);
}

void Copy_reset_proc()
{
        panel_set(source_item,
                PANEL_LABEL_STRING,        "File: ",
                PANEL_VALUE,               "",
                PANEL_SHOW_ITEM,  TRUE,0);

        panel_set(target_item,
                PANEL_SHOW_ITEM,  FALSE,0);

        panel_set(input_done_item,
                PANEL_SHOW_ITEM,  FALSE,0);
}

void Input_done_proc()
{
        char *filename;
        char cmdstring[256], *s_string, *t_string;

        if(!strlen(filename = (char*)panel_get_value(source_item)))
        {
        msg("Enter the source file",1);
        Copy_reset_proc();
        return;
```

```
        }
        if(!strlen(filename = (char*)panel_get_value(target_item)))
        {
        msg("Enter the target file",1);
        Copy_reset_proc();
        return;
        }
        s_string = panel_get_value(source_item);
        t_string = panel_get_value(target_item);
        sprintf(cmdstring, "cp %s %s \n", s_string, t_string);
        ttysw_input(File_tty,cmdstring, strlen(cmdstring));
        Copy_reset_proc();
}

/******** Delete_proc: Delete file procedure ********/
void Delete_proc()
{
        char cmdstring[256], *filename;

        if(!strlen(filename = (char*)panel_get_value(source_item)))
        {
        msg("Enter the file to be deleted!",1);
        Copy_reset_proc();
        return;
        }
        sprintf(cmdstring, "rm %s\n", panel_get_value(source_item));
        ttysw_input(File_tty,cmdstring, strlen(cmdstring));
}

/****************** End of Delete_proc **************************/

extern char ptstring[];

void ftoa(pt,dec,place)
        int pt,dec,place;
{
        int     sign,i,declust,ptlast,j,k,l,decorg;

        if((sign = pt) < 0)
                pt=-pt;
        decorg = dec;
        l = 0;
        if(dec != 0)
        {
        do {
                declust = dec % 10;
                ptstring[l++] = declust + '0';
                dec = dec/10;
                } while((dec /10) > 0);
        ptstring[l++] = dec + '0';
        if(l < place)  ptstring[l++] = 0 + '0';
        if(l < place)  ptstring[l++] = 0 + '0';
        if(l < place)  ptstring[l++] = 0 + '0';

        ptstring[l++] = '.';
        }
        if(pt !=0)
        {
        do {
                ptlast = pt % 10;
                ptstring[l++] = ptlast + '0';
                pt = pt/10;
                } while((pt /10) > 0);
```

```
        }
        if(pt > 0)
                ptstring[i++] = pt + '0';

        if(sign < 0)
                ptstring[i++] = '-';
        ptstring[i++] = '\0';
        for(j=0, k = strlen(ptstring)-1; j < k; j++,k--)
        {       l = ptstring[j];
                ptstring[j] = ptstring[k];
                ptstring[k] = l;
        }
}

int power(c1,c2)
        int c1,c2;
{
        int i , p=1;

        for(i=1; i <= c2; ++i)
                p = p*c1;
        return p;
}
```

Call.c : This module performs time-to-mass calibration.

```
#include <stdio.h>
#include <math.h>
#include <string.h>
#include <ctype.h>
#include <floatingpoint.h>
#include <stdlib.h>
#include <fcntl.h>
#include <suntool/sunview.h>
#include <suntool/textsw.h>
#include <suntool/panel.h>
#include <suntool/canvas.h>
#include <suntool/tty.h>
#include <suntool/alert.h>
#include <pixrect/pixrect_hs.h>
#include <sys/stat.h>
#define MAXIMUM                 26000
#define X_BASE                  100

Frame           Cent_frame, Mark_frame;
Canvas          canvas;
Panel           Cent_panel, Mark_frame;
Panel_item      mass_item, chan_cent_item, spectrum_mode_item, datamo_item,
                save_cali_item, ex_cal_item, charge_item, cluster_item,
                symbol_item, mass_apply_item, dec_apply_item, polarity_item;

Pixwin *pw;
Pixfont *dis_font;

extern int cent_on, spectrum_load;
void Calibration_proc()
{

        if(!spectrum_load)
        {
        msg("No spectrum is loaded!!",1);
        return;
        }

        cent_on = 1;
        msg("Locate the cross-hair onto the peaktop and kick on the right mouse button",1);
        return;
}

extern  int     hf_cent_chan, sum_int, xmin, ix, ix1, ix2;
extern  int     cent_count, spectrum_load;
extern  float   time_center, x_calibration;
extern char ptstring[];
void    cent_mass_proc()
{
void    peak_max_search_proc();
void    flon();
float   hf_cent_length;
char    cmdstring[10];

        if(!spectrum_load)
        {
        msg("No spectrum is loaded!!",1);
        return;
        }

        sprintf(cmdstring,panel_get_value(chan_cent_item));
```

```
        hf_cent_chan = (atoi(cmdstring))/2;
        hf_cent_length = (hf_cent_chan*sam_int*1.0)/1000;

        peak_max_search_proc();

        ix = (int)((X_BASE )+
                ((time_center/1000)-xmin)*x_calibration);
        ix1 = (int)((X_BASE )+
                ((time_center/1000)-xmin-hf_cent_length)*x_calibration);
        ix2 = (int)((X_BASE )+
                ((time_center/1000)-xmin+hf_cent_length)*x_calibration);

        pw_vector(pw, ix, 100,ix, 110, PIX_SRC,1);
        pw_vector(pw, ix1, 110,ix2, 110, PIX_SRC,1);
        pw_vector(pw, ix1, 110,ix1, 130, PIX_SRC,1);
        pw_vector(pw, ix2, 110,ix2, 130, PIX_SRC,1);

        ftos(cent_count+1,0,0);
        panel_set(distance_item,
                PANEL_VALUE, ptstring,0);
        panel_set(mass_item,
                PANEL_VALUE,"",0);
        window_set(Cent_frame, WIN_SHOW, TRUE,0);
        return;
}

extern int cent_count, sam_int;
extern float time_center, xdig[];
extern double time_tip[],mass_tip[];
void mass_acquire_proc()
{
        void display_cancel_proc();

        float     mass_center;
        char      cmdstring[10], *massvalue;
        int       i;

        if(!strlen(massvalue = (char*)panel_get_value(mass_item)))
        {
        msg("Enter the calibration mass",1);
        return;
        }

        sprintf(cmdstring,panel_get_value(mass_item));
        mass_center = atof(cmdstring);
        ++cent_count;


        time_tip[cent_count] = time_center/1000;
        mass_tip[cent_count] = sqrt(mass_center);

        display_cancel_proc();

        return;
}

extern   int       cent_count;

void mass_reset_proc()
{
        void display_cancel_proc();

        cent_count = 0;
```

```
        display_cancel_proc();
        return;
}

extern  int     hf_cent_chan, sam_int, xmin, ix, ix1, ix2, cent_on;
extern  float   time_center, x_calibration;

void    display_cancel_proc()
{


        pw_vector(pw, ix, 100,ix, 110, PIX_SRC,0);
        pw_vector(pw, ix1, 110,ix2, 110, PIX_SRC,0);
        pw_vector(pw, ix1, 110,ix1, 130, PIX_SRC,0);
        pw_vector(pw, ix2, 110,ix2, 130, PIX_SRC,0);

        window_set(Cent_frame, WIN_SHOW, FALSE,0);
        cent_on =0;
        return;
}

extern  int     cent_count, dig_max,xmin, sam_int, hf_cent_chan;
extern  float   xdig[], ydig[], time_center;

void peak_max_search_proc()
{
        int     i, chan_center, s_chan_center;
        float   pkarea, sub1, uppkarea, dnpkarea;

        for(i=0; i<= dig_max; i++)
                {
                sub1 = (xdig[i] - time_center);
                if(sub1 <= 0)       chan_center= i;
                }

        pkarea = ydig[chan_center];

        for(i=1; i <= hf_cent_chan; i++)
                pkarea = pkarea + ydig[chan_center+i] + ydig[chan_center-i];
        i=0;
        do
        {
        s_chan_center = 0;

        uppkarea = pkarea + ydig[chan_center + hf_cent_chan + 1] -
                        ydig[chan_center - hf_cent_chan];

        dnpkarea = pkarea + ydig[chan_center - hf_cent_chan - 1] -
                        ydig[chan_center + hf_cent_chan];

        if((uppkarea-pkarea) > 0 && (dnpkarea-pkarea) < 0)
                {
                ++chan_center;
                pkarea = uppkarea;
                s_chan_center = 1;
                }

        if((dnpkarea-pkarea) > 0 && (uppkarea-pkarea) < 0)
                {
                --chan_center;
                pkarea = dnpkarea;
                s_chan_center = 1;
                }
```

```
        if((uppkarea-pkarea) > 0 && (dnpkarea-pkarea) >0)
                {
                if(uppkarea > dnpkarea)
                        {
                        ++chan_center;
                        pkarea = uppkarea;
                        s_chan_center = 1;
                        }
                else if(dnpkarea > uppkarea)
                        {
                        --chan_center;
                        pkarea = dnpkarea;
                        s_chan_center = 1;
                        }
                }
        ++i;

        }
        while((s_chan_center > 0) || (i > 1000));

        time_center = chan_center*sam_int;
        return;
}

/*****************************************************************
*       Linear regression method:                                *
*                               n(E(xiyi)) - E(xi)E(yi)          *
*               Slope(m) =      ---------------------            *
*                               nE(sq(xi)) - sq(E(xi))           *
*                                                                *
*                               E(sq(xi))E(yi) - E(xi)E(xiyi)    *
*               Intercept(s) =  ---------------------            *
*                               nE(sq(xi)) - sq(E(xi))           *
*                                                                *
*       time = A + B(sqrt(mass))                                 *
*****************************************************************/

extern int cent_count, calibrated, dig_max, spectrum_load;
extern   float x_scale, time_pix;
extern float time_center, xdig[], cal_coeff1, cal_int;
extern double time_tip[],mass_tip[];
;
void In_Call_proc()
{
        void Whole_spectrum_proc();
        int i;
        double  sumxy=0,sumx=0,sumy=0,sumsqx =0;

        if(!spectrum_load)
        {
        msg("No spectrum is loaded!!",1);
        return;
        }

        if(cent_count < 2)
        {
        msg("Internal calibration requires at least two calibration points!!",1);
        return;
        }

        for(i=1; i <= cent_count; i++)
                {
```

```
                sumxy = sumxy + time_tip[i]*mass_tip[i];
                sumx = sumx + mass_tip[i];
                sumy = sumy + time_tip[i];
                sumsqx = sumsqx + mass_tip[i]*mass_tip[i];
                }
        cal_coeff1 = ((cent_count*sumxy) - (sumx*sumy)) /
                ((cent_count*sumsqx) - (sumx*sumx));

        cal_int = ((sumsqx*sumy) - (sumx*sumxy)) /
                ((cent_count*sumsqx) - (sumx*sumx));

        for(i=1; i<=dig_max; i++)
                {
                xdig[i] = ((xdig[i]-cal_int)/cal_coeff1);
                if(xdig[i] < 0) xdig[i]=0;
                xdig[i] = xdig[i]*xdig[i];
                }

        x_scale = xdig[dig_max];
        time_pix = x_scale/dig_max;

        panel_set(spectrum_mode_item,
                PANEL_LABEL_STRING,
                "Spectrum mode : Mass spectrum",
                0);

        calibrated = 1;

        panel_set(spectrum_mode_item,
                PANEL_LABEL_STRING,"Spectrum mode : Mass spectrum",
                PANEL_LABEL_BOLD,       TRUE,
                0);
        Whole_spectrum_proc();

        return;
}

extern int spectrum_load;
extern  float cal_int, cal_coeff1;
void save_cali_proc()
{
        FILE *fp;
        char candstring[50], *filename;

        if(!spectrum_load)
        {
        msg("No spectrum is loaded!!",1);
        return;
        }

        if(!calibrated)
        {
        msg("Do internal calibration first!!",1);
        return;
        }

        if(!strlen(filename = (char*)panel_get_value(save_cali_item)))
        {
        msg("Enter the calibration file",1);
        return;
        }
/*
        if (stat_file(filename))
```

```
        {
                sprintf(cmdstring, "%s is already exit.", filename);
                msg(cmdstring, 1);
                return;
        }
*/
        sprintf(cmdstring, "%s", filename);

        fp=fopen(cmdstring,"w");
        fprintf(fp,"%f\n%f",cal_int, cal_coeff1);
        fclose(fp);

        msg("Calibration data stored",1);

        return;
}

/**********Calibration : TOF = SQRT(M/z)*cal_coff1 + cal_int *****/
extern int calibrated, dig_max, spectrum_load;
extern float x_scale, xdig[], time_pix;
extern float cal_coeff1, cal_int;
void Ex_Cali_proc()
{
        void Whole_spectrum_proc();

        FILE *fp;
        char *filename, cmdstring[50];

        int i;

        if(!spectrum_load)
        {
        msg("No spectrum is loaded!!",1);
        return;
        }

        if(!strlen(filename = (char*)panel_get_value(ex_cal_item)))
        {
        msg("Enter the calibration file",1);
        return;
        }

        sprintf(cmdstring, "%s", filename);
        fp=fopen(cmdstring,"r");
        fscanf(fp,"%f \n %f",&cal_int, &cal_coeff1);
        fclose(fp);
        printf("%f\n%f",cal_int, cal_coeff1);
        for(i=1; i<=dig_max; i++)
                {
                xdig[i] = ((xdig[i]-cal_int)/cal_coeff1);
                if(xdig[i] < 0) xdig[i]=0;
                xdig[i] = xdig[i]*xdig[i];
                }
        x_scale = xdig[dig_max];
        time_pix = x_scale/dig_max;

        panel_set(spectrum_mode_item,
                PANEL_LABEL_STRING,"Spectrum mode : Mass spectrum",
                PANEL_LABEL_BOLD,       TRUE,
                0);

        calibrated = 1;
        Whole_spectrum_proc();
```

```
        return;
}

extern int spectrum_load, marking_on;

void    Marking_proc()
{
        if(!spectrum_load)
        {
        msg("No spectrum is loaded!!",1);
        return;
        }

        marking_on = 1;
        msg("Locate the cross-hair onto the peaktop and kick on the right mouse button",1);

        return;
}

void    mark_acquire_proc()
{
        window_set(Mark_frame, WIN_SHOW, TRUE,0);
        return;
}

extern float x_center, y_center, x_calibration, y_calibration, time_center;
extern float cal_int, cal_coeff1;
extern int xmin, ymin, m_space1, m_length, hf_cent_chan, calibrated;
void put_mark_proc()
{
        void    peak_max_search_proc();
        int     power();
        int     ptx, pty, ix, decx, mass_apply, dec_apply, m_space;
        char    charge[3], cluster[3],symbol[10], polarity[3];
        char    cmdstring1[10],cmdstring2[10];

        sprintf(cmdstring1,panel_get_value(chan_cent_item));
        hf_cent_chan = (atoi(cmdstring1))/2;

        peak_max_search_proc();
        if(calibrated)
        {
                x_center = time_center/1000;
                x_center = ((x_center-cal_int)/cal_coeff1);
                x_center = x_center*x_center;
        }
        else
        {
                x_center = time_center/1000;
        }

        dis_font = pf_open("/usr/lib/fonts/fixedwidthfonts/cour.b.16");

        ptx = (int)((x_center-xmin)*x_calibration)+100;
        pty = 400-((y_center-ymin)*y_calibration);

        sprintf(cluster,panel_get_value(cluster_item));
        sprintf(symbol,panel_get_value(symbol_item));

        sprintf(charge,panel_get_value(charge_item));
        sprintf(polarity,panel_get_value(polarity_item));

        if(atoi(cluster) ==1)
```

```
            sprintf(cmdstring1, "%s",symbol);
        else
            sprintf(cmdstring1, "%s%s",cluster,symbol);
        m_space = 10*(strlen(cmdstring1));


        if(atoi(charge) ==1)
            sprintf(cmdstring2, "%s",polarity);
        else
            sprintf(cmdstring2, "%s%s",charge, polarity);

        m_space1 = (m_space + (strlen(cmdstring2)*10))/2;

        pw_text(pw, ptx-m_space1, pty-12, PIX_SRC, dis_font,cmdstring1);
        pw_text(pw, ptx-m_space1+m_space, pty-16, PIX_SRC, dis_font,cmdstring2);

        pf_close(dis_font);

        dis_font = pf_open("/usr/lib/fonts/fixedwidthfonts/cour.r.10");

        mass_apply = (int)panel_get_value(mass_apply_item);
        dec_apply = (int)panel_get_value(dec_apply_item);

        if(!mass_apply)
        {
            ix = (int)x_center;
            decx = (int)((x_center-ix)*power(10,dec_apply));
            if(dec_apply==0 && decx > 4) ix = ix+1;
            ftos(ix,decx,dec_apply);
            sprintf(cmdstring1, "(%s)",ptstring);
            m_length = (6*strlen(cmdstring1))/2;
            pw_text(pw, ptx-m_length, pty, PIX_SRC, dis_font,cmdstring1);
            printf("%d %d %d \n", dec_apply, ix, decx);
        }
        return;
}


extern float x_center, y_center, x_calibration, y_calibration;
extern int xmin, ymin, m_space1, m_length;
void remove_mark_proc()
{
        int pty, ptx,i;

        ptx = (int)((x_center-xmin)*x_calibration)+100;
        pty = 400-((y_center-ymin)*y_calibration);

        dis_font = pf_open("/usr/lib/fonts/fixedwidthfonts/cour.b.14");

        for(i=0; i<= m_space1*2; i++)
            pw_text(pw, ptx-m_space1+i, pty-12, PIX_SRC, dis_font," ");

        for(i=0; i<= m_space1*2; i++)
            pw_text(pw, ptx-m_space1+i, pty-16, PIX_SRC, dis_font," ");

        pf_close(dis_font);

        dis_font = pf_open("/usr/lib/fonts/fixedwidthfonts/cour.r.12");

        for(i=0; i<= m_length*2; i++)
            pw_text(pw, ptx-m_length+i, pty, PIX_SRC, dis_font," ");
        pf_close(dis_font);
```

```
        return;
}

extern int marking_on;
void    mark_done_proc()
{
        marking_on = 0;
        window_set(Mark_frame, WIN_SHOW, FALSE,0);
        return;
}
```

dso2.c : This module performs data transfer to and from the LeCroy 9400A digital oclilloscope and the Sun 3/80 workstation (RS232-C serial transfer using Hexadecimal data format).

```
/*****************************************************************
Data format :
File : *.des
                #L              : data starts
                nnnn            : header information
                                  (no. of data)
                n..nn,nnnn      : data in hexadecimal,
                                  variable length
                #1              : end of data

File : *.dat
                #L              : data starts
                nnnn            : total number of data
                nn,.... nn      : data in hexadecimal (nn)
                #1              : end of data
*****************************************************************/
#include <stdio.h>
#include <suntool/sunview.h>
#include <suntool/panel.h>
#include <suntool/canvas.h>
#include <stdlib.h>
#include <fcntl.h>
#include <sys/termios.h>
#include <unistd.h>
#include <errno.h>
#include <sys/call.h>

Frame           DSO_to_Sun_frame, Sun_to_DSO_frame;

Panel_item      identifier_item, channel_item, nsweep_item,
                idata_file_item, sdata_file_item, wsweep_item,
                time_scale_item, voltage_item, average_item;

extern int fd, fd1, errno;
extern char ptstring[];
void DtoS_RS232_proc()

{
        void ftos();
        int power();
        struct termios t;
        int consok, Any_key, n=0, i=0;
        int channel_no, ndata, t_scale, tot_dat, left_dat, nsweep;
        char c;
        char buf[BUFSIZ], k[2], parameter[10], cmdstring[50];
        float td;

        fd = open("/dev/ttya",O_RDWR,0);
        t.c_iflag = 0;
        t.c_oflag = 0;
        t.c_cflag = B19200|CS8|CREAD;
        t.c_lflag = 0;
        consok = tcsetattr(fd,TCSANOW,&t);

        write(fd,"\033\103\r",3);
        write(fd,"\033\050\r",3);
        write(fd,"CTRL,OFF\r",9);
        write(fd,"\033\133\0190I2",4);
        write(fd,"\033\122\r",3);
```

```
write(fd,"CFMT,L,BYTE,HEX\r",16);
write(fd,"KEY 3,\"DSO TO SUN\"\r",19);
write(fd,"CBLS,0\r",7);
write(fd,"CTRL,OFF\r",9);

sprintf(parameter, panel_get_value(idata_file_item));
sprintf(cmdstring,"%s%s",parameter,".dat");
fd1 = creat(cmdstring,0666);
if(fd1 < 0)
        {
        printf("%d \n",errno);
        return;
        }
i = 0;
tot_dat = 302;
write(fd,"RD,",3);
channel_no = (int)panel_get_value(identifier_item);
if(channel_no == 0)     write(fd,"C1",2);
if(channel_no == 1)     write(fd,"C2",2);
if(channel_no == 2)     write(fd,"MC",2);
if(channel_no == 3)     write(fd,"MD",2);
if(channel_no == 4)     write(fd,"FE",2);
if(channel_no == 5)     write(fd,"FF",2);
write(fd,",DEu",4);

do
{
        do
        {
        read(fd,&c,1);
        }
        while(c != 'L');
read(fd,&c,1);
}
while(!(c >= '0' && c <= '9'));

write(fd1,"0L",2);
write(fd1,&c,1);

do      {
        n = read(fd,buf,BUFSIZ);
        write(fd1,buf,n);
        tot_dat = tot_dat - n;
        i = i+n;
        }       while(tot_dat > 254);
n = read(fd,buf,tot_dat);
write(fd1,buf,n);
write(fd1,"01",2);
close(fd1);

sprintf(parameter, panel_get_value(idata_file_item));
sprintf(cmdstring,"%s%s",parameter,".dat");
fd1 = creat(cmdstring,0666);

write(fd,"RD,",3);
channel_no = (int)panel_get_value(identifier_item);
if(channel_no == 0)     write(fd,"C1",2);
if(channel_no == 1)     write(fd,"C2",2);
if(channel_no == 2)     write(fd,"MC",2);
if(channel_no == 3)     write(fd,"MD",2);
if(channel_no == 4)     write(fd,"FE",2);
if(channel_no == 5)     write(fd,"FF",2);
write(fd,",DA,,,,",7);
```

```
        sweep = (int)panel_get_value(nsweep_item);
        if(sweep == 0)   write(fd,"1\r",2);
        if(sweep == 1)   write(fd,"2\r",2);
        if(sweep == 2)   write(fd,"3\r",2);
        if(sweep == 3)   write(fd,"4\r",2);
        if(sweep == 4)   write(fd,"5\r",2);
        if(sweep == 5)   write(fd,"6\r",2);
        if(sweep == 6)   write(fd,"7\r",2);
        if(sweep == 7)   write(fd,"8\r",2);

        tot_dat = 0;
        do
                read(fd,&c,1);
                while(c != 'L');
        write(fd1,"0L",2);
        for(i=0; i < 4 ; i++)
                {
                read(fd,&c,1);
                write(fd1,&c,1);
                if(c < '0' || c > '9')
                        c = c - '7';
                else
                        c = c - '0';

                tot_dat = tot_dat + c*(power(16,3-i));
                }
        i = 0;
        tot_dat = (tot_dat - 1)*2;
        do      {
                n = read(fd,buf,BUFSIZ);
                write(fd1,buf,n);
                tot_dat = tot_dat - n;
                i = i+n;
                }       while(tot_dat > 254);

        n = read(fd,buf,tot_dat);
        write(fd1,buf,tot_dat);
        i = i+n;
        write(fd1,"0I",2);
        close(fd1);
        write(fd,"\033\114\r",3);
        close(fd);
        window_set(DSO_to_Sun_frame, WIN_SHOW, FALSE,0);
}

extern int fd, fd1,errno;
extern char ptstring[];

void StoD_RS232_proc()
{
        FILE *fp;
        void floa();
        int power();
        struct termios t1;
        int conob1, n, i, fn;
        int channel_no, mdata,no_of_ave, t_scale, v_scale, sweep;
        int fix_ver_gain, tim_div, index, tim_axis, ver_axis;
        char buf[BUFSIZ], parameter[10], condstring[50];
        char c;
        float td, var_ver_gain;

        fd = open("/dev/ttya",O_RDWR,0);
```

```
t1.c_iflag = 0;
t1.c_oflag = 0;
t1.c_cflag = B19200|CS8|CREAD;
t1.c_lflag = 0;
cond1 = tcsetattr(fd,TCSANOW,&t1);

write(fd,"\033\103\r",3);
write(fd,"\033\050\r",3);
write(fd,"CTRL,OFF\r",9);
write(fd,"\033\133\015\012",4);
write(fd,"\033\122\r",3);
write(fd,"CFMT,L,BYTE,HEX\r",16);
write(fd,"KEY 3,\"SUN TO DSO\"\r",19);
write(fd,"CBLS,0\r",7);
write(fd,"CTRL,OFF\r",9);

sprintf(parameter, panel_get_value(sdata_file_item));
sprintf(cmdstring,"%s%s",parameter,".dat");

fd1 = open(cmdstring,O_RDWR,0);

if(fd1 < 0)
        {
        printf("%d\n",errno);
        return;
        }
write(fd,"WT,",3);
channel_no = (int)panel_get_value(channel_item);
if(channel_no == 0)       write(fd,"MC",2);
if(channel_no == 1)       write(fd,"MD",2);
write(fd,",DA,,,,",7);
sweep = (int)panel_get_value(waweep_item);
if(sweep == 0)   write(fd,"1\r",2);
if(sweep == 1)   write(fd,"2\r",2);
if(sweep == 2)   write(fd,"3\r",2);
if(sweep == 3)   write(fd,"4\r",2);
if(sweep == 4)   write(fd,"5\r",2);
if(sweep == 5)   write(fd,"6\r",2);
if(sweep == 6)   write(fd,"7\r",2);
if(sweep == 7)   write(fd,"8\r",2);

while((n = read(fd1,buf,BUFSIZ))>0)
        write(fd,buf,n);

write(fd,"\r",1);
close(fd1);
for(i=0;i < 5000; i++) i++;
write(fd,"\033\114\r",3);
close(fd);
window_set(Sun_to_DSO_frame, WIN_SHOW, FALSE,0);
return;
}
```

prt.c : This module produces bit mapping file for the time-of-flight spectrum.

```
#include    <stdio.h>
#include    <sys/types.h>
#include    <pixrect/pixrect.h>
#include    <pixrect/pr_io.h>
#define     RT_STANDARD     1
#define     RMT_NONE 0

void Prt_graph_proc()
{
        Pixrect         *screen, *icon;
        FILE            *c_ras;
        colormap_t      *colormap = 0;
        int             type = RT_STANDARD;
        int             copy_flag = 1;
        char            cmdstring[256];

        if(!(screen = pr_open("/dev/fb")) ||
                !(icon = pr_region(screen,210,360,780,470)))
                return;
        c_ras = fopen("c_ras","w");

        pr_dump(icon, c_ras, colormap, type, copy_flag);
        pr_close(screen);
        fclose(c_ras);
}
```